

AO-A191 900

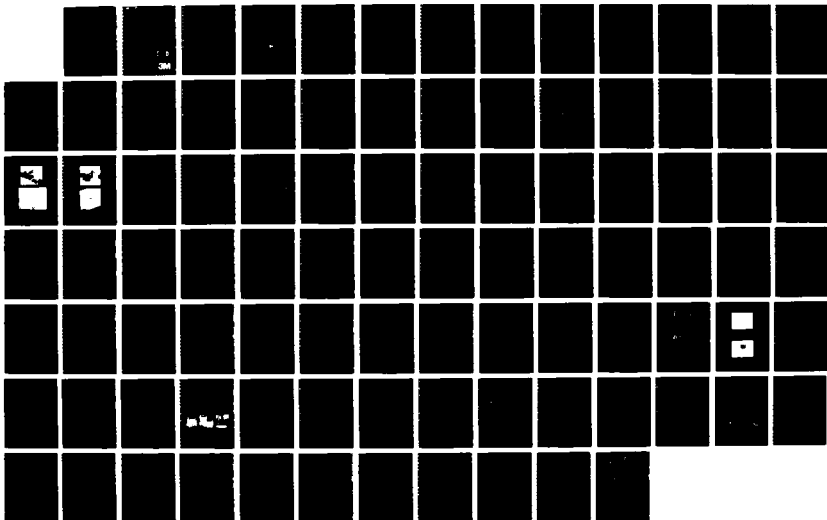
BLUE-GREEN LASER DIODE RESEARCH PROGRAM(U) MINNESOTA  
MINING AND MFG CO ST PAUL ELECTRONIC AND INFORMATION  
SECTOR LAB J E POTTS ET AL. FEB 88 N00014-03-C-0552

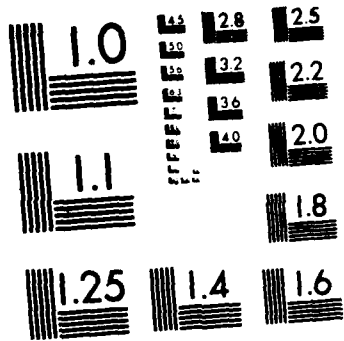
1/1

UNCLASSIFIED

F/G 9/3

NL





MICROCOPY RESOLUTION TEST CHART  
NATIONAL BUREAU OF STANDARDS-1963 A

**DTIC FILE COPY**

4

**BLUE-GREEN LASER DIODE RESEARCH PROGRAM**

**AD-A191 980**

**Final Technical Progress Report  
For The Period October 1, 1985 To December 31, 1987**

**Prepared Under  
Contract Number N00014-85-C-0552**

**FEBRUARY, 1988**

**APPROVED FOR PUBLIC RELEASE  
DISTRIBUTION UNLIMITED**

The views and conclusions contained in this document are those of the authors and should not be interpreted as necessarily representing the official policies, either expressed or implied, of the Defense Advanced Research Projects Agency or the U.S. Government.

Work supported in part by the:

**DEFENSE ADVANCED RESEARCH PROJECTS AGENCY  
1400 Wilson Boulevard  
Arlington, VA 22209**

Under the:

**OFFICE OF NAVAL RESEARCH  
Department Of The Navy  
800 N. Quincy Street  
Arlington, VA 22217-5000**

**DTIC  
ELECTE  
MAR 09 1988  
S D  
G-H**

**Electronic and Information  
Sector Laboratories/3M**

St. Paul, MN 55144-1000

**3M**

**88 3 05 001**

UNCLASSIFIED

SECURITY CLASSIFICATION OF THIS PAGE

## REPORT DOCUMENTATION PAGE

1a. REPORT SECURITY CLASSIFICATION UNCLASSIFIED			1b. RESTRICTIVE MARKINGS		
2a. SECURITY CLASSIFICATION AUTHORITY			3. DISTRIBUTION/AVAILABILITY OF REPORT Approved for Public Release Distribution Unlimited		
7b. DECLASSIFICATION/DOWNGRADING SCHEDULE					
4. PERFORMING ORGANIZATION REPORT NUMBER(S) Final Technical Progress Report			5. MONITORING ORGANIZATION REPORT NUMBER(S)		
6a. NAME OF PERFORMING ORGANIZATION 3M Company		6b. OFFICE SYMBOL (If applicable)	7a. NAME OF MONITORING ORGANIZATION Defense Advanced Research Projects Agency		
6c. ADDRESS (City, State and ZIP Code) E&I Sector Laboratory - 201-1N-36 3M Center - St. Paul, MN 55144			7b. ADDRESS (City, State and ZIP Code) 1400 Wilson Boulevard Arlington, VA 22209		
8a. NAME OF FUNDING/SPONSORING ORGANIZATION Office of Naval Research		8b. OFFICE SYMBOL (If applicable)	9. PROCUREMENT INSTRUMENT IDENTIFICATION NUMBER Contract No. N00014-85-C-0552		
8c. ADDRESS (City, State and ZIP Code) Dept. of the Navy 800 N. Quincy St. Arlington, VA 22217-5000			10. SOURCE OF FUNDING NOS.		
11. TITLE (Include Security Classification) Blue-Green Laser Diode Research Program			PROGRAM ELEMENT NO.	PROJECT NO.	TASK NO.
			WORK UNIT NO.		
12. PERSONAL AUTHOR(S) Drs. J. E. Potts, H. A. Mar, and C. T. Walker					
13a. TYPE OF REPORT Final Tech. Progress		13b. TIME COVERED FROM 85/10/01 TO 87/12/31		14. DATE OF REPORT (Yr., Mo., Day) 1988, February	15. PAGE COUNT 90
16. SUPPLEMENTARY NOTATION					
17. COSATI CODES			18. SUBJECT TERMS (Continue on reverse if necessary and identify by block number)		
FIELD	GROUP	SUB. GR.			
			Blue-Green Laser or Lasers, Blue-Green		
19. ABSTRACT (Continue on reverse if necessary and identify by block number)					
<p>This report presents the results of work during the final quarter of ONR Contract No. N00014-85-C-0552 (July 1, 1987 to September 30, 1987) and during a three-month extension of the original twenty-four month program (October 1, 1987 to December 31, 1987). This report concludes with a Summary Report describing the highlights and major accomplishments under this contract during the period October 1, 1985 to December 31, 1987 in the following areas:</p> <p>i. Growth of unintentionally-doped ZnSe epitaxial films by MBE on (100) GaAs substrates in order to fully characterize the material and to understand the effects of varying growth conditions on the resultant film properties.</p> <p style="text-align: right;">(Contd.)</p>					
20. DISTRIBUTION/AVAILABILITY OF ABSTRACT UNCLASSIFIED/UNLIMITED <input type="checkbox"/> SAME AS RPT. <input checked="" type="checkbox"/> DTIC USERS <input type="checkbox"/>			21. ABSTRACT SECURITY CLASSIFICATION UNCLASSIFIED		
22a. NAME OF RESPONSIBLE INDIVIDUAL L. C. McGraw			22b. TELEPHONE NUMBER (Include Area Code) (612) 733-9816	22c. OFFICE SYMBOL	

DD FORM 1473, 83 APR

EDITION OF 1 JAN 73 IS OBSOLETE.

UNCLASSIFIED

SECURITY CLASSIFICATION OF THIS PAGE

Block 19 (Continued)

- ii. Growth of unintentionally-doped ZnSe on alternate substrates (Ge, Si, Ge with Ge buffer layer, Si with Ge/ZnSe strained-layer superlattice buffer layer) in an attempt to reduce the deleterious effects caused by lattice mismatch between the substrate and the epilayer and/or possible autodoping by contaminants from the substrate which had been suspected to occur when using GaAs substrates,
- iii. p-doping of ZnSe films on (100) GaAs substrates,
- iv. Examination of the lasing properties of ZnSe films using electron-beam pumping,
- v. Studies of metal contacts on ZnSe for Ohmic contacts and Schottky barriers.



Accession For	
NTIS GRA&I	<input checked="" type="checkbox"/>
DTIC TAB	<input type="checkbox"/>
Unannounced	<input type="checkbox"/>
Justification _____	
By _____	
Distribution/	
Availability Codes	
Dist	Avail and/or Special
A-1	

## EXECUTIVE SUMMARY

In this report we present the results of our work during the final quarter of ONR Contract No. N00014-85-C-0552 (July 1, 1987 to September 30, 1987) and during a three-month extension of the original twenty-four month program (October 1, 1987 to December 31, 1987). This report concludes with a Summary Report describing the major accomplishments under this contract during the period October 1, 1985 to December 31, 1987.

During the final quarter of this contract we demonstrated that the use of 6N super-grade Zn rod as a source material offered no improvement in sample quality over that produced using 6N Zn and 6N super-grade Se. We have found that the high levels of Cu impurities found by SIMS analyses and reported earlier for some of our undoped and Li-doped films, and suspected of compensating our intentionally-incorporated acceptor atoms, were in fact due to a high background contamination in the SIMS chamber. We have extended our X-ray studies of tilting phenomena in ZnSe/Ge and ZnSe/GaAs epilayers in an effort to understand why the magnitude of the tilt is much larger in the former system than in the latter. We found that the tilt depends strongly on the crystallographic orientation of the substrate as well as on the thickness of the epilayer. In a simple microscopic model of the substrate/epilayer interface, we have shown how the relocation of atoms in the interface region near steps on the substrate surface triggers the formation of the tilt. By growing 0.3-0.4  $\mu\text{m}$  thick Ge buffer layers prior to initiating growth of the ZnSe epilayer, we have been able to reduce the tilt angle as well as the FWHM of the double-crystal rocking curve reflection peaks and the 4.2K PL excitonic peaks. TEM examination showed these layers to be free of the cellular structure found previously in unbuffered layers.

The main thrust of our efforts during the past six months has been in a detailed study of p-type doping of ZnSe epilayers using the alkali metal dopants Li and Na. Following on the first achievement of p-type ZnSe in MBE growth reported in Quarterly Technical Progress Report No. 5, we have examined the properties of films grown using three alternate sources of Li and covering a broad range of MBE growth parameter space. Li source #2 was of a different composition than source #1; source #3, while of the same composition as source #1, was chosen on the basis of a SIMS analysis of similar materials from several different vendors. Samples grown using these

three sources exhibit similar 9K PL spectra and all are unquestionably p-type, although it is still not possible to do Hall measurements on these films and the hole concentrations deduced from I-V measurements appear to be anomalously low. The similarities in the PL spectra and electrical measurements for samples grown using radically different sources of Li indicate that either extrinsic impurities have a negligible effect on the activity of Li acceptors or that the relevant unintentionally-incorporated donor impurities are common to all three of the sources used.

An alternate explanation for the electrical inactivity of the Li acceptors involves the gettering of the Li atoms by macroscopic structural defects propagating from the substrate. Incorporation of an undoped ZnSe buffer layer prior to initiating the growth of Li-doped ZnSe was attempted in order to bury the interface and offer a defect-free surface on which to begin growing the doped layer. Little improvement in the film quality was realized by this modification. In particular, no improvement occurred in the electrical activation of the Li acceptors. There remains the possibility that the presence of Li atoms at the growth surface results in the formation of structural defects.

Our examination of Li-doped films grown in various regions of ZnSe growth parameter (substrate temperature and Zn/Se beam pressure ratio) space found that the film properties were altered very little by large changes in the growth conditions. This is in striking contrast to the results obtained in the case of undoped ZnSe. The optimum growth conditions for the Li-doped films were found to lie in the Se-stabilized growth region ( $T_g = 250-300^\circ\text{C}$ , BPR = 1/4:1); growth of undoped ZnSe under these conditions would have yielded films of extremely poor quality.

For Na-doping we have used the same source material as was described in Quarterly Technical Progress Report No. 5, but we have used a new method for loading the source material, designed to provide better control over the Na flux. Samples grown using this Na source #3 have PL spectra which are dominated by a strong broad band of near 2.62 eV, as was the case with samples grown using source #2. The origin of this band is unknown, but it lies in a spectral region where structural-defect-related peaks usually occur. Electrically, these films have not been shown to be p-type, and

there are indications that donors are being incorporated into the ZnSe films from this Na beam. We continue to search for a source which can give us a cleaner Na beam.

Studies of Li diffusion using Li-modulation-doped films have demonstrated that Li i) diffuses readily into an underlying ZnSe film and ii) sticks to the growing surface and continues to dope the film even after the Li source has been shuttered off. These effects must be dealt with if clean, abrupt interfaces are to be grown in ZnSe films which employ Li-doping. A similar study performed by Na-modulation-doping a ZnSe film demonstrated that Na diffuses very little, making Na more amenable to device construction if it can be made to behave suitably as a p-type dopant.

The final work reported during the final quarter was in the area of contact studies. Examination of the Li-doped films using a potential profiling technique has led to a confirmation of the p-type activity of these films. In addition, these measurements have shown that the actual resistivity of these films is quite low and the hole concentrations deduced from these measurements are quite reasonable in view of the incorporated Li concentrations. Thus it would appear that i) the electrical activation of the Li acceptors is much larger than our two-point I-V measurements had indicated, and ii) Au may not be forming a good Ohmic contact to p-ZnSe as had been predicted. These results have led us to shift the emphasis of our project from altering the electrical activation of the Li acceptors to finding suitable Ohmic contacts to p-ZnSe.

The Summary Report highlights the accomplishments under this contract in the following areas:

- i. Growth of unintentionally-doped ZnSe epitaxial films by MBE on (100) GaAs substrates in order to fully characterize the material and to understand the effects of varying growth conditions on the resultant film properties.
- ii. Growth of unintentionally-doped ZnSe on alternate substrates (Ge, Si, Ge with Ge buffer layer, Si with Ge/ZnSe strained-layer superlattice buffer layer) in an attempt to reduce the

deleterious effects caused by lattice mismatch between the substrate and the epilayer and/or possible autodoping by contaminants from the substrate which had been suspected to occur when using GaAs substrates.

- iii. p-doping of ZnSe films on (100) GaAs substrates.
- iv. Examination of the lasing properties of ZnSe films using electron-beam pumping.
- v. Studies of metal contacts on ZnSe for Ohmic contacts and Schottky barriers.

In brief, all of the goals set out in the work statements for this contract have been met within the timelines set forth in that contract. The highlight of the work done under this contract has been the achievement of p-type ZnSe films by molecular beam epitaxy. In spite of some potential limitations set by the use of Li as the acceptor impurity, this is an accomplishment of major significance since it demonstrates that p-type conversion can be achieved in this wide-bandgap material (and, undoubtedly, in similar materials). As we suggested in our initial proposal, the thermodynamic limitations on type conversion set by self-compensation processes can be overcome by using a kinetically-controlled growth process such as MBE. Further developments in this area are certain to follow rapidly, as other suitable p-type dopant sources, having lower diffusivity than Li, are identified. We have suggested that Na may be such a source. The fundamental materials problems now appear solvable and the time for development of visible light-emitting devices based on wide-bandgap II-VI semiconductors is at hand.

## TABLE OF CONTENTS

<u>Section</u>	<u>Page</u>
1.0 INTRODUCTION.....	1
2.0 PROGRESS REPORT: JULY 1, 1987 TO DECEMBER 31, 1987.....	2
2.1 Project 1, Task 1: Materials Research - Undoped ZnSe.....	2
2.1.1 Unintentionally-Doped ZnSe Heteroepitaxy on (100) GaAs..	2
2.1.1.1 Use of Ultra-High-Purity Zn and Se Sources.....	2
2.1.1.2 SIMS Analysis for Copper Impurities.....	2
2.1.2 X-Ray Study of Tilting Phenomenon in ZnSe/Ge and	
ZnSe/GaAs Epilayers.....	4
2.1.2.1 ZnSe Layers on (100) Ge Substrates.....	4
2.1.2.2 ZnSe/(100) Ge with a Ge Buffer Layer.....	13
2.2 Project 1, Task 2: Materials Research - p-ZnSe.....	18
2.2.1 Li-Doped ZnSe on GaAs.....	18
2.2.1.1 Li-Doping Source #2.....	18
2.2.1.2 SIMS Comparison of Lithium Sources.....	22
2.2.1.3 Li-Doping Source #3.....	24
2.2.1.4 Undoped ZnSe Buffer Layers.....	27
2.2.1.5 Examination of Growth Space with Li-Doping.....	33
2.2.2 Na-Doped ZnSe on (100) GaAs.....	37
2.2.2.1 Na-Doping Source #3.....	37
2.2.3 Lithium and Sodium Diffusion Studies.....	40
2.3 Project 2, Task 2: Contact Studies.....	43
3.0 SUMMARY REPORT.....	45
3.1 Unintentionally-doped ZnSe.....	45
3.2 Growth of MBE-ZnSe Epilayers on Alternate Substrates.....	53
3.2.1 Ge Substrates.....	54
3.2.2 Si Substrates.....	59
3.2.3 Ge Buffer Layers.....	60
3.2.4 ZnSe/Ge Superlattice Buffer Layers.....	60
3.3 p-Doping of ZnSe Films.....	63
3.3.1 N.....	63
3.3.2 P.....	64
3.3.3 Sb.....	67
3.3.4 Li.....	68
3.3.5 Na.....	72
3.4 Electron-Beam Pumping of ZnSe Laser Cavities.....	74
3.5 Metal Contacts to ZnSe.....	74
4.0 REFERENCES.....	77
5.0 PUBLICATIONS RESULTING UNDER ONR CONTRACT NO. N00014-85-C-0552.....	79
5.1 Refereed Papers.....	79
5.2 Published Conference Proceedings (not refereed).....	80
5.3 Oral Presentations (no published proceedings).....	81
5.4 In Preparation.....	81

LIST OF FIGURES

<u>Figure</u>	<u>Page</u>
2-1. Tilt angle between (400) planes of the epilayer and the substrate versus epilayer thickness.....	5
2-2. Tilt angle between (400) planes of the epilayer and the substrate versus the cut-off angle of the Ge substrate.....	6
2-3. Linewidth of the (400) DCRC X-ray peak in ZnSe films versus epilayer thickness.....	7
2-4. Linewidth of the (400) DCRC peak of ZnSe films versus the cut-off angle of the Ge substrate.....	8
2-5. Linewidth of the donor-bound exciton line in PL versus the cut-off angle of the Ge substrate.....	10
2-6. Atomic model of the ZnSe/(100) GaAs interface cut off toward the (110) direction.....	11
2-7. Schematic model of the (100) Ge substrate cut towards the (100) direction.....	13
2-8. Bond distortion at the Ge step edge versus cut-off angle of the Ge substrate.....	14
2-9. Differences between the tilt of the (400) planes of Ge and ZnSe and between the DCRC FWHM values of ZnSe layers for samples grown with and without Ge buffer layers.....	14
2-10. Planar view of ZnSe epilayers grown in (100) Ge substrate.....	16
2-11. Cross-sectional transmission electron micrographs of ZnSe on (100) Ge.....	17
2-12. PL spectra of two samples with similar Li concentrations (approximately $5 \times 10^{17} \text{ cm}^{-3}$ ).....	19
2-13. PL spectra of two samples with similar Li concentrations (approximately $3 \times 10^{18} \text{ cm}^{-3}$ ).....	20
2-14. PL spectra of three samples grown using Li Source #2.....	21
2-15. PL spectra of two samples with similar Li concentrations (approximately $1.4 \times 10^{17} \text{ cm}^{-3}$ ).....	28
2-16. SIMS depth profiles of Li concentrations.....	30
2-17. PL spectra for Li-doped samples with and without a $1 \mu\text{m}$ thick undoped ZnSe buffer.....	31
2-18. PL spectra for two Li-doped samples with and without a $1 \mu\text{m}$ thick undoped ZnSe buffer.....	32
2-19. SIMS depth profiles of Na concentration in sample ZSE158 grown with Na source #3 and with a thick undoped ZnSe buffer layer.....	38

LIST OF FIGURES (continued)

<u>Figure</u>	<u>Page</u>
2-20. PL spectra for Na-doped ZnSe films grown using Na-sources #2 and #3 to compare the effects of the new source loading procedure.....	39
2-21. SIMS profile of Li-modulation-doped ZnSe film.....	42
2-22. SIMS profile of Na-modulation-doped ZnSe film.....	42
2-23. Results of potential profiling measurements on a Li-doped film....	44
3-1. Growth matrix used to study the properties of undoped ZnSe using different growth temperatures and Zn/Se beam pressure ratios.....	47
3-2. (a) Positions of exciton-related PL features versus film thickness. (b) Relaxation of the ZnSe lattice parameter versus film thickness.....	49
3-3. ZnSe lattice relaxation as a function of layer thickness.....	50
3-4. Two-electron and resonant Raman scattering signals for sample ZSE37A.....	51
3-5. AES spectrum of sputter/annealed (100) Ge substrate showing the absence of both C and O.....	55
3-6. RHEED patterns of Ge substrates.....	56
3-7. DCRC linewidths of ZnSe on (100) Ge and (100) GaAs versus layer thickness.....	57
3-8. DBE linewidth of ZnSe layers on (100) Ge and (100) GaAs substrates.....	58
3-9. SEM micrographs of surface morphologies of ZnSe layers grown directly on Si and with superlattice buffers incorporated.....	61
3-10. 4.2K PL spectrum of ZnSe on (100) Si with a two-period superlattice is dominated by excitonic emission.....	62
3-11. (a) 4.2K PL excitonic spectrum of unintentionally-doped ZnSe is dominated by free excitonic-related emission. (b) Spectrum of n-doped ZnSe layer is dominated by the acceptor-bound excitonic peak, $I_1$ .....	65
3-12. 9K PL spectra of lightly and heavily phosphorous-doped ZnSe films, showing a dramatic increase in the deep level emission as the P-concentration increases.....	66
3-13. 9K PL spectra for an undoped and a Li-doped ZnSe film.....	70
3-14. I-V characteristics for an undoped and a Li-doped ZnSe film using different metal contacts and electrode configurations.....	71

LIST OF FIGURES (continued)

<u>Figure</u>	<u>Page</u>
3-15. 9K PL spectra for three Na-doped samples with increasing Na concentrations.....	73
3-16. 16K lasing spectrum of a 4.3 $\mu\text{m}$ ZnSe cavity at 35 kV and an electron beam current just above threshold.....	75

LIST OF TABLES

<u>Table</u>	<u>Page</u>
2-1. Comparison of Cu Concentrations Determined by SIMS Measurements for Several Samples Grown Using Different Zn and Se Starting Materials.....	3
2-2. Tetrahedral Covalent Radii of Some Elements of Interest According to Pauling.....	12
2-3. Summary of Growth Conditions and Incorporated Li Concentrations (measured by SIMS) for Samples Grown Using Li Source #2.....	18
2-4. Results of +SIMS Analysis of Three Different Li Sources.....	23
2-5. Results of -SIMS Analysis of Three Different Li Sources.....	23
2-6. Summary of Growth Conditions and Incorporated Li Concentrations for All Samples Grown Using Li Source #3.....	25
2-7. Results of SIMS, Electrical, and PL Measurements for Samples Grown Using Li Sources #1 and #3.....	26
2-8. Growth Matrix Used to Study the Variation of Film Properties with Different Growth Conditions at a Constant Li-flux of 3.....	35
2-9. Growth Matrix used to Study the Variation of Film properties with Different Growth Conditions at a Constant Li-flux of 60.....	36
2-10. Summary of Growth Conditions and Incorporated Na Concentrations (measured by SIMS) for Samples Grown Using Na Source #3.....	37

## 1.0 INTRODUCTION

This is a final technical report under ONR contract No. N00014-85-C-0552 that (1) covers progress during the last six months (July through December, 1987), and (2) summarizes the results and major areas of study during the entire 27 months of this contract.

All work was completed through parallel and coordinated efforts done in the laboratories at 3M St. Paul, Minnesota and 3M Toronto, Canada.

## 2.0 PROGRESS REPORT: JULY 1, 1987 TO DECEMBER 31, 1987

### 2.1 Project 1, Task 1: Materials Research - Undoped ZnSe

#### 2.1.1 Unintentionally-Doped ZnSe Heteroepitaxy on (100) GaAs

##### 2.1.1.1 Use of Ultra-High-Purity Zn and Se Sources

As we discussed in Quarterly Technical Progress Report No. 3, the Se starting material plays a most important role in achieving uncompensated high-resistivity ZnSe films. These undoped films usually exhibit an extremely high resistivity and show dominant free exciton emission and very weak  $I_{20}$  and  $I_x$  donor-bound exciton emission in the low-temperature photoluminescence. This indicates that there is very little contamination by extrinsic donor impurities. Whether the quality of the film can be improved further by using higher purity Zn is unclear; however it is desirable to use Zn starting material in such a form that the charging capacity can be maximized and at the same time any potential overgrowth problem can be significantly reduced.

Super-grade Zn rods of 99.9999+% (6N) purity with a shape similar to that of the pyrolitic boron nitride (PBN) crucible were purchased from Osaka Asahi Metals. After being loaded in the MBE system, the material was outgassed under UHV for several hours. An undoped ZnSe sample was grown before any other growth run to examine the effect of purer Zn starting material on the quality of the film. Optical and electrical characterizations of this sample showed no discernible change in its properties. Undoped films grown at later stages had similar results. Therefore we conclude that the high purity Zn starting material available commercially is adequate for MBE growth of ZnSe. In addition, because we are now using a solid Zn rod rather than Zn shot, we find we can now grow more films from each load of Zn starting material. The actual increase of total film thickness per load amounts to more than 80%.

##### 2.1.1.2 SIMS Analysis for Copper Impurities

We have recently questioned whether or not the origin of the deep level PL emission in our Li-doped ZnSe samples might lie in Cu-related recombination centers. The copper concentrations reported in Quarterly

Technical Progress Report No. 4 were between  $5 \times 10^{16}$  and  $1.5 \times 10^{17} \text{ cm}^{-3}$  for both undoped and Na-doped samples. During this quarter, we have undertaken more thorough measurements of the copper concentration in various undoped and Li-doped samples in order to determine if this might be causing problems in our films, particularly in the Li-doped samples. Cu-implanted standards with known ion doses were used for calibration purposes. This allows for determination of the absolute copper concentration. The results are shown in Table 2-1, along with the relevant information on the starting materials:

TABLE 2-1. Comparison of Cu Concentrations Determined by SIMS Measurements for Several Samples Grown Using Different Zn and Se Starting Materials. Alfa and Spex are material vendors. 6NS represents the 6N supergrade materials obtained from Osaka Asahi. The notation "z.r." refers to zone-refined zinc.

Sample	Zn Source	Se Source	(Cu) earlier report	(Cu) new measurements	(Cu) after Si sputtering	(Cu) 3 days later
Undoped						
67C	Alfa	Spex	---	$5.8 \times 10^{16}$	$6.6 \times 10^{15}$	
75C	Alfa	Alfa	---	$4.9 \times 10^{16}$	$8.4 \times 10^{15}$	
77C	Alfa	6NS	$4.4 \times 10^{16}$	$4.2 \times 10^{16}$	$9.6 \times 10^{15}$	
88C	z.r.	6NS	$9 \times 10^{16}$	$4.2 \times 10^{16}$	$5.7 \times 10^{15}$	
131C	6NS	6NS	---	$3.6 \times 10^{16}$	$4.6 \times 10^{15}$	$1.9 \times 10^{16}$
94C	z.r.	6NS	$1.3 \times 10^{17}$			$7.8 \times 10^{15}$
Li-doped						
147C*	6NS	6NS				$8.4 \times 10^{15}$

\* (Li)  $\sim 7 \times 10^{18} \text{ cm}^{-3}$

As shown in Table 2-1 the Cu concentration is about the same in all samples in the same series of study. In order to reduce the background concentration of Cu in the SIMS system, the walls of the SIMS specimen chamber were coated with sputtered Si. Since this procedure reduced the Cu levels significantly, we have concluded that the high Cu signal observed for these samples does come from the background rather than from the samples themselves. This high background level of copper in the SIMS system is probably due to an Al-Cu grid used for primary ion beam alignment and focusing. The upper limit of Cu concentration in our samples is in the upper  $10^{15} \text{ cm}^{-3}$  and it is very likely that most of the Cu signal is still coming from the background. The heavily Li-doped sample 147 does not show a higher Cu level when compared with undoped samples. Hence it is safe to say the Li source is free of Cu contamination problems, at least at the temperature at which it is used for doping.

## 2.1.2 X-ray Study of Tilting Phenomenon in ZnSe/Ge and ZnSe/GaAs Epilayers

As was reported previously [1, 2], tilting between (400) planes of ZnSe epilayers and Ge and GaAs substrates was observed. Because the magnitude of the tilt in the ZnSe/Ge system was much larger than in the ZnSe/GaAs system, the behavior of the tilt was studied more extensively in the former. It was found that the tilting phenomenon depends strongly on the crystallographic orientation of the substrate surface, as well as on the thickness of the epilayer.

### 2.1.2.1 ZnSe Layers on (100) Ge Substrates

Figure 2-1 shows the tilt dependence on layer thickness for films grown on Ge substrates with surfaces cut to a nominal  $2^\circ$  off (100) towards the (110) direction. As can be seen, all data points fall along two lines. One is where the tilt decreases with the thickness of the epilayer (Region I of Figure 2-1). The other is where the tilt increases with film thickness (Region II of Figure 2-1). Tilts for films grown on substrates cut  $0.5^\circ$  and  $4^\circ$  off (100) towards (110) exhibited a similar dependence on the thickness of the layer. Tilt angles were, in general, smaller for the  $0.5^\circ$  cut-off substrates and larger for the  $4^\circ$  cut-off substrates as compared to the  $2^\circ$  cut-off substrates. Figure 2-2 illustrates that tilt dependence on the cut-off angle of the substrate for two sets of samples grown to 1.2 - 1.5  $\mu\text{m}$  and 4.0 - 4.5  $\mu\text{m}$  ranges. As can be seen from the figure, for thin epilayers the tilt angle decreases monotonically with the cut-off angle. For thick films it goes through a minimum at around  $1.5^\circ$ .

Figure 2-3 represents the dependence of the linewidth (FWHM) of the epilayer peak on the layer thickness. It is seen to decrease monotonically with layer thickness. However note that for the 8.5  $\mu\text{m}$  thick sample, there is an apparent slight increase. The bars on the values of FWHM in Figure 2-3 are not error bars. Instead, they represent the range of FWHM values as measured upon rotation of the sample through  $360^\circ$  about an axis normal to the sample surface. This effect is due to absorption in the layer and results in changes in the integrated intensity of the signal from the epilayer upon rotation.

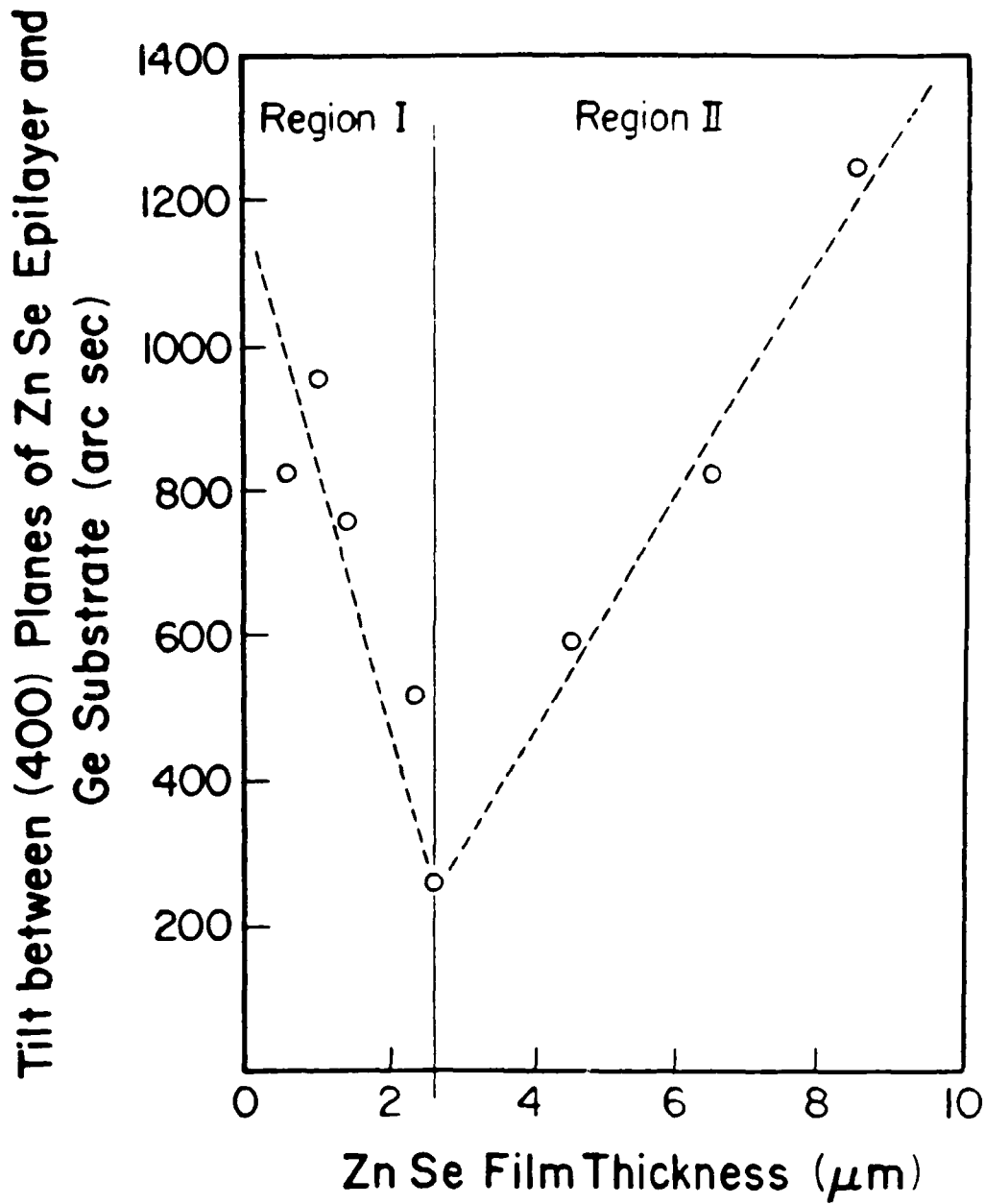


Figure 2-1. Tilt angle between (400) planes of the epilayer and the substrate versus epilayer thickness. The cut-off angle of the Ge substrate is  $2^\circ \pm 0.5^\circ$ .

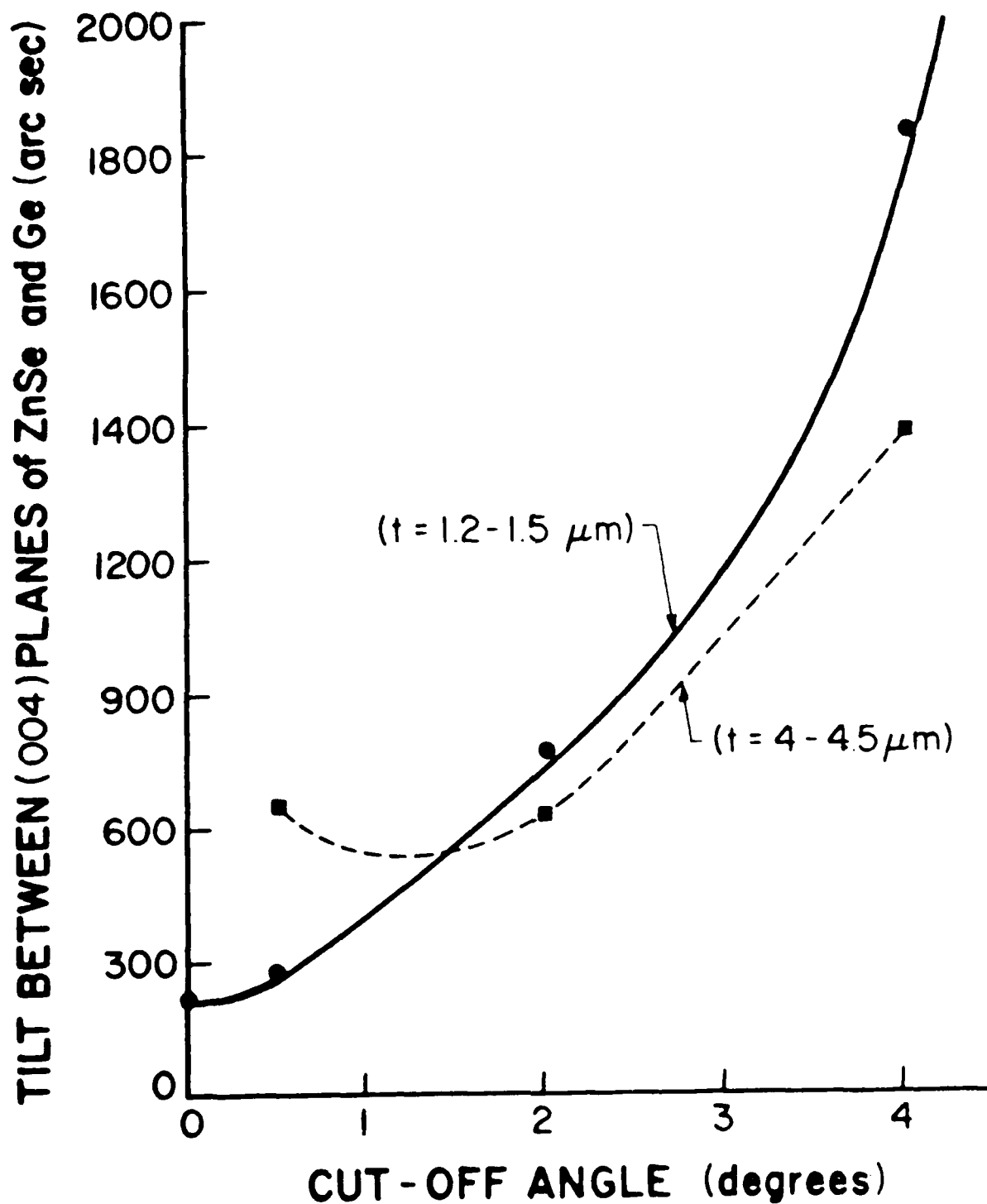


Figure 2-2. Tilt angle between (400) planes of the epilayer and the substrate versus the cut-off angle of the Ge substrate. The lines connecting the data points in this and the following figures are drawn for eye convenience only.

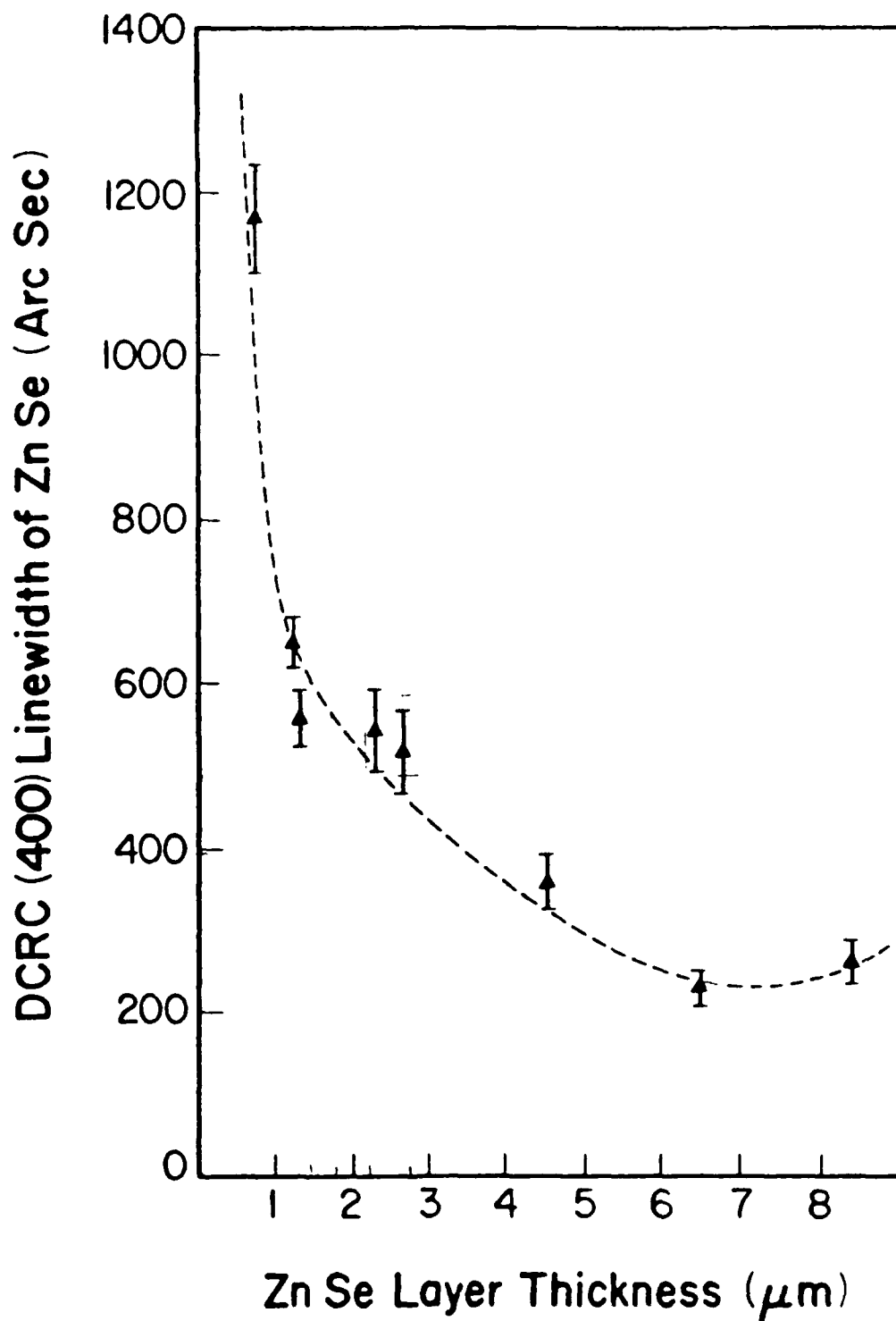


Figure 2-3. Linewidth of the (400) DCRC X-ray peak in ZnSe films versus epilayer thickness.

As can be seen from Figures 2-1 and 2-3, while the DCRC linewidth of the epilayers decreases monotonically with layer thickness, the tilt angle is observed to decrease with increasing thickness up to 2.5 - 3.0  $\mu\text{m}$  and then to increase for layers thicker than these values. From an examination of Figures 2-1 and 2-2, it is also evident that tilting depends strongly on the value of the cut-off angle (Figure 2-2) and on thickness (Figure 2-1). It is suggested here that the latter dependence is related to the stresses that develop in the layers during growth and subsequent cooling.

It should be noted that our results of tilt versus the cut-off angle for thick layers (Figure 2-2) is in accord with observations made on 5 - 10  $\mu\text{m}$  thick layers of  $\text{Ga}_x\text{In}_{1-x}\text{As}$  deposited by chemical vapor deposition onto GaAs. It was shown [2] that the tilt angle between the (100) planes of the epilayer and the substrate goes through zero as the inclination of the substrate surface from (100) was increased (the  $1^\circ$  cut-off angle being the optimum for parallel epitaxy). Because of the fact that there is an optimum cut-off angle for, at least, thick layers as our data and others [3] indicate, it would be interesting to check other properties of the layer versus the cut-off angle. Figure 2-4 shows the linewidth of the DCRC (400) peak of ZnSe as a function of the cut-off angle, as measured for thin and thick layers.

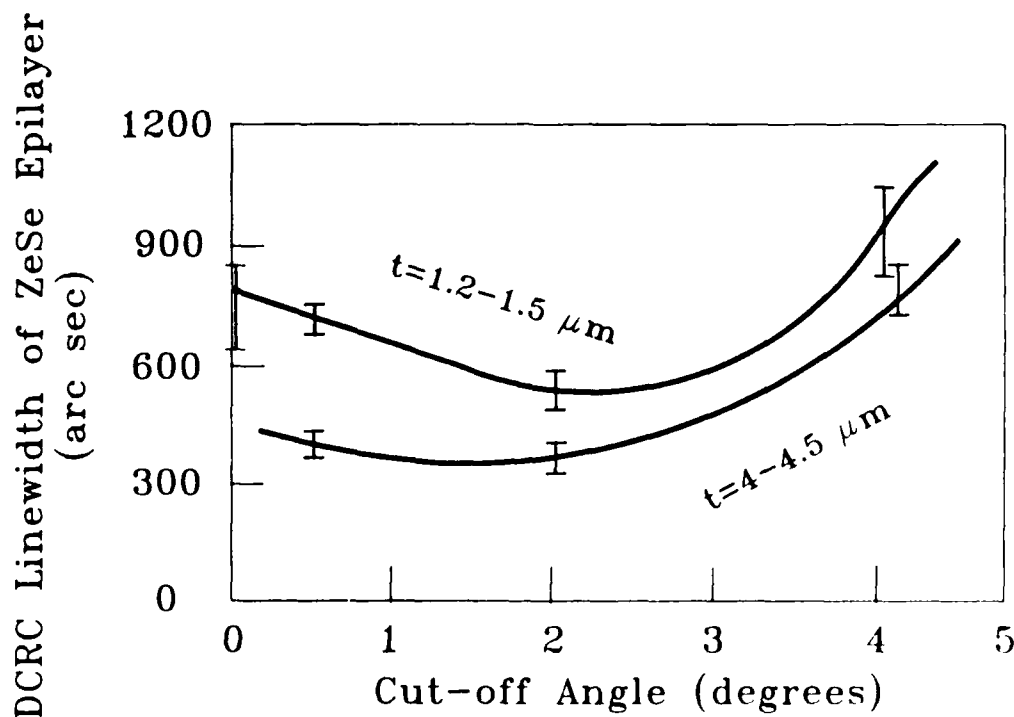


Figure 2-4. Linewidth of the (400) DCRC peak of ZnSe films versus the cut-off angle of the Ge substrate.

Similarly, Figure 2-5 shows the relation between the donor-bound exciton (DBE) emission linewidth, as measured by PL at 4.2K as a function of the cut-off angle of the substrate surface for thin and thick layers. As can be seen from Figures 2-4 and 2-5, the ZnSe layers indeed exhibit superior behavior around a certain ( $1.5^\circ - 2^\circ$ ) cut-off angle for the substrate surface.

In an attempt to explain the formation of tilt, we propose a simple atomic model of the interface between the epilayer and the substrate. In our model, the relocation of the atoms in the interface region around the steps present on the surface is the main factor that triggers the formation of the tilt.

Let us consider the atomic model of a Ge surface. It is cut at an arbitrary angle,  $\gamma$ , off the (100) plane towards the (110) direction onto which a few monolayers of ZnSe were deposited as shown in Figure 2-6. In constructing the model, we followed the assumptions and rules listed below:

- (i) steps introduced as a result of the cut-off procedure were assumed to have an average height of  $a_s/2$ , where  $a_s$  is the Ge lattice constant, and an average terrace length,  $L$ ,
- (ii) atoms that comprise the first monolayer of ZnSe on the Ge surface are attached to every available Ge dangling bond and are Se atoms, and
- (iii) the second monolayer of atoms to arrive will be Zn and these will attach themselves to all newly available Se free-bonds, etc.

Figure 2-6 illustrates the region around a step on the Ge surface after five monolayers of ZnSe were deposited following the rules given above. As can be seen from Figure 2-6, the ZnSe layer grows free of anti-phase domains, a result that is expected for a step of height  $a_s/2$  [4]. In addition, a distorted area propagating in the (111) direction (marked by two broken lines in Figure 2-6) is seen to develop around the step. The width of this distorted region, as it follows from the model, will depend on the height of the step becoming wider for larger steps.

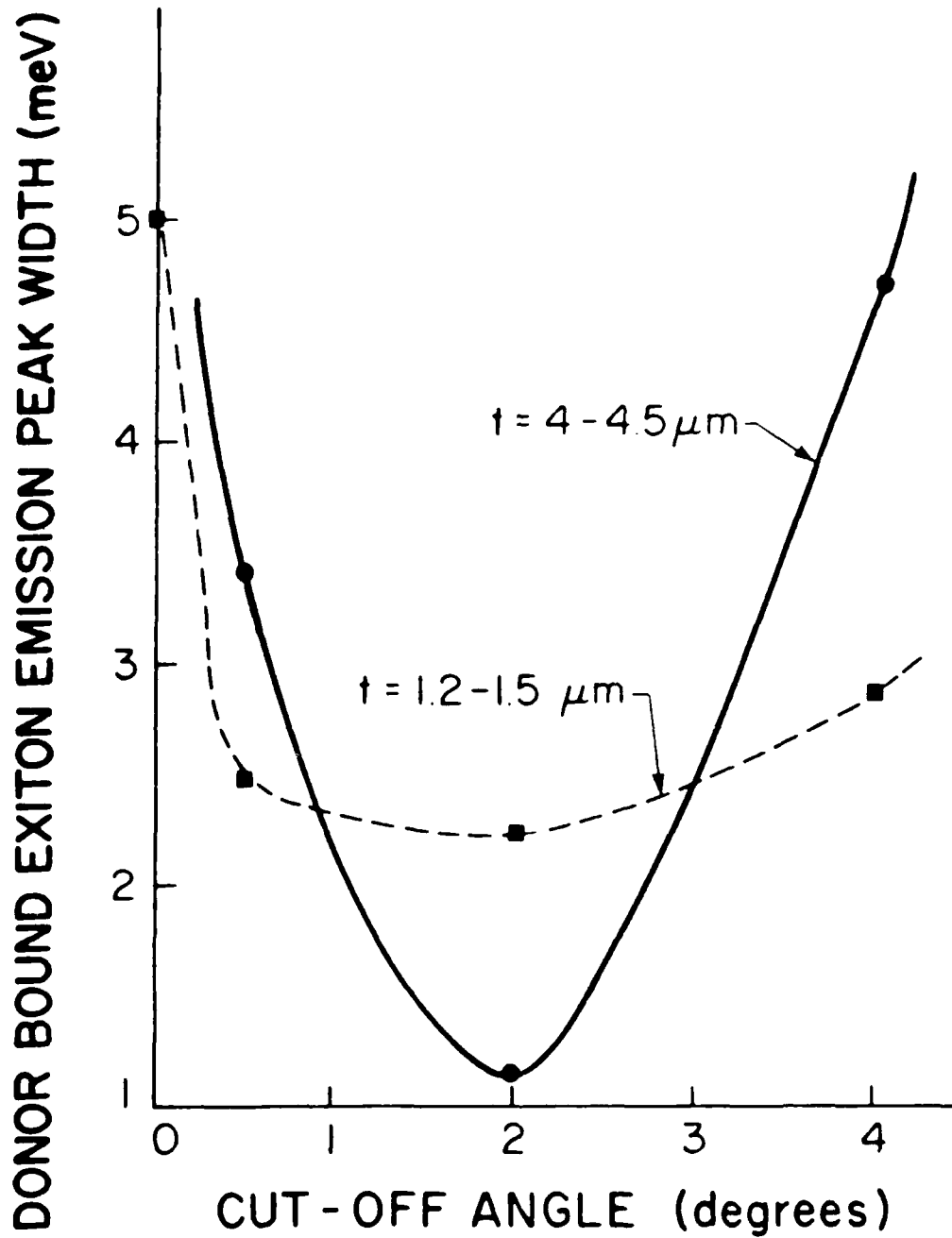


Figure 2-5. Linewidth of the donor-bound exciton line in PL versus the cut-off angle of the Ge substrate.

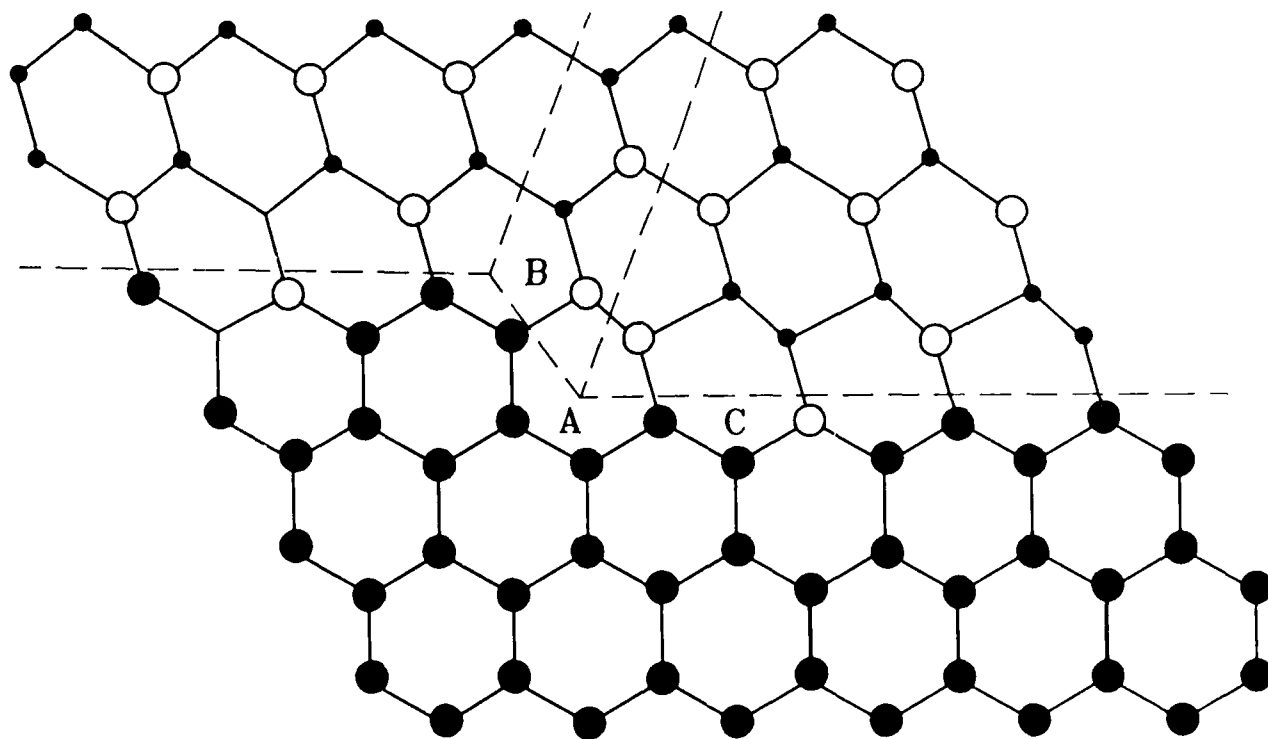


Figure 2-6. Atomic model of the ZnSe/(100)GaAs interface cut off toward the (110) direction showing the details near a step on the Ge surface. The links between the atoms in the epilayer are drawn with an exaggerated tilt. Large black circles represent Ge atoms, small black circles Zn atoms, and open circles Se atoms.

The bond lengths between the atoms in the few hexagons around the step (Figure 2-6) will be different from the rest of the bonds in the epilayer. It is clear from Figure 2-6 that the bonds comprising hexagons A, B, and C are formed between different types of atoms; that is Ge-Se Ge-Ge, and Se-Se, as opposed to the rest of the ZnSe lattice which consists of Zn-Se bonds only (excluding the distorted areas round the steps). Table 2-2 shows data on tetrahedral covalent radii of some elements of interest. As can be seen from the table, following the rules of bond length determination [5], the Ge-Se and Se-Se bonds are indeed shorter than the Ge-Ge and Zn-Se bonds, thus distorting hexagons A, B, and C as illustrated in Figure 2-6(b). As a result of this distortion, the atoms that comprise the first few monolayers of the film will be displaced from their ideal bulk positions. It is clear that the atoms closest to the step will be affected the most with the displacement distances becoming shorter away from the step. In this way a "tilt" angle between the plane formed from first or second monolayer atoms and the equivalent plane in the substrate is introduced. The steps on the substrate surface, therefore, act as initiators of the tilting in the epilayer planes. Because the rest of the growing epilayer comprises only the Zn-Se bonds, the tilt formed in the interface region around the steps will be replicated in the rest of the lattice.

**TABLE 2-2. Tetrahedral Covalent Radii of Some Elements of Interest According to Pauling [6].**

Element	Zn	Ga	Ge	As	Se
Radius (Å)	1.31	1.26	1.22	1.18	1.14

It should be noted here that the distorted area shown by two broken lines in Figure 2-6 will grow into the layer. Because it is formed from Se-Se and Zn-Zn bonds that are shorter in the former case and longer in the latter than the Zn-Se bond, it will help to maintain the tilt angle throughout the thickness of the layer. The mechanism proposed above may be visualized as a rotation of the epilayer lattice around the steps present on the surface of the substrate.

The tilting may be described by the simple model shown in Figure 2-7 where  $\gamma$  is the cut-off angle of the substrate surface,  $\Delta a_t$  is the effective lattice distortion at the step edge,  $L$  is the terrace length and  $\phi$  is the tilt. The lattice distortion is therefore given by:

$$\Delta a_t = L \tan \Delta \phi$$

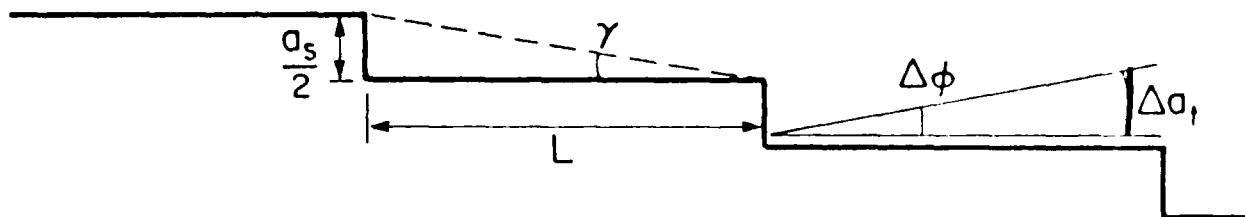


**Figure 2-7.** Schematic model of the (100) Ge substrate cut towards the (100) direction.  $\gamma$  is the cut-off angle,  $a_s$  is the Ge lattice constant,  $L$  is the average terrace length,  $\Delta a_t$  is the effective lattice distortion at the step edge, and  $\Delta\phi$  is the epilayer tilt.

It is interesting to note here that using this model and the empirical data of  $\Delta\phi(\gamma)$  obtained from Figure 2-2, a dependence between lattice distortion,  $\Delta a_t$ , and the substrate surface cut-off angle,  $\gamma$ , was found as shown in Figure 2-8. As can be seen from Figures 2-4, 2-5, and 2-8, the narrowest DCRC and DBE linewidths occur in the range of cut-off angle where the total distortion goes through a minimum. The interpretation of this finding is not quite clear at present. However, the fact that the best optical and structural properties (as determined by PL and DCXD measurements in this study) occur in the layers with minimum lattice distortion may be of significant importance.

#### 2.1.2.2 ZnSe/(100) Ge with a Ge Buffer Layer

Because the surface of the substrate is so important in achieving good epitaxy, a study was conducted where Ge buffer layers of different thicknesses were deposited prior to ZnSe deposition. The behavior of the tilt and FWHM of the ZnSe signal as a function of the buffer layer thickness was analyzed. Because the thickness of the ZnSe layers was not kept constant, a correction factor was used to eliminate the effect of thickness variation. Figure 2-9 shows the difference between the tilt of the (400) planes of ZnSe and Ge for samples grown with and without the Ge buffer as indicated by the crosses. In addition, the differences between the FWHM values of ZnSe layers grown with and without the buffer layer are shown by the full dots.

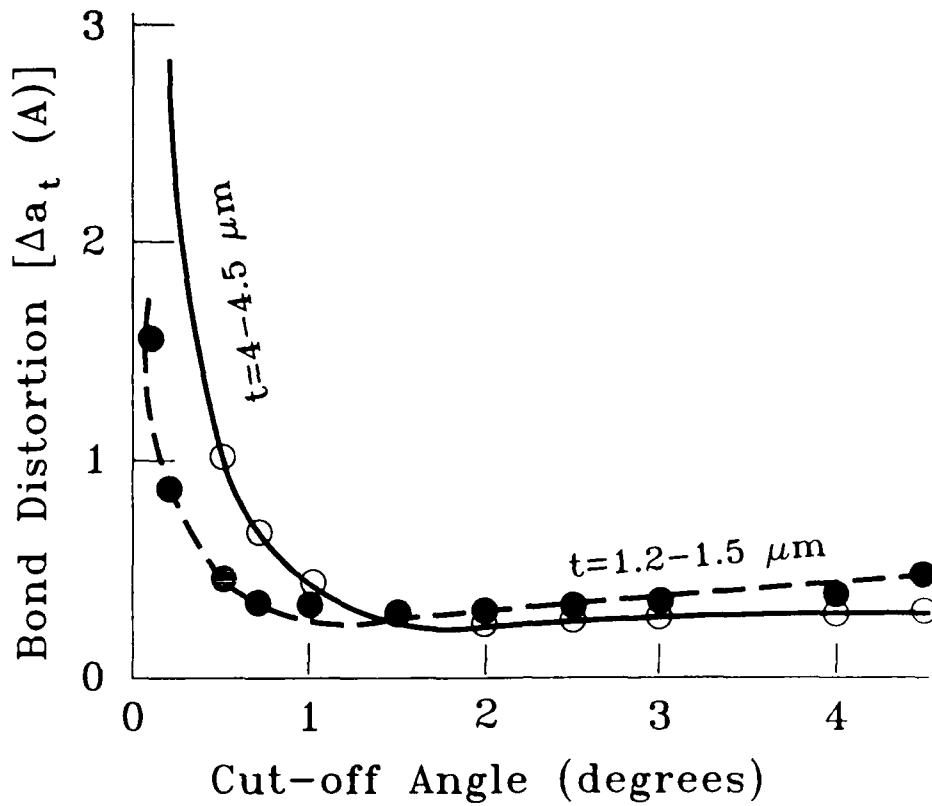


Figure 2-8. Bond distortion at the Ge step edge versus cut-off angle of the Ge substrate.

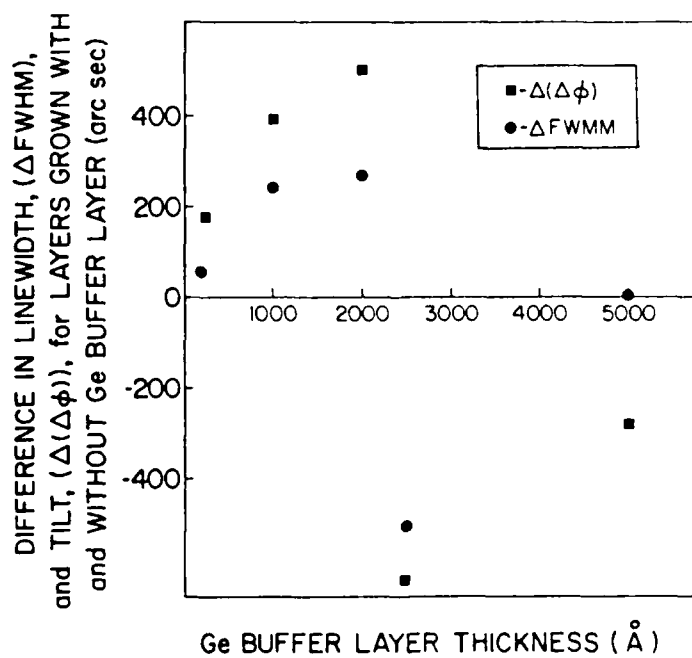


Figure 2-9. Squares: difference between the tilt of the (400) planes of Ge and ZnSe for samples grown with and without Ge buffer layers. Circles: difference between the DCRC FWHM values of ZnSe layers grown with and without Ge buffer layers.

As can be seen, in general the tilt angles and the FWHM linewidth of ZnSe layers are smaller for layers grown with Ge buffer layers to a thickness of around 0.3 - 0.4  $\mu\text{m}$ . However, for ZnSe layers grown on a 0.5  $\mu\text{m}$  Ge buffer, the value of the tilt angle is much larger than for a layer grown without a buffer. Yet the FWHM is only marginally increased. This result indicates that the tilt does not introduce any significant additional structural imperfections into the layer.

A conventional transmission electron microscopy (CTEM) study of the ZnSe epilayers grown with and without a buffer layer on Ge was also conducted both in cross-sectional and planar modes. As was established earlier, the ZnSe epilayers grown in (100) Ge without a buffer layer possessed a cell structure with dislocations lying in the boundaries of the cells. The exact nature of the cell structure is not clear at the moment. They could be anti-phase domains or represent grains with low-angle boundaries. A similar study of ZnSe epilayers grown on (100) Ge substrates with buffer layers revealed that the cell structure is not present. The only defects that were visible were dislocations scattered throughout the film. Figure 2-10 shows two planar views of ZnSe epilayer grown of (100) Ge substrate without [Figure 2-10(a)] and with [Figure 2-10(b)] a Ge buffer layer. As can be seen from Figure 2-10, the cell structure that is obvious in the ZnSe/(100) Ge system is absent in the ZnSe/Ge/(100) Ge system. The cross-sectional CTEM analysis revealed that the buffer layers of high quality, as can be seen in Figure 2-11.

Finally, it should be noted that 4.2K PL measurements of ZnSe on (100) Ge with and without a Ge buffer show that, in general, the DBE linewidths are significantly smaller for the latter case. For example, 2  $\mu\text{m}$  thick ZnSe layers grown on 0.6  $\mu\text{m}$  Ge buffers exhibit DBE linewidths of around 0.8 meV, whereas the narrowest linewidth with direct growth onto (100) Ge is around 1.2 meV. The 0.8 meV linewidth is comparable with the best ZnSe/(100) GaAs layers grown in this laboratory for which the linewidths were  $\sim$  0.65 meV.



Figure 2-10. Planar view of ZnSe epilayers grown on (100) Ge substrate. (a) shows that heavily dislocated cellular structure for direct growth on the (100) Ge substrate, and (b) shows that better quality ZnSe is grown when an intermediary Ge buffer layer is first deposited.

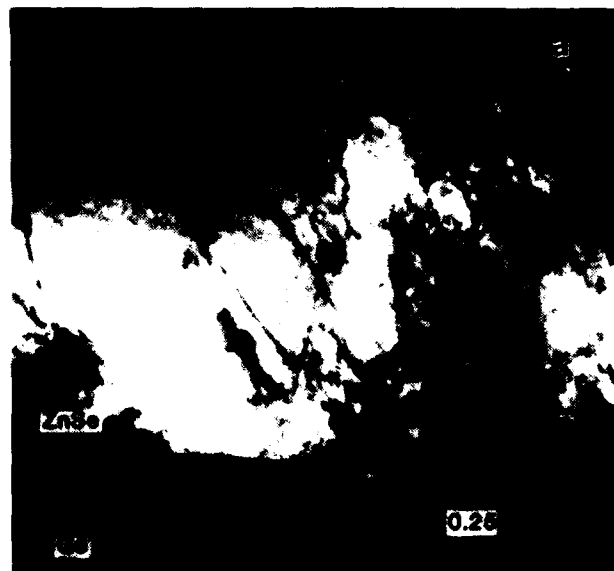


Figure 2-11. Cross-sectional transmission electron micrographs of ZnSe on (100) Ge (a) without a Ge buffer, and (b) with a Ge buffer reveals a ZnSe layer of higher quality is obtained with the presence of the Ge buffer.

## 2.2 Project 1, Task 2: Materials Research - p-ZnSe

### 2.2.1 Li-Doped ZnSe on GaAs

#### 2.2.1.1 Li-doping Source #2

In the previous Li doping study, the purity of the dopant source was our major concern. In order to understand what problems might arise when using this less pure source, a new Li source (described elsewhere and referred to hereafter as Li source #2) was used. Eight ZnSe samples doped with Li from Li source #2 were grown on (100) GaAs under various conditions. The control of Li doping level in the films was achieved by monitoring the Li signal level of the quadrupole mass analyzer (QMA) prior to the growth. The growth conditions of these runs are summarized in Table 2-3.

TABLE 2-3. Summary of Growth Conditions and Incorporated Li Concentrations (measured by SIMS) for Samples Grown Using Li Source #2.

Sample	T <sub>g</sub>	BPR	Li Flux (rel. units)	[Li] (SIMS)	
ZSE120	350	1/2:1	-	5.9 x 10 <sup>15</sup>	check run
ZSE121	350	1/2:1	3	4.6 x 10 <sup>17</sup>	
ZSE122	350	1/2:1	30	3.2 x 10 <sup>18</sup>	
ZSE123	350	1:1	3	1.1 x 10 <sup>17</sup>	
ZSE124	350	1:1	300	1.8 x 10 <sup>19</sup>	
ZSE125	350	1.5:1	2	6.4 x 10 <sup>16</sup>	
ZSE126	350	1.5:0.7	2	4.4 x 10 <sup>16</sup>	
ZSE129	350	1:1	3	6.8 x 10 <sup>16</sup>	
ZSE130	350	1:1	6	7.9 x 10 <sup>17</sup>	modulation doping

SIMS analysis of the most heavily Li-doped sample indicated that the major contaminants in the source were Mn, Mg, Cr, Na, and K. Their influence on the properties of the ZnSe films is unclear, although several of these elements might be expected to give rise to deep levels. Sample ZSE130A was grown with a Li-doped layer sandwiched between two undoped ZnSe layers in order to study the Li diffusion rate in ZnSe. These results will be discussed in Section 2.2.3.

The photoluminescence spectra of samples produced using Li source #2 appear very similar to those made with source #1. Figures 2-12 and 2-13 compare the PL spectra for samples grown using source #1 (top figure) and source #2 (bottom figure); samples were selected for this comparison based on the similarity of their Li concentrations.

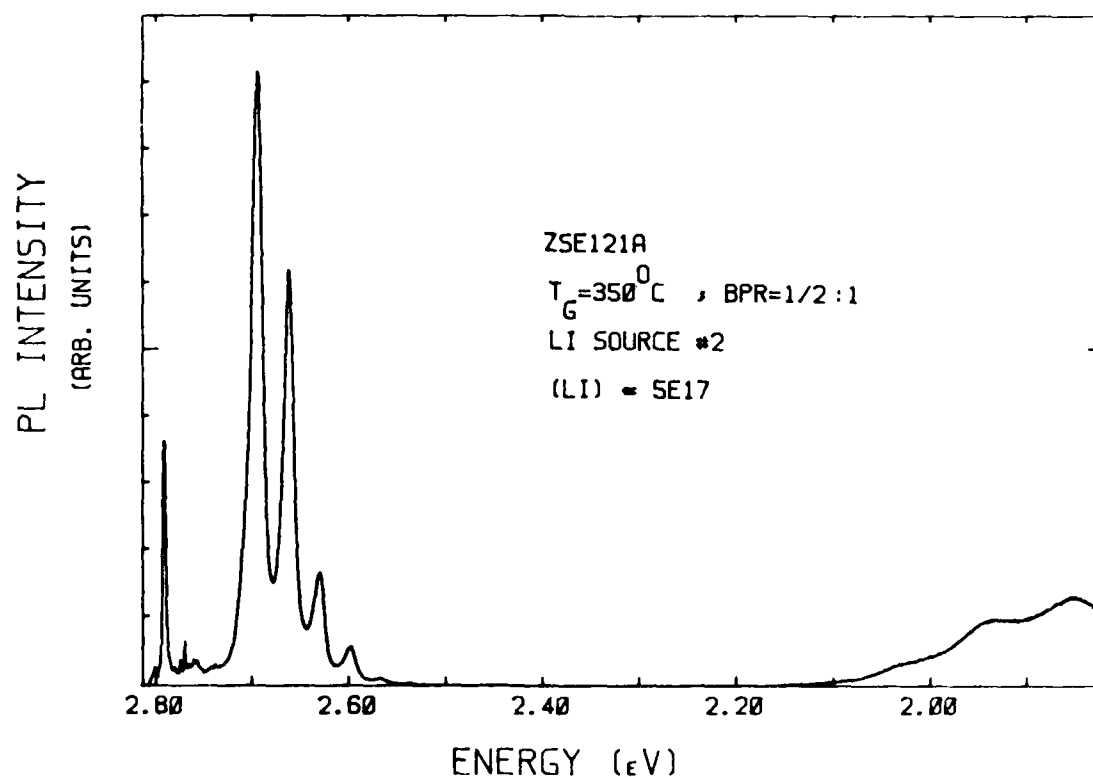
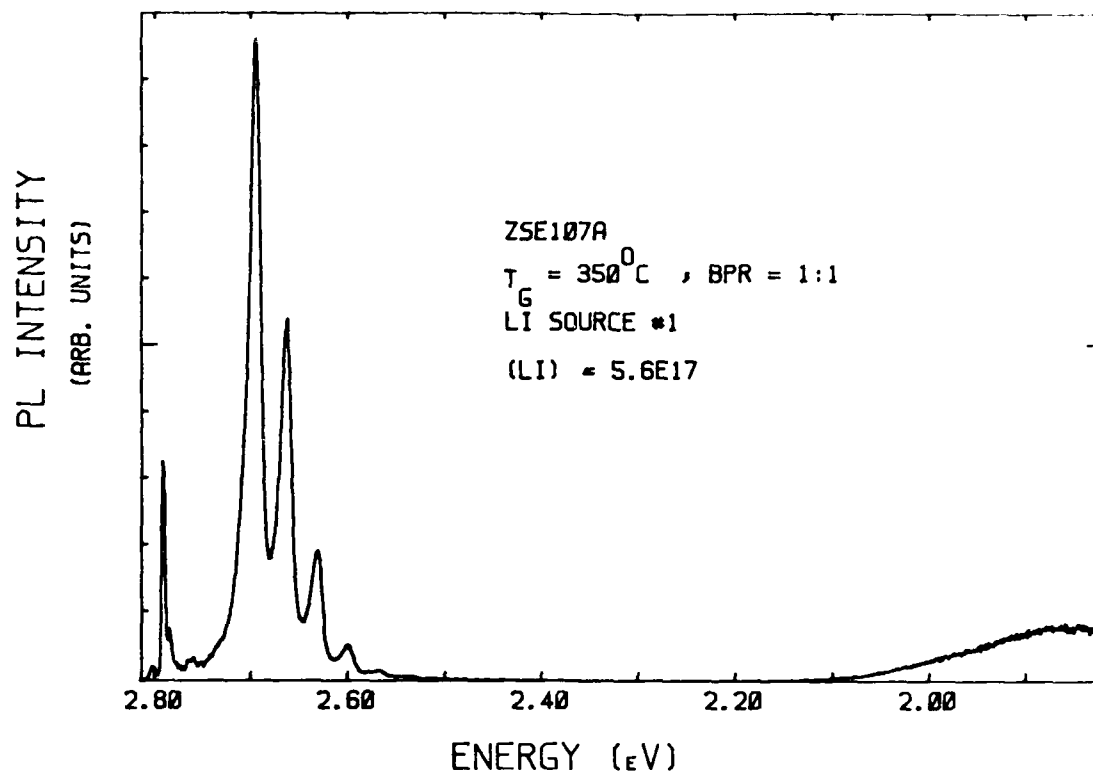


Figure 2-12. PL spectra of two samples with similar Li concentrations (approximately  $5 \times 10^{17} \text{ cm}^{-3}$ ) grown using Li Source #1 (upper) and Li Source #2 (lower).

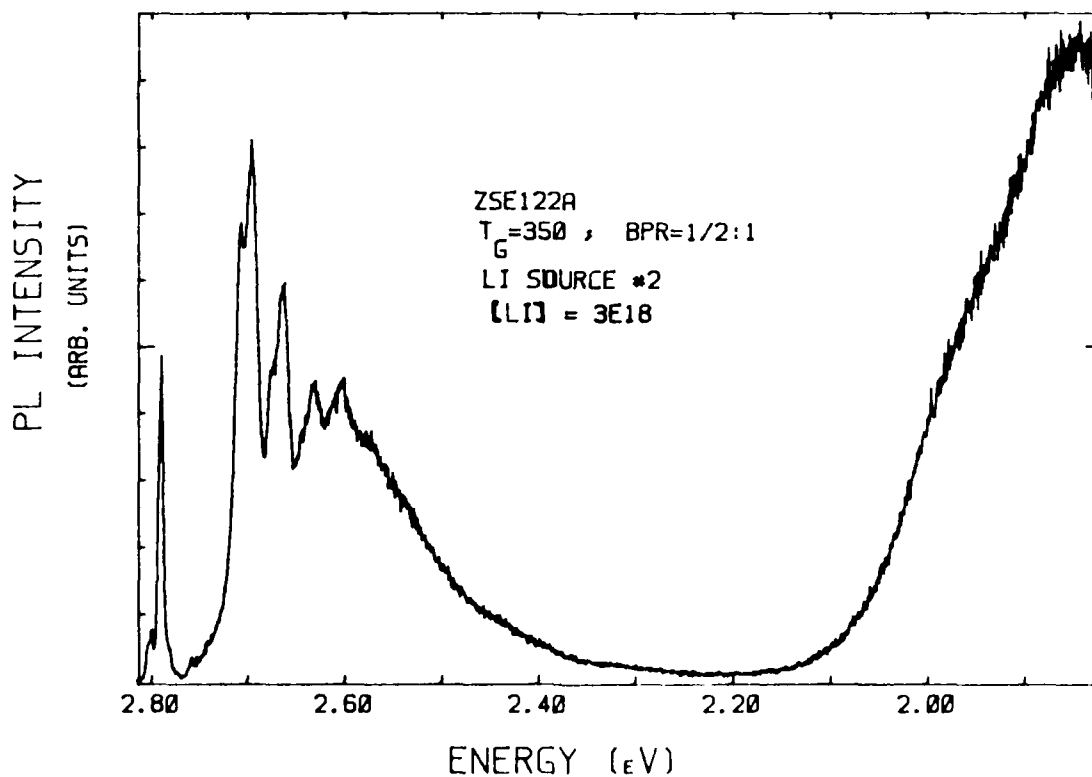
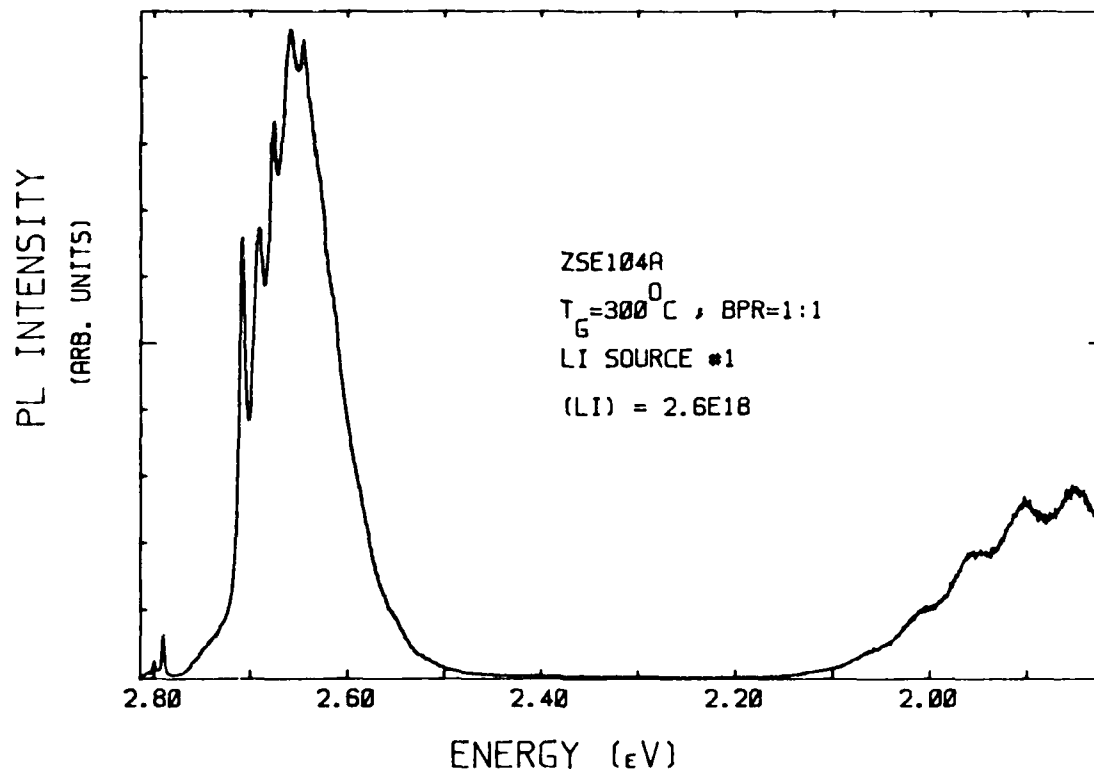


Figure 2-13. PL spectra of two samples with similar Li concentrations (approximately  $3 \times 10^{18} \text{ cm}^{-3}$ ) grown using Li Source #1 (upper) and Li Source #2 (lower).

Figure 2-12 shows that the similarity between samples ZSE107A and ZSE121A, both with Li concentrations of about  $5 \times 10^{17} \text{ cm}^{-3}$ , is most striking. The relative intensities of the free exciton, acceptor-bound exciton, donor-acceptor pair, and deep level emission peaks are nearly identical in the two samples. When the Li concentration rises to near  $3 \times 10^{18} \text{ cm}^{-3}$  (Figure 2-13), the major features are still qualitatively similar for the two samples. In particular, we see the emergence of a strong, broad emission at about 2.62 eV and a 1.9 eV deep level band in both samples. The evolution of these two peaks with increasing Li concentration is better seen in Figure 2-14 which shows the PL spectra for samples (grown using Li source #2) with Li concentrations of 0 (i.e., undoped),  $5 \times 10^{17} \text{ cm}^{-3}$  and  $3 \times 10^{18} \text{ cm}^{-3}$ .

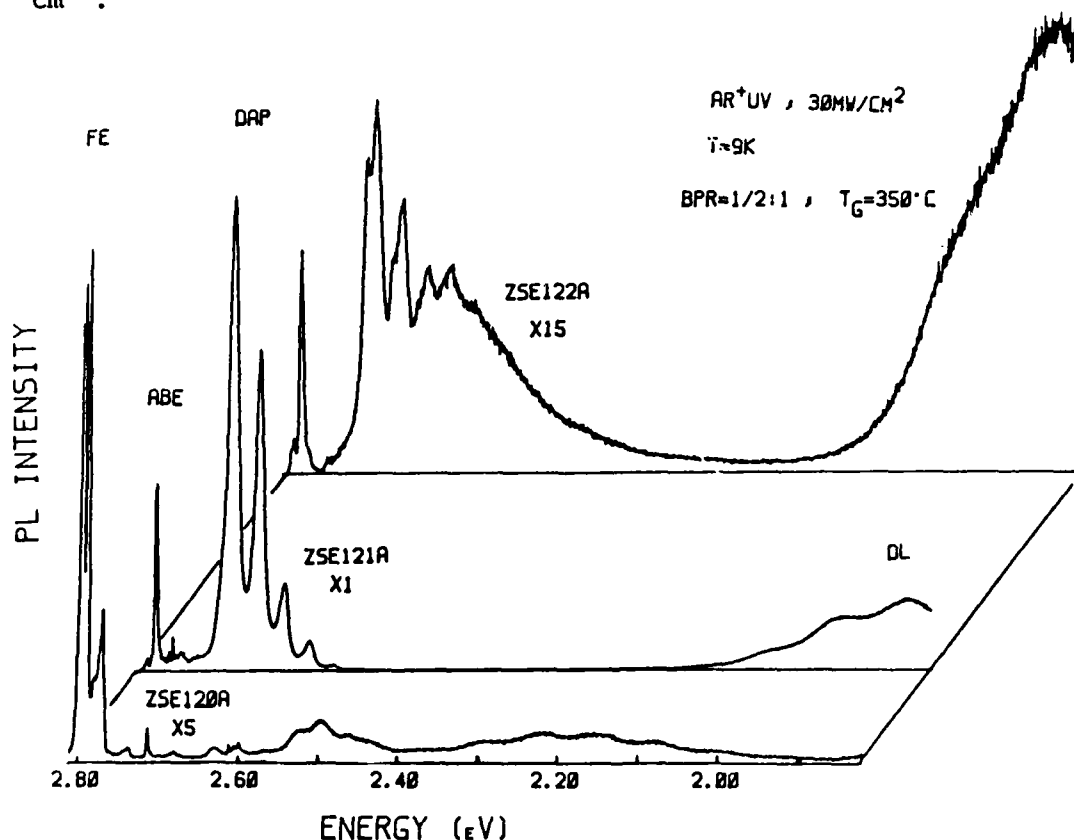


Figure 2-14. PL spectra of three samples grown using Li Source #2 with increasing amounts of Li. (Li) = 0 (i.e., undoped; lower curve),  $4.6 \times 10^{17} \text{ cm}^{-3}$  (middle curve, and  $3.2 \times 10^{18} \text{ cm}^{-3}$  (upper curve).

The similarity in PL spectra for samples grown from radically different Li sources would appear to rule out extrinsic impurities as the source of the two emission features highlighted above. Instead, these would appear to be features associated with some type of Li complex which forms at sufficiently high Li concentrations.

Two-point current versus voltage measurements similar to those described in Quarterly Technical Progress Report No. 5 were made on the samples doped with Li using source #2. Using this measurement technique, these Li-doped samples were found to be p-type with the exception of ZSE124A; the carrier type for ZSE124A could not be determined. The results for ZSE124A are not completely understood, but the absence of p-type conversion is likely to be related to the extreme doping of this sample ( $[Li] = 1.8 \times 10^{19} \text{ cm}^{-3}$ ). The hole densities estimated from the two-point I-V measurement for the remaining samples measurements were less than  $10^{15} \text{ cm}^{-3}$ . These values are comparable to those estimated in the samples doped using source #1. To date, the electrical measurements provided no clear distinction between the samples doped with Li using source #1 and those doped using source #2.

#### 2.2.1.2 SIMS Comparison of Lithium Sources

The severity of unintentional doping by impurities emanating from the dopant source was not known during our earliest Li-doping attempts. The free hole densities in samples doped with Li at levels greater than  $10^{17} \text{ cm}^{-3}$  were estimated to be less than  $10^{15} \text{ cm}^{-3}$  from 2-point I-V measurements. One possible explanation of the low measured carrier density is that extreme compensation occurs as a result of unintentional co-doping by impurities released from the dopant source. This possibility certainly must be addressed since strong compensation by impurities was observed in some of our earlier studies where  $\text{Na}_2\text{Se}$  was used as a source in Na-doping studies.

Alternative lithium sources of the highest available purity were obtained from two vendors. These sources are of the same composition as Li source #1 and they will be referred to as Li sources #3 and #4. The degree of contamination of the Li source materials was studied in two steps. In the first step, the three sources (#'s 1, 3, and 4) were analyzed using secondary ion mass spectrometry (SIMS). The second step involved the comparison of the optical and electrical properties of Li-doped ZnSe films grown under similar conditions with the exception of placing lithium source #3 in the dopant effusion cell rather than lithium source #1. The results of this latter comparison will be discussed in Section 2.2.1.3.

The SIMS analyses involved both positive and negative SIMS measurements. In positive SIMS (+ SIMS), positively charged ions were detected while sputtering with an  $O_2^+$  primary ion beam. The second measurement was carried out on each sample with the detection of negatively charged ions (- SIMS). The results of these two measurements are shown in Tables 2-4 and 2-5.

**TABLE 2-4. Results of +SIMS Analysis of Three Different Li Sources.**

<u>Impurity</u>	<u>Source #1</u>	<u>Source #3</u>	<u>Source #4</u>
Mg	2900	3800	1300
** Al	17000	2900	4000
Si	8700	3000	2000
Ca	19000	4700	930
Ti	100	--	--
Mn	130	--	110
Fe	6200	73	100
Ni	--	--	150
** Ga	--	--	13000
** In	--	230	17
Ta	--	--	25

The values listed here are given by  $(6.7 \times 10^3) \times [\text{ion count}/^6\text{Li}^+]$  where "ion count" is the number of counts of the indicated ion and  $^6\text{Li}^+$  is the number of counts obtained for  $^6\text{Li}^+$  ions. The elements indicated with \*\* are believed to act as shallow donor impurities ZnSe.

**TABLE 2-5. Results of -SIMS Analysis of Three Different Li Sources.**

<u>Impurity</u>	<u>Source #1</u>	<u>Source #3</u>	<u>Source #4</u>
** F	9000	1100	5500
Si	500	68	1600
** Cl	700	830	2200
Fe	13	--	12
Ni	5	--	--
Ge	5	--	35
Rb	20	--	7
Sn	8	--	--
** I	1	--	--

The values are given by  $(2.5 \times 10^4) \times [\text{ion count}/^7\text{Li}^-]$ . The elements indicated with \*\* are believed to act as shallow donors in ZnSe. The primary ion beam used on source #1 was  $\text{Cs}^+$  ions whereas an  $O^-$  beam was used as the primary beam on sources #3 and #4.

The results of the SIMS study described here are not fully quantitative in that yield factors have not been taken into account and calibration runs have not been completed. Comparison between rows of the tables, therefore, are meaningless and quantitative values for the impurity concentrations cannot be extracted. Comparison between columns, however, is meaningful as it does directly indicate the relative concentration of impurities present in the three sources. This is the case only because all correction factors for the three samples are identical. Upon examination of the two tables it is seen that none of the three sources is obviously "cleaner" than the other two. Source #1 has the largest concentration of Al and F, source #3 has the largest concentration of In, and source #4 has the largest concentration of Ga and Cl. Overall, source #3 appears to contain the lowest relative concentration of impurities and source #1 appears to contain the largest.

#### 2.2.1.3 Li-Doping Source #3

In our second attempt at p-type conversion, using Li source #2, no significant improvement in either optical or electrical properties could be found as compared with the results obtained when lower purity Li source #1 was used. Significant amounts of Mn were detected with SIMS in the films grown using source #2 and its concentration varied as the temperature of Li source was changed. In addition, modulation of contaminant Mn concentration was observed in a sample (ZSE130) in which modulation doping of Li was attempted. This was done in order to study a potential problem of high diffusivity of Li in ZnSe. These findings indicate that Mn originates from Li source #2 and its presence in the films makes the analysis of those samples more complicated. Therefore, a Li source with still higher purity is desired for the p-type conversion study.

A new Li source (#3) was purchased and was used as the p-type dopant. Purity analysis by SIMS (see Section 2.2.1.2) indicated that this material has fewer impurities than Li source #1 used previously. The results of this SIMS comparison of different Li sources are described in Section 2.2.1.2. A prebaked new PBN crucible was used for the new Li source and the loaded oven was then outgassed thoroughly in the II-VI chamber. Twenty-five ZnSe specimens were grown after the material recharge. Their growth conditions are summarized in Table 2-6 as follows:

TABLE 2-6. Summary of Growth Conditions and Incorporated Li Concentrations for All Samples Grown Using Li Source #3. The Li flux is given in the same arbitrary units used in Quarterly Technical Progress Report No. 5.

Sample	TG	BPR	Li Flux (rel. units)	[Li] (SIMS)	
ZSE131	350	1/2:1	---	$5.0 \times 10^{14}$	check run
ZSE132	350	1:1	3	$1.6 \times 10^{17}$	
ZSE133	350	1:1	3	$1.5 \times 10^{17}$	undoped buff. layer
ZSE134	350	1/2:1	3	$1.1 \times 10^{17}$	undoped buff. layer
ZSE135	350	1/2:1	3	$9.8 \times 10^{16}$	
ZSE136	350	1/4:1	3	$7.7 \times 10^{16}$	undoped buff. layer
ZSE137	350	1/4:1	3	$5.2 \times 10^{16}$	
ZSE138	350	1:1	30	$1.4 \times 10^{17}$	modulation doping
ZSE139	350	1:1	---	$9.4 \times 10^{14}$	
ZSE140	350	1:1	3	$1.6 \times 10^{17}$	
ZSE141	375	1:1	30	$1.0 \times 10^{18}$	
ZSE142	350	1:1	3	$1.2 \times 10^{17}$	
ZSE143	350	1:1	---	-----	thin film
ZSE144	300	1:1	3	$1.4 \times 10^{17}$	
ZSE145	260	1:1	---	$< 2.0 \times 10^{15}$	
ZSE146	260	1:1	3	$3.8 \times 10^{17}$	
ZSE147	350	1:1	60	$6.7 \times 10^{18}$	
ZSE148	250	1:1	60	$4.9 \times 10^{19}$	
ZSE149	350	1:1	3	$6.0 \times 10^{16}$	in-situ met.
Source reloading					
ZSE150	350	1/2:1	---	---	check run
ZSE151	350	1/2:1	1.5	$3.1 \times 10^{16}$	in-situ met.
ZSE152	300	1/4:1	3	$6.9 \times 10^{16}$	
ZSE153	250	1/4:1	3	$1.5 \times 10^{17}$	
ZSE154	375	1:1	3	$1.1 \times 10^{17}$	
ZSE155	350	1/2:1	3	mod. ( $2.7 \times 10^{16}$ )	

The Li concentrations in those samples grown at the same temperature decrease slightly as the Zn-to-Se BPR diminishes. The same trend was also found for samples from #ZSE132 to ZSE137 in their growth sequence despite the fact that the same effusion cell temperature was used. Sample ZSE140 was grown under the same conditions as ZSE132 in order to determine whether the observed variations in Li concentration were due to beam pressure ratio effects or to irreproducibility of the Li flux. The Li concentrations measured by SIMS are the same for both samples ZSE132 and ZSE142, indicating that the Li flux from this source is quite reproducible. We are left to conclude that the Zn/Se beam pressure ratio which did decrease over this series, does have some effect on the Li incorporation in ZnSe.

It was also found in this study that the growth temperature does affect the incorporation of Li in ZnSe. Under the same Li flux, the incorporation coefficient increases as the growth temperature decreases, which is exactly what we observed in the past with Na and P.

The Li concentration in sample ZSE151, grown after source reloading, is lower than those grown in the previous series by a factor of 3. The reduction in Li concentration has been observed previously after source reloading. It is speculated that a thin surface layer on the Li source was formed during the reloading despite the fact that the MBE chamber was backfilled with inert gas. This thin surface layer reduces the evaporation rate of the material. In the future, measurements made using the residual gas analyzer can be used to fine tune the flux before each growth run.

Samples ZSE152 and ZSE153 were grown under Se-stabilized conditions. Our previous experiences with Li-doping in this region of growth space had given indications that the optical and electrical properties of the films were beginning to deteriorate as we moved away from the Zn-stabilized region (see, e.g., our discussion of sample ZSE102 in Quarterly Technical Progress Report No. 5.) In contrast to these earlier results, we found that ZSE152 and ZSE153 had very good optical and electrical properties. Acceptor-bound exciton emission is the dominant feature in their low temperature PL spectra. They are much less resistive than other Li-doped films. The film (ZSE154) grown at higher temperature, on the other hand, has dominant DAP emission. This is what we observe for most Li-doped samples under Zn-stabilized growth conditions.

To test the effects of the Li source on film properties, several Li-doped samples which were grown under identical conditions using source #3 instead of source #1 are compared. The sample numbers, growth conditions, and Li concentrations of samples used during the comparison with the two Li sources are given in Table 2-7.

**TABLE 2-7. Results of SIMS, Electrical and PL Measurements for Samples Grown Using Li Sources #1 and #3. Samples ZSE106A, 101A and 103A were doped using Source #1. Samples ZSE132A, 144A and 152A were doped using Source #3. Along with the sample number and growth conditions are shown the magnitude of the current measured at 2.0 volts, the ratio of the intensity of the acceptor-bound exciton ( $I_1$ ) to the donor-acceptor pair intensity ( $I_{DAP}$ ), and the R-value.**

Sample	TG	BPR	Li ( $\times 10^{17} \text{ cm}^{-3}$ )	i (nA)	$I_1 / I_{DAP}$	R
ZSE106A	350	1:1	1.2	1.0	10.7	1160
ZSE132A	350	1:1	1.6	0.4	3.1	690
ZSE101A	300	1:1	1.2	6.6	1.2	84
ZSE144A	300	1:1	1.4	4.7	1.0	13
ZSE103A	300	1/4:1	0.7	8.3	2.6	2
ZSE152A	300	1/4:1	3.2	14.0	3.0	2400

There were no obvious differences in the photoluminescence spectra between samples produced using the new Li (source #3) and those grown using Li source #1. Figure 2-15 compares the PL emission spectra for sample ZSE106A, grown using Li source #1, with that of ZSE132A, grown using Li source #3. Apart from some slight differences in the relative intensities of the ABE and DAP peaks, there are no qualitative differences between these two spectra. In particular, ZSE132A exhibits no more or less emission from donor-bound excitons or deep levels which might indicate a change in the density of unintentionally-incorporated donors from impurities in the source material.

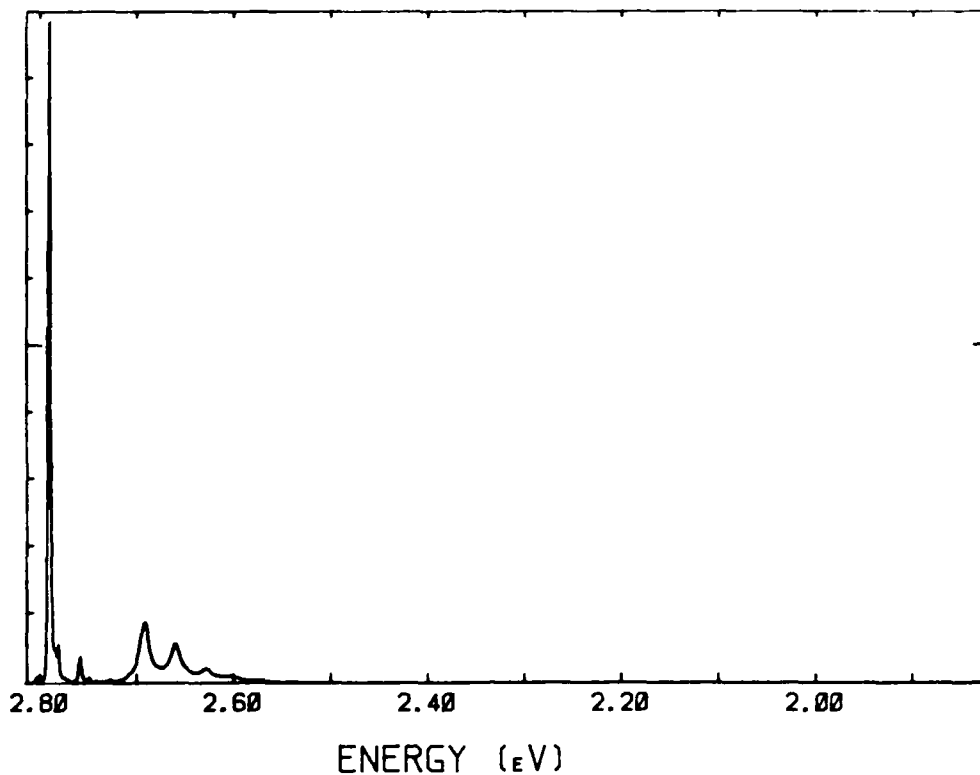
Contact studies showed all samples in Table 2-7 to be p-type. Column 5 of this table gives the current measured at 2.0 volts for the Au-to-Au 2-point contact configuration. No significant changes were observed in the electrical properties of the films when Li source #3 was substituted for Li source #1.

It would appear that either extrinsic donor-type contaminants in the Li starting materials are negligible, or that whatever donor-type impurities are affecting the electrical activity of the Li are common to both Li sources #1 and #3.

#### 2.2.1.4 Undoped ZnSe Buffer Layers

Although most of our epitaxial ZnSe films doped with Li show p-type conversion, high conductivity has not been achieved. Hole densities in all the Li-doped films have been estimated from two-point I-V measurements to be less than  $10^{15} \text{ cm}^{-3}$  even though doping densities exceeded  $10^{17} \text{ cm}^{-3}$ . One possible explanation for the apparent electrical inactivity of the Li is compensation by extrinsic impurities; this possibility is addressed elsewhere in this report. An alternative explanation of the inactivity of the Li involves dopant gettering by macroscopic structural defects. In such a case most of the dopant resides in the immediate vicinity of an extended defect rather than substitutionally in the bulk of the crystal. In this study an undoped ZnSe buffer layer was grown in an attempt to bury the interface prior to opening the Li shutter.

PL INTENSITY  
(ARB. UNITS)



PL INTENSITY  
(ARB. UNITS)

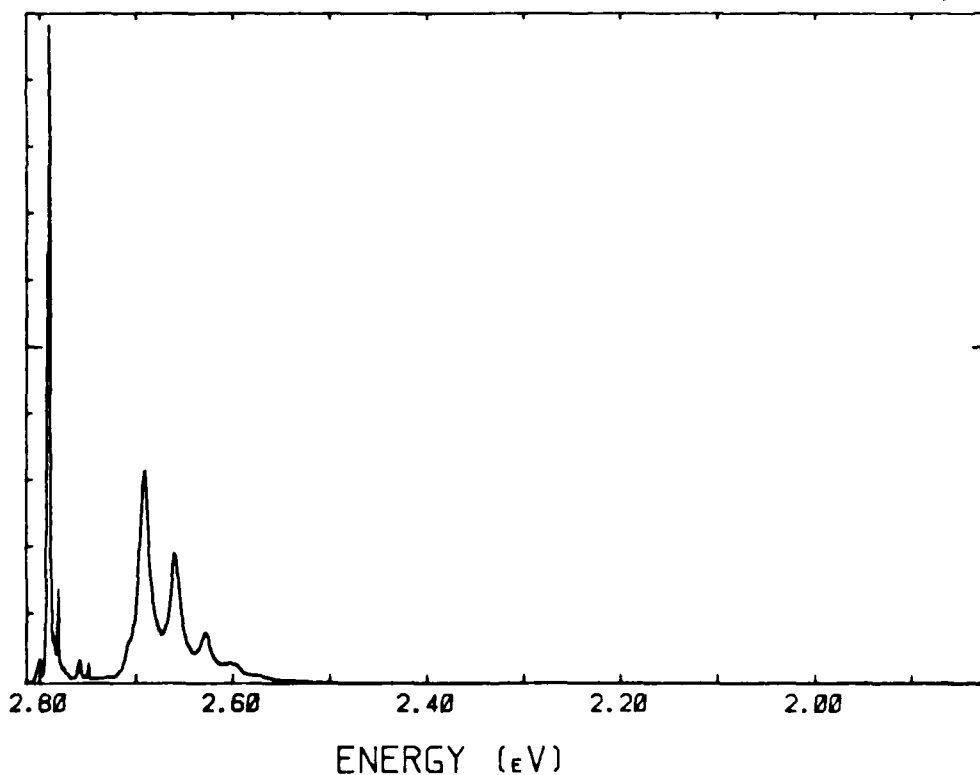


Figure 2-15. PL spectra of two samples with similar Li concentrations (approximately  $1.4 \times 10^{17} \text{ cm}^{-3}$ ), grown using Li Source #1 (upper; #ZSE106) and Li Source #3 (lower; #ZSE132).

Figures 2-16(a) and (b) show the SIMS depth profile of Li in two samples grown under otherwise identical conditions without and with a thick undoped ZnSe buffer layer. The Li concentration is very constant throughout the film for sample without a buffer layer, indicating the stability of the Li flux. The Li level in the sample with a buffer layer shows a constant doping region and a gradual decrease near the ZnSe/GaAs interface. The details of the gradual decrease in Li concentration will be discussed later.

Two-point I-V measurements using various contact configurations were made on the samples grown on top of ZnSe buffer layers. Conversion to p-type conductivity was confirmed in all samples grown in this manner, however high conductivity was still not achieved. The hole densities measured in films grown in this study were comparable to those found in samples grown under similar conditions without buffer layers. From the electrical studies no improvement was observed with the use of undoped ZnSe buffer layers.

In Figure 2-17 we compare the PL spectra for samples grown under identical conditions [same growth temperature (350°C), Zn/Se beam pressure ratio (1/2:1), and Li flux] and containing nearly the same Li concentrations ( $1 \times 10^{17} \text{ cm}^{-3}$ ) but in one case (ZSE134) with and in the other case (ZSE135) without a 1- $\mu\text{m}$  undoped ZnSe buffer layer. While the major features of these two spectra are qualitatively identical, there may be some modest improvement in the case of the sample grown with the buffer layer. Specifically, there is less emission at  $I_1^{\text{D}^{\text{e}^{\text{e}^{\text{p}}}}$  (2.783 eV) than is seen in the ZSE135 spectrum (this peak is frequently seen in samples of poor surface quality grown under conditions considerably removed from the optimal). We also see a considerable  $Y_0$  peak at 2.60 eV; this peak has been associated with the presence of impurities associated with structural defects in ZnSe [7]. Finally, the  $I_1$  and DAP peaks are somewhat narrower and better defined in ZSE134.

Similar results are seen in Figure 2-18 where an unbuffered (ZSE137) and a buffered (ZSE136) sample are compared. In both cases the growth conditions were  $T_g = 350^\circ\text{C}$ ,  $\text{BPR}=1/4:1$  and the Li concentrations were approximately  $6 \times 10^{16} \text{ cm}^{-3}$ . Again, we see a large defect-related  $Y_0$  peak in the case of the unbuffered sample. Note, however, that the ABE peak is more intense and the ABE/DAP peak intensity ratio larger for the unbuffered sample in this case.

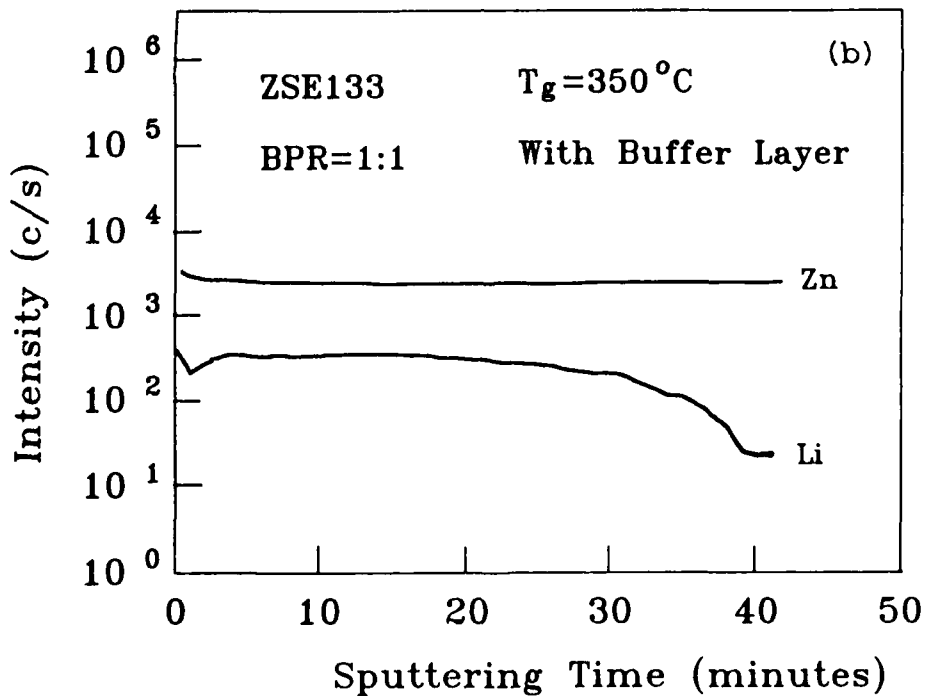
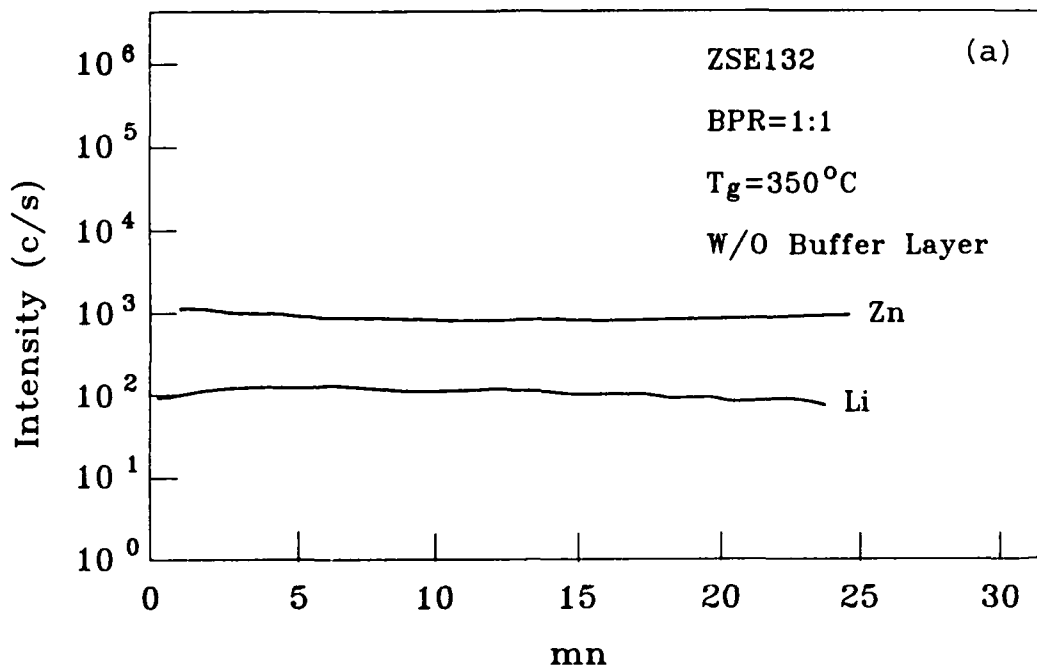


Figure 2-16. SIMS depth profiles of Li concentrations in samples grown (a) without and (b) with a  $1\ \mu\text{m}$  thick ZnSe buffer layer. The  $^{68}\text{Zn}$  signal is also shown as a reference.

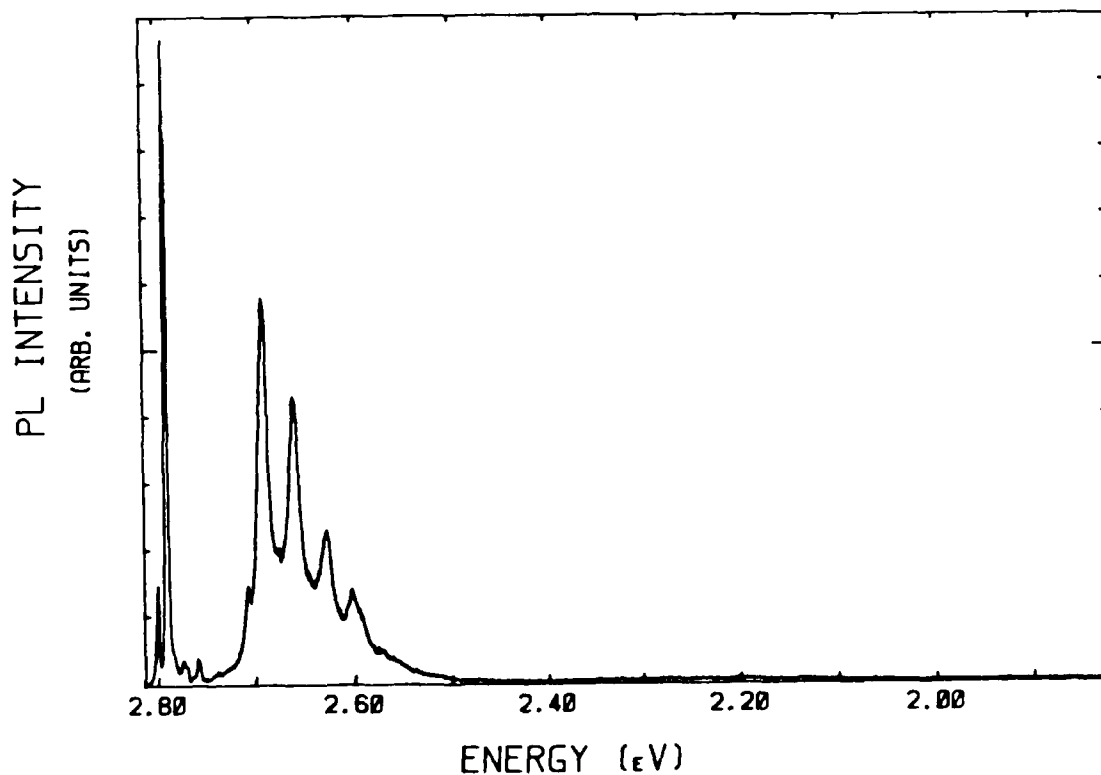
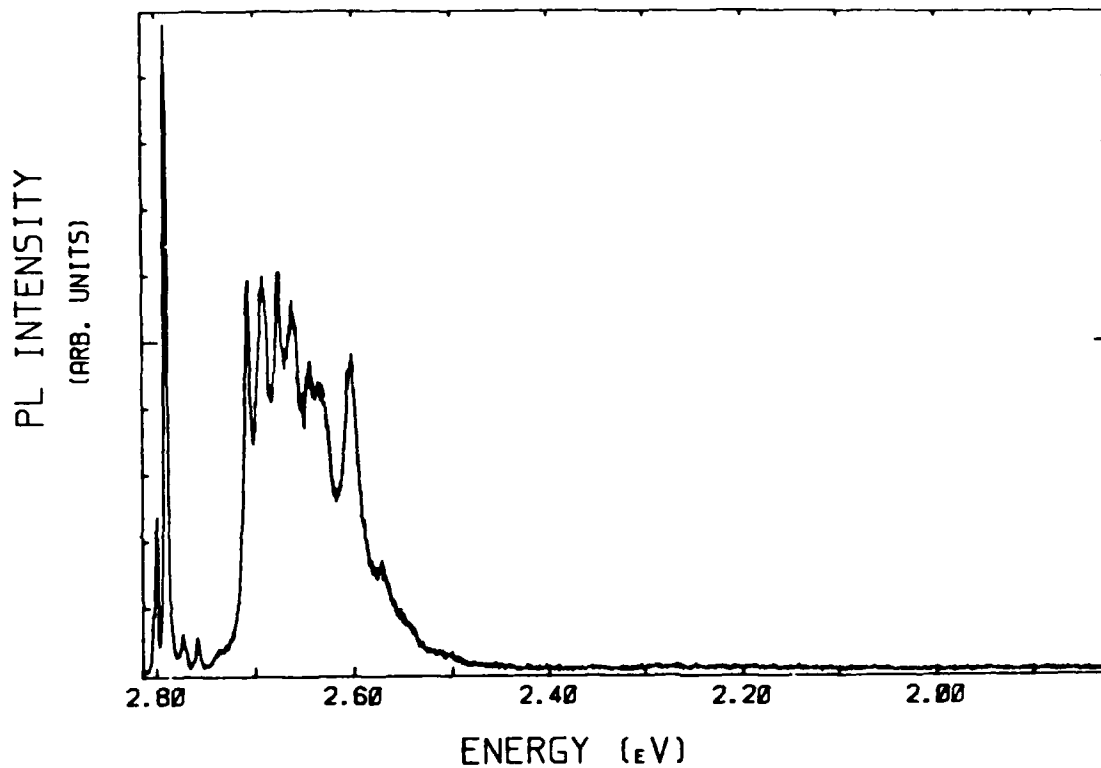


Figure 2-17. PL spectra for two Li-doped samples grown under similar conditions ( $T_g = 350^\circ\text{C}$ , BPR = 1/2:1, Li flux = 3) and with nearly equal Li concentrations (approximately  $1 \times 10^{17} \text{ cm}^{-3}$ ) but in one case (upper curve; #ZSE135) without a  $1 \mu\text{m}$  thick undoped ZnSe buffer layer and in the other case (lower curve; #ZSE134) with the buffer layer.

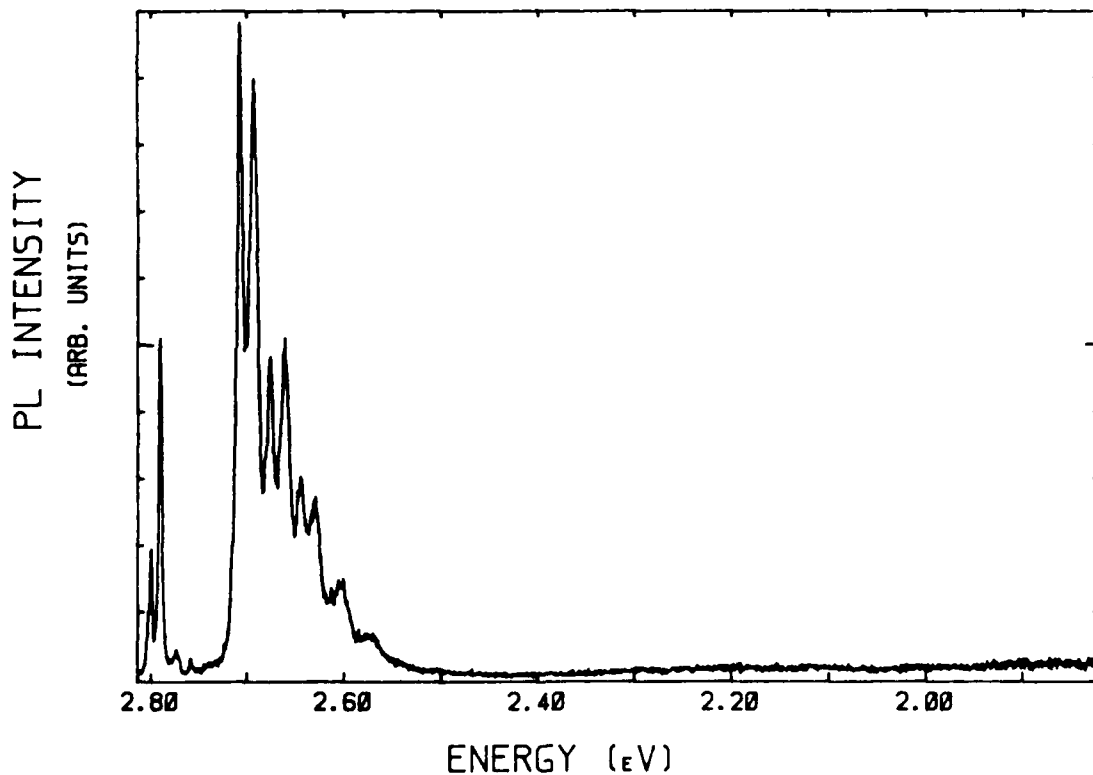
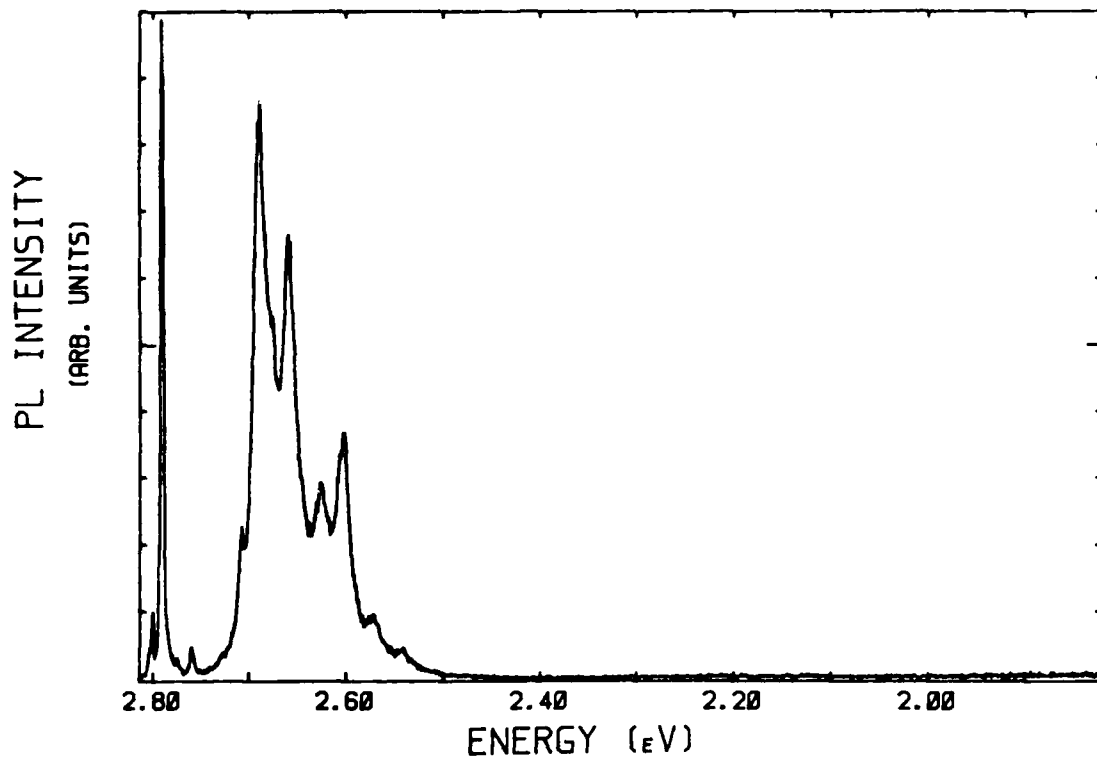


Figure 2-18. PL spectra for two Li-doped samples grown under similar conditions ( $T_g = 350^\circ\text{C}$ , BPR = 1/4:1, Li flux = 3) and with nearly equal Li concentrations (approximately  $6 \times 10^{16} \text{ cm}^{-3}$ ) but in one case (upper curve; #ZSE137) without a  $1 \mu\text{m}$  thick undoped ZnSe buffer layer and in the other case (Lower curve; #ZSE136) with the buffer layer.

This runs counter to what one would expect if the film were smoother and less contaminated when grown in the presence of the buffer layer.

Finally, we note that in both Figures 2-17 and 2-18 the higher-energy DAP series (R-series) is much more prominent in the PL spectrum of the buffered sample. This series has been associated [8] with a  $\text{Li}_{\text{int}}-\text{Li}_{\text{zn}}$  donor-acceptor pair, although some of our recent results have cast some doubt on this interpretation. If so, it is not clear to us how the concentration of such pairs might be influenced by the use of an undoped ZnSe buffer layer prior to beginning the Li doping.

In summary, it would appear that the use of an undoped buffer layer has little effect on the properties of the ZnSe:Li film. In particular, macroscopic structural defects propagating from the substrate do not appear to be limiting the electrical activity of the Li dopant. Of course, the presence of Li at the growth surface may itself lead to the formation of structural defects.

#### 2.2.1.5 Examination of Growth Space with Li-Doping

In previous reports we have discussed our extensive studies of the MBE growth parameter space for undoped ZnSe. Specifically, we have examined the effects of sample growth temperatures ( $T_g$ ) from 250 to 400°C and of Zn/Se beam pressure ratios (BPR) from 1/4:1 to 2:1. In these studies, we used RHEED diffraction patterns to observe for the first time the transition from the Zn-stabilized to Se-stabilized regions of growth space and we used surface morphological studies to identify a region of transition from smooth growth surface to one of rough (three-dimensional) growth. We identified the intersection of these two transition lines as being an important fixed point which could be used in "calibrating" one MBE growth system to another. Taking all of our film quality criteria into account, we found that the optimum conditions for growth of unintentionally-doped ZnSe lay in the vicinity of  $T_g = 300-350^\circ\text{C}$  and  $\text{BPR} = 2:1-1:1$ .

During the final quarter of this contract period we undertook a similar, though less extensive examination of growth space for Li-doped ZnSe. Of course, the additional degree of freedom in this case was the Li flux. We have limited our studies to taking scans through different growth temperatures and Zn/Se beam pressure ratios (BPR) at two different Li

fluxes. The results of our SIMS and photoluminescence measurements for these scans are shown in Tables 2-8 and 2-9. All of these samples were found to be p-type, as determined from I-V measurements. All were of sufficiently high resistivity that Hall effect measurements could not be done, so no meaningful values for free hole concentrations can be quoted for these samples.

In observing the RHEED patterns during the growth of these samples, we found that:

- (i) the RHEED pattern of the Li-doped layer depends only upon the regime of the growth condition, namely Zn- or Se-stabilized, in which the sample was grown. The RHEED pattern was spotty under Zn-stabilized conditions and streaky under Se-stabilized conditions. The Li concentration also affects the RHEED pattern.
- (ii) the RHEED pattern of the Li-doped layer is independent of the thickness of the underlying undoped buffer layer and it is also independent of the RHEED pattern of that buffer layer. Specifically, the RHEED pattern for a Li-doped layer grown under Zn-stabilized conditions was spotty whether the RHEED pattern for its buffer layer was streaky or spotty.

The overwhelming impression one gets from examining the data in Tables 2-8 and 2-9 is that the quality of these samples, insofar as it can be judged from PL measurements, is relatively insensitive to these broad variations in the sample growth conditions. This is in marked contrast to the case of unintentionally-doped ZnSe where we saw extreme variations in the film quality as we moved about in this growth space. In Table 2-8 we see only a slight increase in the Li concentration, R-value (ratio of near-band-edge emission intensity to deep level intensity), and  $I_1/\text{DAP}$  (ratio of acceptor-bound exciton intensity to donor-acceptor pair intensity) as the BPR is increased from 1/4:1 to 1:1 at 350°C. The luminescence efficiency (as measured, approximately, by the intensity  $I_1$  of the ABE since this is the dominant feature in all of these spectra) increases slightly over this range. This may indicate a slight improvement in the surface quality (less surface recombination), but far less than our studies of the undoped material would have suggested.

As we scan  $T_g$  at constant BPR, we find the Li concentration increases, without any serious degradation of the PL properties, with decreasing  $T_g$ . This result can be seen at both of the Li flux values used. The magnitude of this effect is not large, but it does appear to be the case that the Li incorporation is influenced more by the growth temperature than by the Zn/Se beam pressure ratio.

TABLE 2-8. Growth Matrix Used to Study the Variation of Film Properties with Different Growth Conditions at a Constant Li-flux of 3 (same flux units as used in the Quarterly Technical Progress Report No. 5). Data shown are the Li-concentrations [Li], acceptor-bound exciton intensity ( $I_1$ ), and the ratios of  $I_1$  to the free-exciton (FE), donor-acceptor pair (DAP), and deep level ( $R = I_1/DL$ ) emission bands.

BPR	$T_G$	250	300	350	375
1/4:1		ZSE153 [Li]= $1.2 \times 10^{17}$ $I_1=330$ $I_1/FE=35$ $I_1/DAP=5$ R=700	ZSE152 [Li]= $6.9 \times 10^{16}$ $I_1=1000$ $I_1/FE=4.3$ $I_1/DAP=2.6$ R=4600	ZSE137AS [Li]= $5.2 \times 10^{16}$ $I_1=1450$ $I_1/FE=10.35$ $I_1/DAP=1.17$ R=174	
1/2:1				ZSE135 [Li]= $9.8 \times 10^{16}$ $I_1=1240$ $I_1/FE=4.43$ $I_1/DAP=2.58$ R=170	
1:1		ZSE146 [Li]= $3.8 \times 10^{17}$ $I_1=750$ $I_1/FE=15$ $I_1/DAP=1.3$ R=110	ZSE144 [Li]= $1.4 \times 10^{17}$ $I_1=3400$ $I_1/FE=17.4$ $I_1/DAP=1.16$ R=110	ZSE132 [Li]= $1.6 \times 10^{17}$ $I_1=5500$ $I_1/FE=27.5$ $I_1/DAP=3.1$ R=690	ZSE154 [Li]= $1.1 \times 10^{17}$ $I_1=5300$ $I_1/FE=66$ $I_1/DAP=0.43$ R=1100

TABLE 2-9. Growth Matrix Used to Study the Variation of Film properties with Different Growth Conditions at a Constant Li-flux of 60 (same flux units as used in the Quarterly Technical Progress Report No. 5). Data shown are the Li-concentrations [Li], acceptor-bound exciton intensity ( $I_1$ ), and the ratios of  $I_1$  to the free-exciton (FE), donor-acceptor pair (DAP), and deep level ( $R = I_1/DL$ ) emission bands.

BPR	$T_g$	250	300	350	375
1/4:1					
1/2:1					
1:1		ZSE148 [Li]= $4.9 \times 10^{19}$ $I_1=130$ $I_1/FE=5$ $I_1/DAP=0.27$ $R=130$		ZSE147 [Li]= $6.7 \times 10^{18}$ $I_1=500$ $I_1/FE=10$ $I_1/DAP=0.11$ $R=4700$	

It is most significant that some of our best films, as judged by their PL spectra (large  $I_1$  intensity,  $I_1/DAP$  and R-values) were grown under Se-stabilized conditions. For example, ZSE152 and ZSE153 (Table 2-8) were grown under conditions ( $T_g = 250 - 300^\circ\text{C}$ , BPR = 1/4:1) which would have yielded undoped films of extremely poor quality. It would appear, then, that the presence of Li at the growth surface alters the growth dynamics sufficiently to permit growth of high quality doped films under these "extreme" conditions.

Finally, we note that, as the Li concentration grows beyond  $10^{18} \text{ cm}^{-3}$  (see Table 2-9), the luminescence efficiency begins to decrease (poorer surface morphology) and the donor-acceptor pair emission becomes stronger than the ABE peak intensity. This latter fact may reflect (i) an increasing incorporation of Li atoms into interstitial positions where they act as donors or (ii) the formation of some other type of Li-related complex at these high Li concentrations.

## 2.2.2 Na-Doped ZnSe on (100) GaAs

### 2.2.2.1 Na-Doping Source #3

In the previous Na doping study we encountered difficulty in controlling the Na flux and maintaining a constant dopant concentration in the films (Quarterly Technical Progress Report No. 5). Careful analysis of the loading and growth procedures convinced us that an improper loading method was the major cause of this failure. A new batch of the same Na source material as was used for source #2 was loaded into the system using an improved loading procedure. This source will hereafter be referred to as Na source #3. Four Na-doped samples were grown under identical conditions except for the Na flux. One sample, ZSE157, was modulation-doped to study possible Na diffusion; the results of this study will be described in Section 2.2.3. The growth conditions for these runs are listed in the Table 2-10.

TABLE 2-10. Summary of Growth Conditions and Incorporated Na Concentrations (measured by SIMS) for Samples Grown Using Na Source #3.

<u>Sample</u>	<u>T<sub>G</sub></u>	<u>BPR</u>	<u>Na Flux</u> (rel. units)	<u>[Na] (SIMS)</u>
ZSE156	300	1/4:1	0.15	not uniform ( $8.4 \times 10^{15}$ )
ZSE157	300	1/4:1	3.6	modulation-doped
ZSE158	300	1/4:1	4.5	$1.1 \times 10^{19}$ thick buffer
ZSE159	300	1/4:1	0.5	$2.4 \times 10^{15}$ thick buffer

The Na concentration in sample ZSE156 is not uniform. This is probably due to the new Na source having not yet attained a chemically steady state at the time this sample was grown. This is supported by the constant Na concentration in later samples ZSE158 and ZSE159 measured by SIMS depth profiling. Two points are worth mentioning when comparing this series of growth runs with the previous doping study using the same source but with a different loading method. It is found that a higher Na-oven temperature was required to dope the film to the same level of sodium concentration. This result is not unexpected in view of our new loading procedure. The Na flux was also more stable during the growth as monitored with the quadrupole mass analyzer (QMA). This stability in flux is also reflected in the SIMS depth profiling of Na level (Figure 2-19). The abrupt change in Na level reflects the onset of impurity doping and also indicates that diffusion of Na in ZnSe is not a problem.

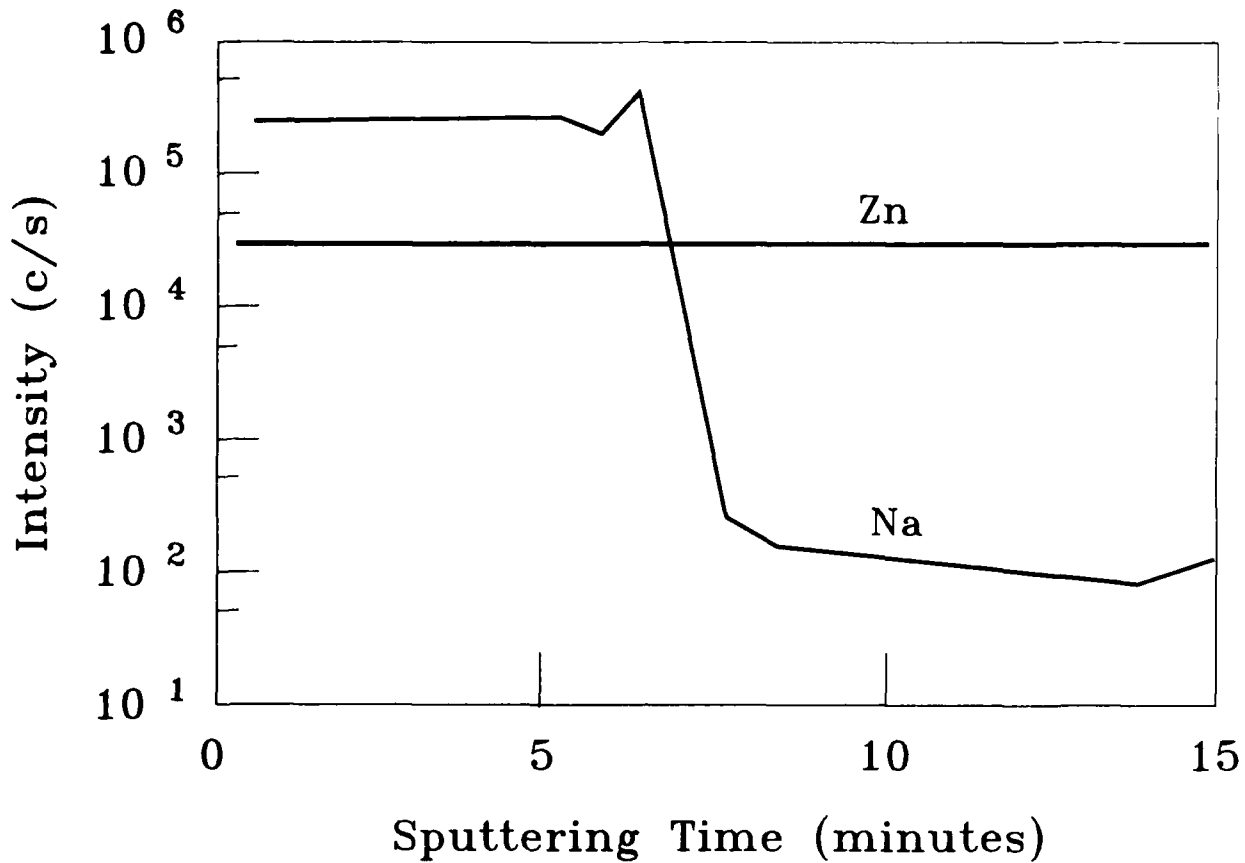


Figure 2-19. SIMS Depth profiles of Na concentration in sample ZSE158 grown with Na Source #3 and with a thick undoped ZnSe buffer layer. The  $^{70}\text{Zn}$  signal is also shown for reference.

PL spectra obtained for samples grown using Na source #3 with the old and new loading procedures are shown in Figure 2-20. Samples ZSE113 and ZSE118 [(Figures 2-20(a) and 2-20(b)] were grown during an earlier series, discussed in Quarterly Technical Progress Report No. 5 (Section 2.2.1). ZSE113 was grown at  $T_g = 300^\circ\text{C}$ , BPR = 1:1 and Na flux = 2 and SIMS analysis showed the Na concentration to be  $1 \times 10^{18} \text{cm}^{-3}$ , while ZSE118 was grown at  $T_g = 350^\circ\text{C}$ , BPR = 1:1, Na flux = 4, and contained  $[\text{Na}] = 5 \times 10^{18} \text{cm}^{-3}$ . In both of these spectra we see some free exciton (2.8 eV) and donor-bound exciton (2.795 eV) emission as well as the large, broad band near 2.62 eV which is observed in all of our heavily-Na-doped films. ZSE158, grown more recently using our new loading procedure to permit better temperature control of the Na source, and with  $T_g = 300^\circ\text{C}$ , BPR = 1/4:1, Na flux = 4.5, and  $[\text{Na}] = 1.1 \times 10^{19} \text{cm}^{-3}$ , is shown in Figure 2-20 (c). This spectrum seems to demonstrate the same trends that were seen in Figures 2-20(a) and 2-20(b) with increasing  $[\text{Na}]$ ; i.e., the 2.62 eV band increasingly dominates the PL spectrum and the  $Y_0$  peak becomes more prominent.

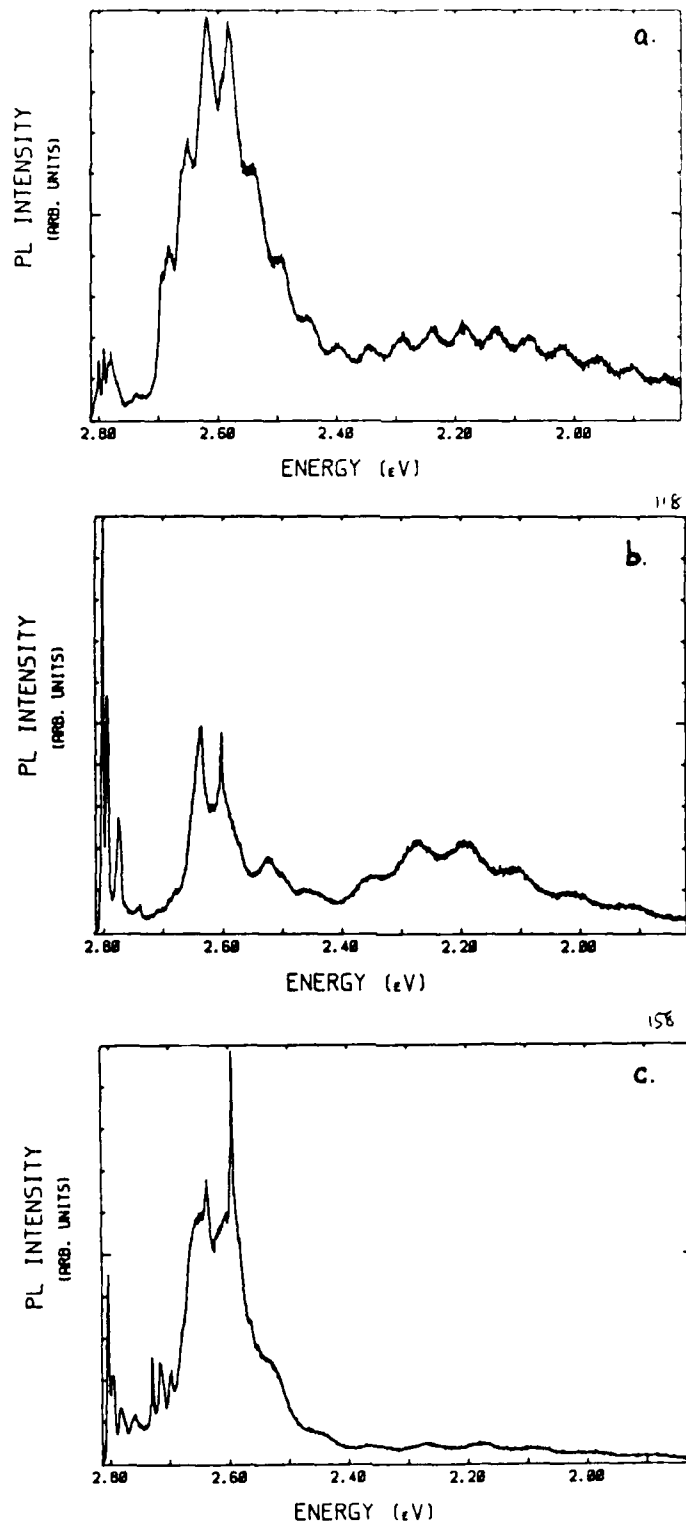


Figure 2-20. PL spectra for Na-doped ZnSe films grown using Na-sources #2 and #3 to compare the effects of the new source loading procedure. (a) #ZSE113:  $T_g = 300^\circ\text{C}$ , BPR = 1:1, Na flux = 2,  $[\text{Na}] = 1 \times 10^{16}$ ; (b) #ZSE118:  $T_g = 350^\circ\text{C}$ , BPR = 1:1, Na flux = 4,  $[\text{Na}] = 5 \times 10^{16}$ ; (c) #ZSE158:  $T_g = 300^\circ\text{C}$ , BPR = 1/4:1, Na flux = 4.5,  $[\text{Na}] = 1.1 \times 10^{16}$ .

We also see a decrease in the relative intensity from deep levels. This latter effect may represent some slight improvement over the earlier samples, but it may also be due to differences in the growth temperature, the ZnSe beam pressure ratio, or to the presence of an undoped buffer layer grown prior to depositing film ZSE158. In addition, we have seen a decrease in the deep level emission with increasing [Li] in the case of the Li-doped samples. This perhaps indicates that the Li atoms in that case, and the Na in the present case, are forming non-radiative complexes with the defects which give rise to the deep level emissions in the more lightly-doped samples.

It is not surprising that we see no systematic differences in the PL from samples grown in this latest series using Na source #3 when compared with samples grown using this source earlier. We have only changed the procedures for loading the source material in order to better control the Na flux. As a result, the uniformity of the Na doping should be improved, but the photoluminescence experiment will not be sensitive to this uniformity.

Studies of the electrical properties of the four samples doped with Na using Na source #2 gave no evidence of p-type activity. Two of the samples were found to be n-type while the results for the remaining two samples were inconclusive. Hall measurements made on ZSE156A showed the free electron density to be  $1.1 \times 10^{15} \text{ cm}^{-3}$  at room temperature. Since the undoped samples in this series were found to have immeasurably small free carrier densities, this somewhat surprising result indicates that donors are being incorporated when the growing films are exposed to the Na beam. Possible origins of the donors include: impurities which are released from the Na source, intrinsic defects which are formed in the presence of Na, or improper substitution of Na into the ZnSe lattice. Regardless of the origin of the donors, Na-doping does not appear promising at this time unless a cleaner Na beam can be found.

### 2.2.3 Lithium and Sodium Diffusion Studies

As was shown in earlier sections, doping ZnSe with Li does appear promising in that conversion to p-type conductivity has been achieved. It is also believed that proper control of the growth conditions will ultimately produce high conductivity materials suitable for device applications. A major concern with the use of Li as a dopant, however, is the problem of

diffusion. Abrupt doping profiles are often required in the fabrication of optoelectronic devices, but such abrupt profiles may not be possible when doping with Li.

Modulation-doping studies were carried out to test the diffusivity of both Li and Na in ZnSe. In these studies the shutter for the dopant cell was opened only for a short time during the middle portion of the growth run. If diffusion of the dopant did not occur, then this type of growth schedule would have produced films in which a narrow, doped region was sandwiched between two undoped layers. SIMS profiles were taken to determine the actual distribution of dopant in samples grown in this manner. The results for two samples, ZSE155A and ZSE157A, are shown in Figures 2-21 and 2-22. In these figures the intended doping profiles are shown by the dashed lines and the actual doping profiles are given by the solid lines.

In the film which was thought to have been modulation-doped with Li (Figure 2-21), it was found that the actual Li concentration was nearly uniform throughout the film with only a moderate decrease occurring away from the region of the sample which had been exposed to the Li beam. The integrated area under the actual concentration profile agrees well with the area under the projected profile. Thus the total number of Li atoms appears to be conserved. This indicates that the measured profile is not an experimental artifact, but that Li diffuses quite readily in films grown under these conditions. The profile of the film which was modulation-doped with Na (Figure 2-22) is quite different from the profile of the Li-doped film. From the measured profile it appears that Na diffusion into the undoped region of the film which was grown prior to the opening of the Na shutter is quite low. When the Na shutter is opened the Na concentration quickly begins to rise. After closing the Na shutter, however, the Na concentration does not quickly drop to zero, but instead slowly decreases as the film is grown. The Na-doping profile may be understood using a model where:

- (i) sodium desorption from the surface is negligible at the growth temperature of 300°C,
- (ii) diffusion of Na is small enough to be neglected, and
- (iii) incorporation of Na at the growing interface is proportional to the surface population of Na,  $C = aN(\text{Na})$  where  $C$  is the concentration of Na near the growing interface,  $a$  is a proportionality constant, and  $N(\text{Na})$  is the number of Na atoms per unit area on the surface.

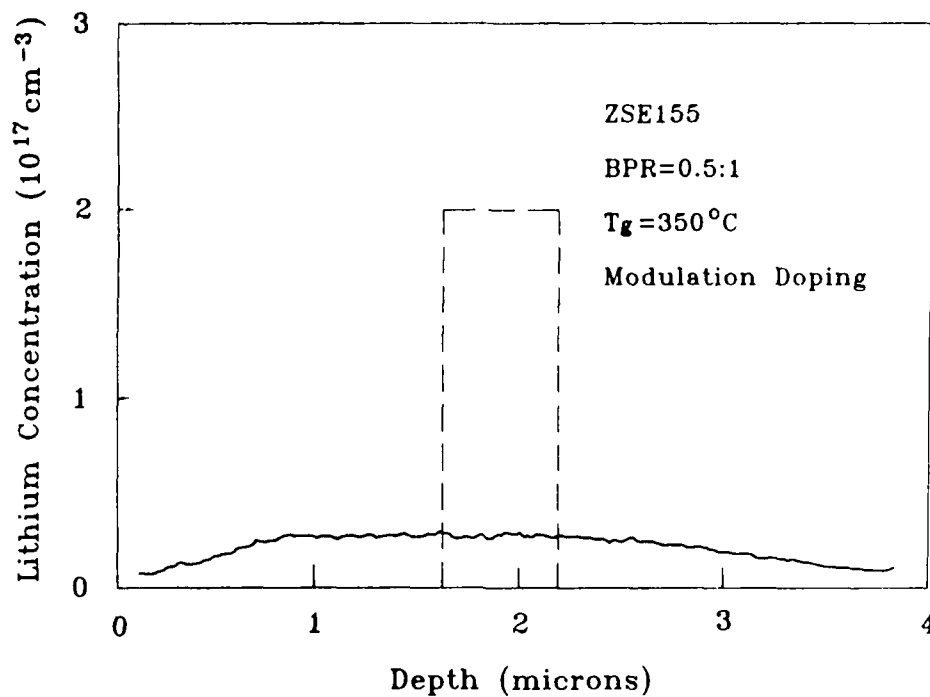


Figure 2-21. SIMS profile of Li-modulation-doped ZnSe film. The dashed line shows the intended Li profile and the solid curve shows the actual measured Li concentrations in units of  $10^{17} \text{ cm}^{-3}$ .

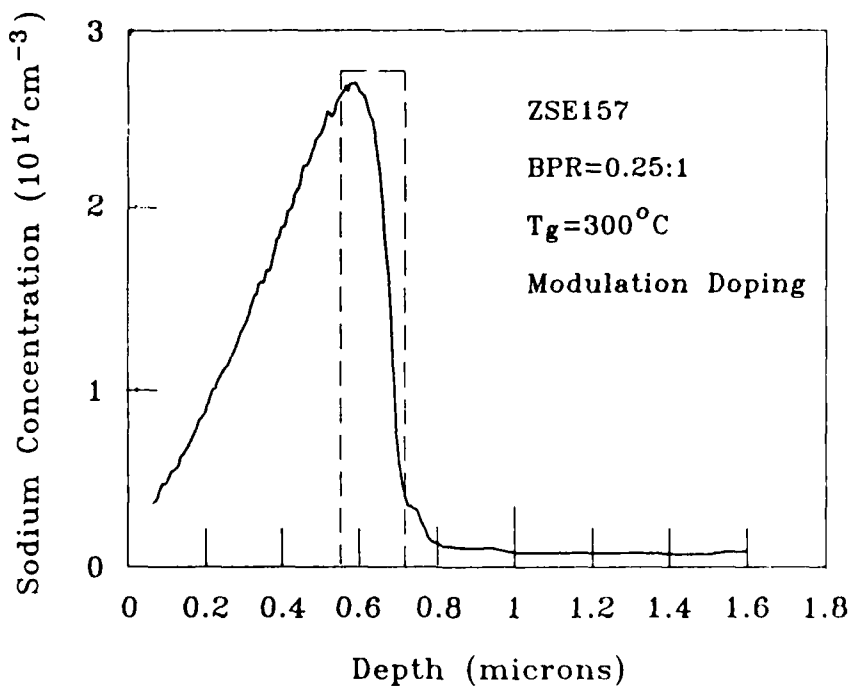


Figure 2-22. SIMS profile of Na-modulation-doped ZnSe film. The dashed line shows the intended Na profile and the solid curve shows the actual measured Na concentrations in Units of  $10^{17} \text{ cm}^{-3}$ .

A model describing the Li profile would be identical to that describing the Na profile except for the larger diffusivity of Li.

The modulation doping studies described here show that Li appears to be a rapid diffuser in ZnSe. Sodium diffusion, on the other hand, appears to be very weak. To date, p-type conversion in ZnSe has not been achieved using Na as a dopant; this may ultimately restrict us to using Li as a p-dopant. If Li-doping is necessary in order to achieve p-type conversion in ZnSe, then either some technique for inhibiting Li diffusion must be developed or devices must be designed which do not rely on abrupt Li concentration profiles.

### 2.3 Project 2, Task 2: Contact Studies

The bulk of the electrical measurements on our Li-doped films relied on the interpretation of two-point I-V measurements. This type of study could be used to determine the majority carrier type of the films, but the reliability of the carrier densities estimated from these measurements may be poor. If, for example, the voltage drops at the contacts are large, then significant underestimation of the hole densities will occur.

A technique used to circumvent the problems associated with poor contacts is the potential profiling technique [9]. With this measurement technique several contacts are deposited in a line. Current is then injected into the sample using the outermost two electrodes while the voltage drop is measured along the line of electrodes using a high input impedance electrometer. The asymmetry of the voltage profile can be used to determine the majority carrier type. Furthermore, since no current is drawn through the inner electrodes, the voltage drop between inner electrodes is due only to the sample resistance and not to contacts. The resistivity of the sample, therefore, can be determined using the voltage profile of the inner electrodes.

Voltage profiles were made on ZSE144A using evaporated Au to form the metal contacts. The results of this measurement are shown in Figure 2-23. From the voltage asymmetry the majority carrier type is found to be hole-like. This agrees with the result of the two-point contact studies. The slope of the potential between the inner electrodes indicates that the resistivity of the sample is reasonably low.

## POTENTIAL PROFILING ZSE144A

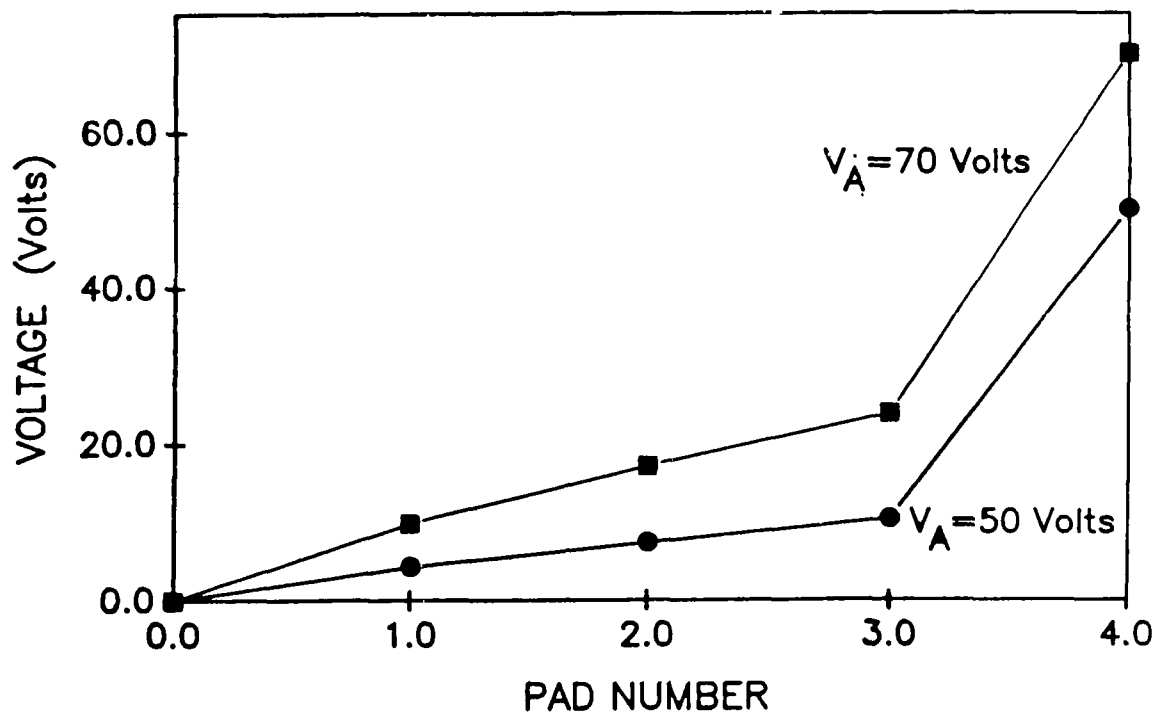


Figure 2-23. Results of potential profiling measurements on a Li-doped film. Data show the potential drop as a function of the distance between two outer electrodes. The asymmetry shows that the film is p-type.

This is in disagreement with the results obtained using the two-point measurements. This measurement also suggests that the Au may not form a good Ohmic contact to p-ZnSe. This is the first indication we have seen that the free hole concentrations in our Li-doped films may actually be much larger than our initial I-V measurements led us to believe.

### 3.0 SUMMARY REPORT

This section summarizes the work done under ONR Contract N00014-85-C-0552 from October 1, 1985 to December 31, 1987. The work was done through parallel and coordinated efforts in two laboratories, one at the 3M Electronic and Information Technology Sector Laboratory in St. Paul, Minnesota, and the other at 3M Canada Corporate Research and Development Laboratory, located at the University of Toronto in Toronto, Canada. The major areas of study during the 27 months of this contract were:

- i. Growth of unintentionally-doped ZnSe epitaxial films on GaAs substrates in order to fully characterize the material and the growth system prior to attempting doping.
- ii. Growth of intrinsic ZnSe on alternate substrates in an attempt to reduce the deleterious effects caused by lattice mismatch between the substrate and epilayer and/or the autodoping by contaminants from the substrate which have been suspected to occur when using GaAs substrates.
- iii. p-doping of ZnSe films on GaAs substrates.
- iv. Examination of the lasing properties of ZnSe films using electron-beam excitation.
- v. Studies of metal contacts on ZnSe.

The results of these studies are detailed below.

#### 3.1 Unintentionally-doped ZnSe

A great deal of work has been done in laboratories throughout the world in an attempt to obtain high conductivity n- and p-type ZnSe, with most of this work aimed toward forming p-n junctions for carrier injection in blue-light-emitting devices. The results have been largely disappointing and, to some extent, contradictory. As we began our attempts at growing ZnSe by molecular beam epitaxy (MBE), we recognized a need to fully characterize, insofar as possible, the intrinsic (i.e., the not-intentionally-doped) ZnSe material system, and to examine the perturbations of this system brought about by variations in our sample growth procedures. We felt that such a thorough knowledge of the undoped system would serve us well in our later attempts at doping. A point of particular concern to us in this study was the question of identifying the residual donors in unintentionally doped n-type ZnSe. Specifically, were these donors due to impurities incorporated

into the film (from the ambient, from the starting materials, or outdiffusing from the substrate) during growth, or were they intrinsic defects (vacancies, interstitials, or anti-site defects)? The answer to this question would have profound implications in the subsequent doping studies.

The quality of the materials we have been able to grow in this study is attested to by the fact that we have reported:

- i. The highest peak electron mobility ever observed for MBE-grown ZnSe in a lightly n-type sample.
- ii. Donor bound exciton (DBE) emission lines in the photoluminescence (PL) spectrum of lightly n-type samples that are as narrow as any ever reported in MBE- or MOCVD-grown samples (LPE-grown samples have DBE peaks which are typically somewhat narrower).
- iii. Extremely high-resistivity samples whose PL spectra are dominated by free-exciton emission and which show no indication of emission from excitons bound to residual donors. The carrier concentration in such samples was too low to measure directly, but we estimate an upper bound of  $n = 1 \times 10^{14} \text{ cm}^{-3}$ .

In the course of this study, we exhaustively examined a broad area of growth-parameter space, varying growth temperatures ( $T_g$ ) from 250 to 400°C and varying the Zn-to-Se beam pressure ratio (BPR) from 1/4:1 to 2:1 [10]. The reflection high energy electron diffraction (RHEED) patterns monitored during the films' growth disclosed heretofore unreported surface reconstructions characteristic of a transition from a Zn- to a Se-stabilized surface as the growth conditions were varied. See Figure 3-1. In addition, a transition from a streaky to a spotty RHEED pattern was observed, indicating a change from high-quality, two-dimensional growth to a rougher surface characterized by three-dimensional growth. The intersection of the lines defining these two transitions in growth space defines a unique point in that growth space. We have emphasized the importance of this intersection in fixing the absolute position in growth space for different growth chambers in order to permit the intercomparison of results from different labs.

From the electrical and optical measurements on the (approximately 30) films grown for this "growth matrix" study we found that, while both the free-carrier and donor concentrations,  $n$  and  $N_d$ , decreased as either  $T_g$  or the BPR increased, PL DBE lines broadened and radiative deep-level emission increased for  $T_g > 350^\circ\text{C}$  and for  $\text{BPR} > 1:1$ .

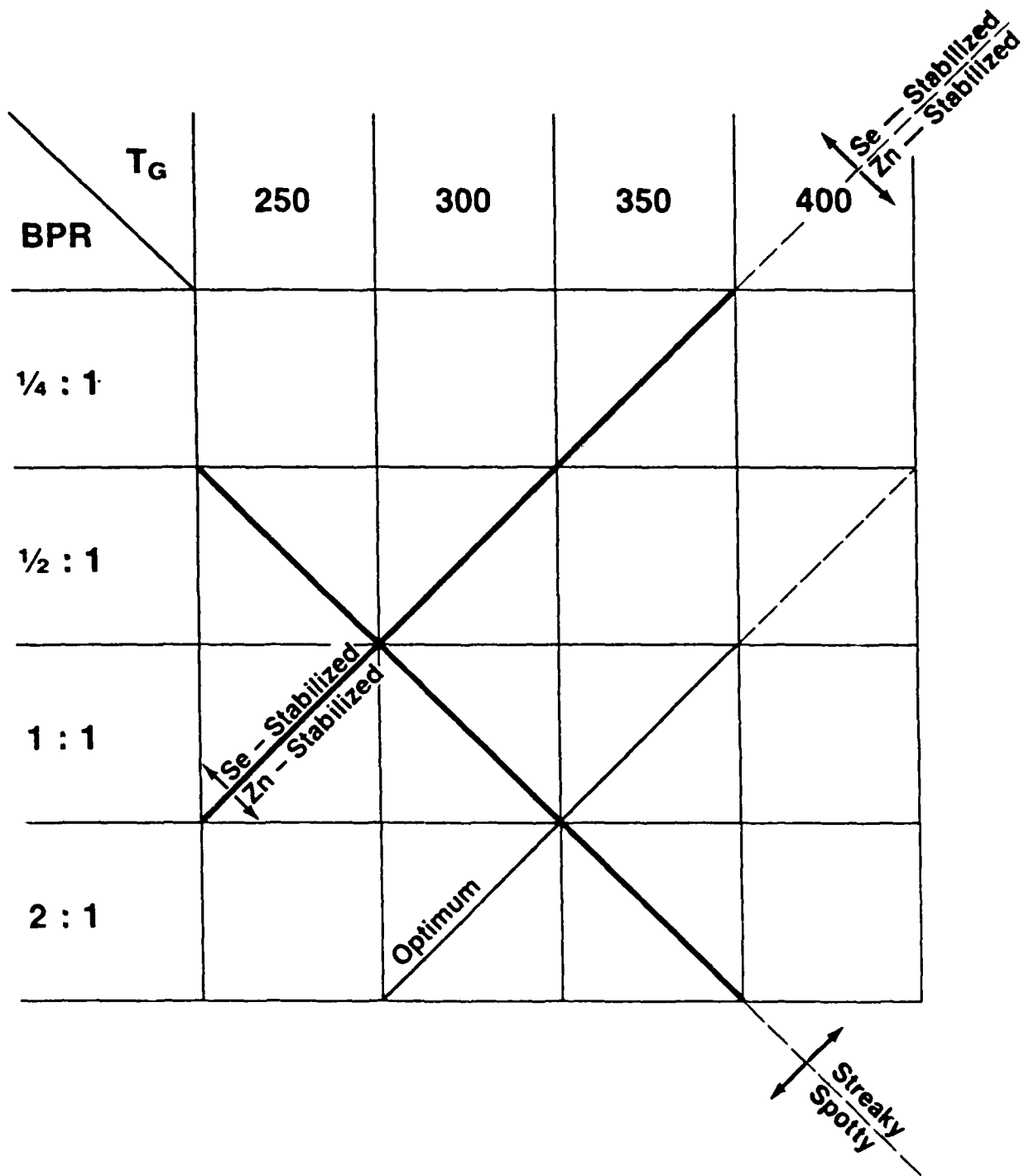


Figure 3-1. Growth matrix used to study the properties of undoped ZnSe grown by molecular beam epitaxy using different growth temperatures and Zn/Se beam pressure ratios. The region of transition from a Se- to a Zn-stabilized region is indicated, as is the transition from a streaky to a spotty RHEED pattern and the optimum conditions for growth of undoped ZnSe films.

Balancing the optimizations indicated by these criteria, we find the "best" growth conditions to occur on a line in growth-parameter space parallel to the Zn- to Se-stabilized surface transition line, but on the Zn-stabilized side of this line, and near the spotty-to-streaky transition line. For our system, this translates to  $T_g = 300 - 350^\circ\text{C}$  and BPR = 2:1-1:1.

By growing samples to the same thickness but at growth rates which differed by a factor of two (by varying the absolute beam pressures in a constant ratio) we have found no effect on the sample quality as judged by PL and electrical measurements. This is in contrast to the findings of some other workers. Thus we are able to grow films at the modestly high growth rate of  $1 \mu\text{m/hr}$  without fear of compromising the film quality.

We observed effects on the PL spectra caused by variations in the sample thickness [11]. In particular, we found the PL excitonic peak positions to increase in energy with decreasing thickness as a result of the increasing biaxial compressive strain in the epilayers, reflecting an increase in the bandgap. See Figure 3-2. Combining our PL measurements with available X-ray measurements of the lattice parameters, we showed the magnitude of this strain to be in agreement with that predicted by properly scaling the bulk elastic constants of ZnSe, in contrast to the behavior that had been predicted by some other researchers. Our X-ray diffraction measurements showed that layers of ZnSe on (100) GaAs are elastically strained up to  $0.15 - 0.2 \mu\text{m}$ , and that misfit dislocations relieve the strain for layers with thicknesses between  $0.2$  and  $0.5 \mu\text{m}$  [12]. See Figure 3-3.

Our secondary ion mass spectrometry (SIMS) measurements [13] have demonstrated that the measured concentrations of the Group III elements (Ga, In, and Al) which are prime candidates as potential residual extrinsic donors in ZnSe are too small, individually or in total, to account for the measured carrier concentrations. Through selective excitation PL (SPL) measurements [14] we have identified Cl and Ga as being the major extrinsic residual donors which cause the DBE emission which usually dominates the PL spectrum of our unintentionally-doped ZnSe. See Figure 3-4. Taken together, these results imply either that Cl is the major source of donor electrons in the unintentionally-doped material or that the residual donors arise from intrinsic defects. This latter possibility can now be dismissed as a result of our examination of the effects of starting material purity.

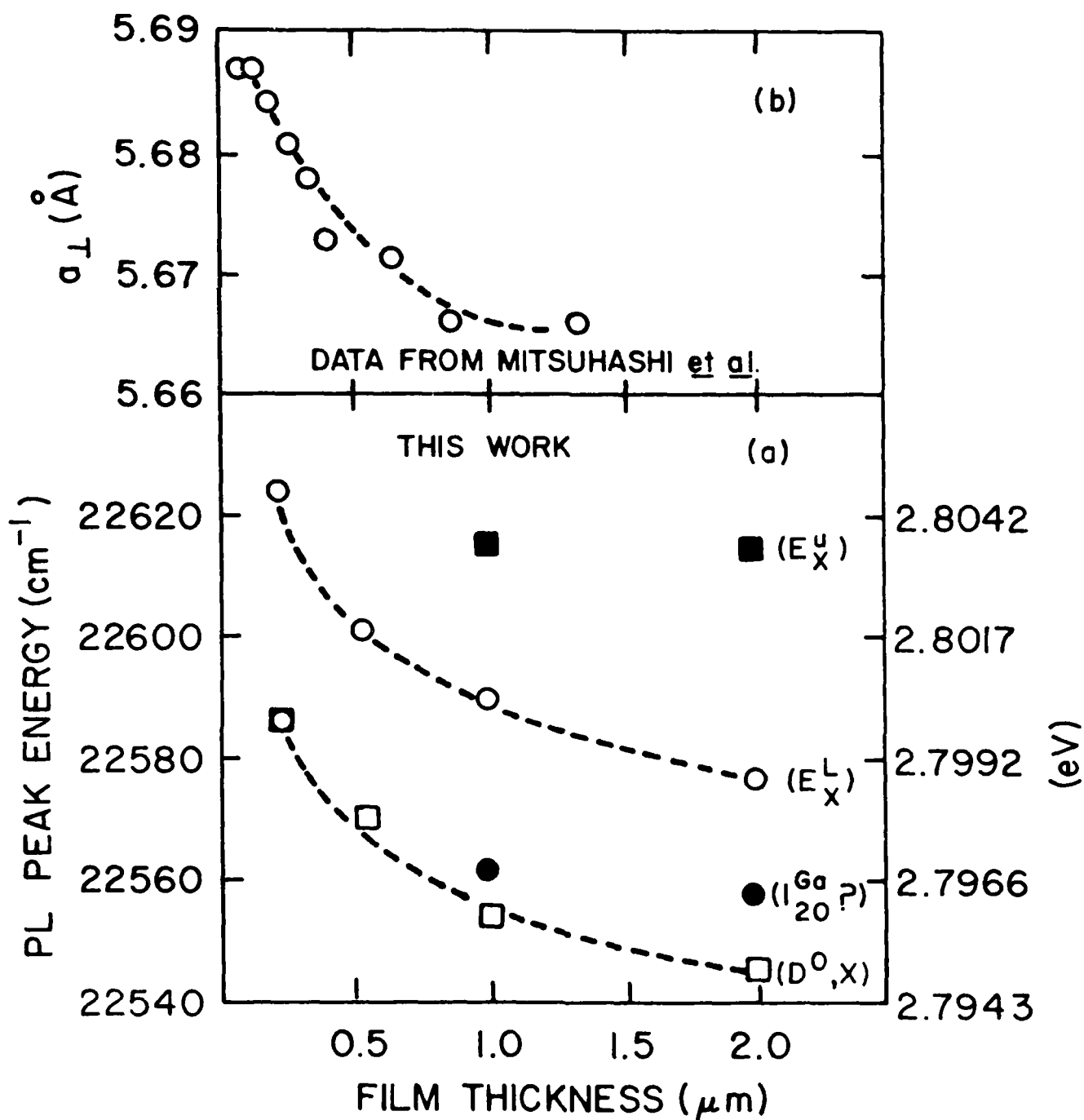


Figure 3-2. (a) Positions of exciton-related PL features versus film thickness, showing the relaxation of the energy gap with a reduction in strain.  $E_X^u$  and  $E_X^L$  are the upper and lower branch polariton peaks,  $I_{20}^{Ga}$  and  $D^0, X$  are donor-bound exciton peaks. (b) Relaxation of the (perpendicular) ZnSe lattice parameter versus film thickness, reflecting the relief of strain with increasing film thickness. These X-ray data are from H. Mitsuhashi, et al., Jpn. J. Appl. Phys., 24 L578 (1985).

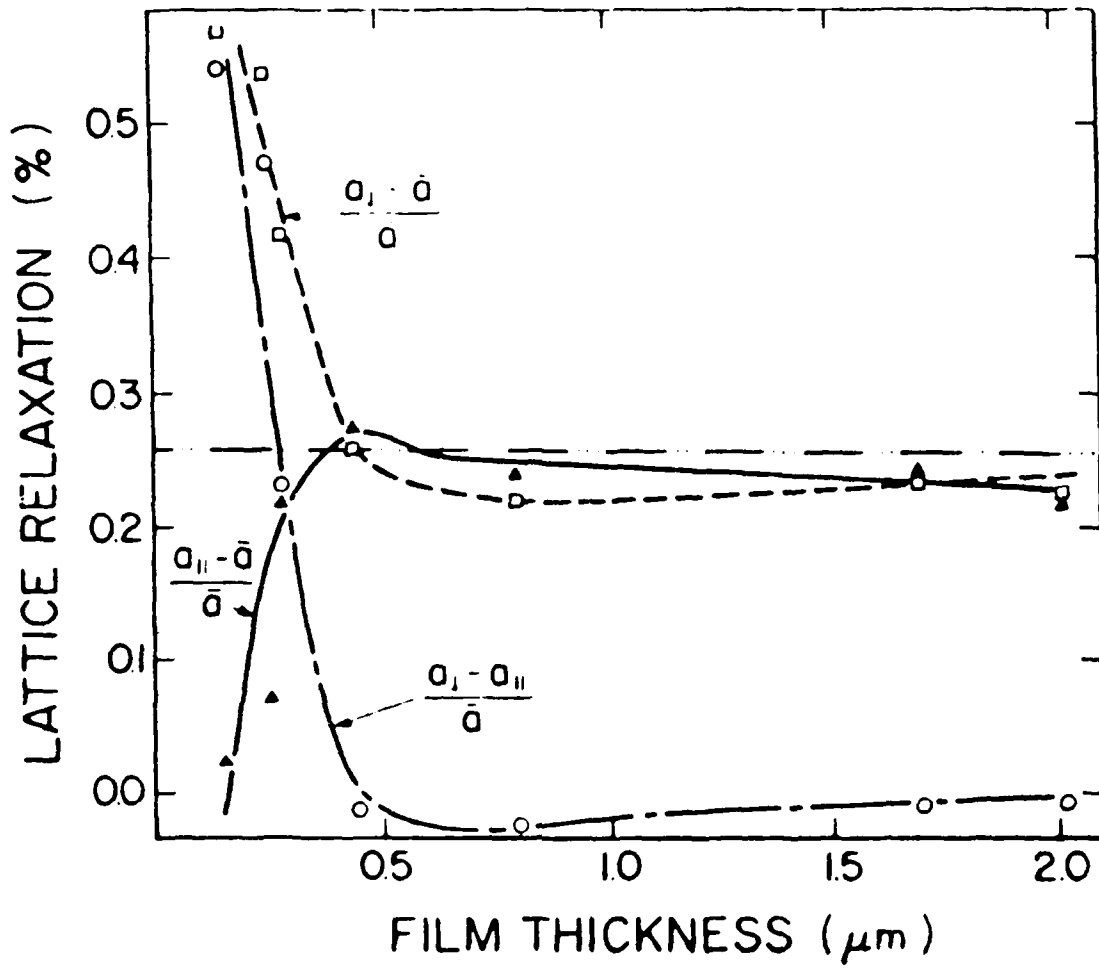


Figure 3-3. ZnSe lattice relaxation as a function of layer thickness. The lattice parameter  $a_1$  is the ZnSe lattice parameter normal to the heterointerface while  $a_{11}$  and  $\bar{a}$  are the ZnSe and GaAs lattice parameters parallel to the interface, respectively.

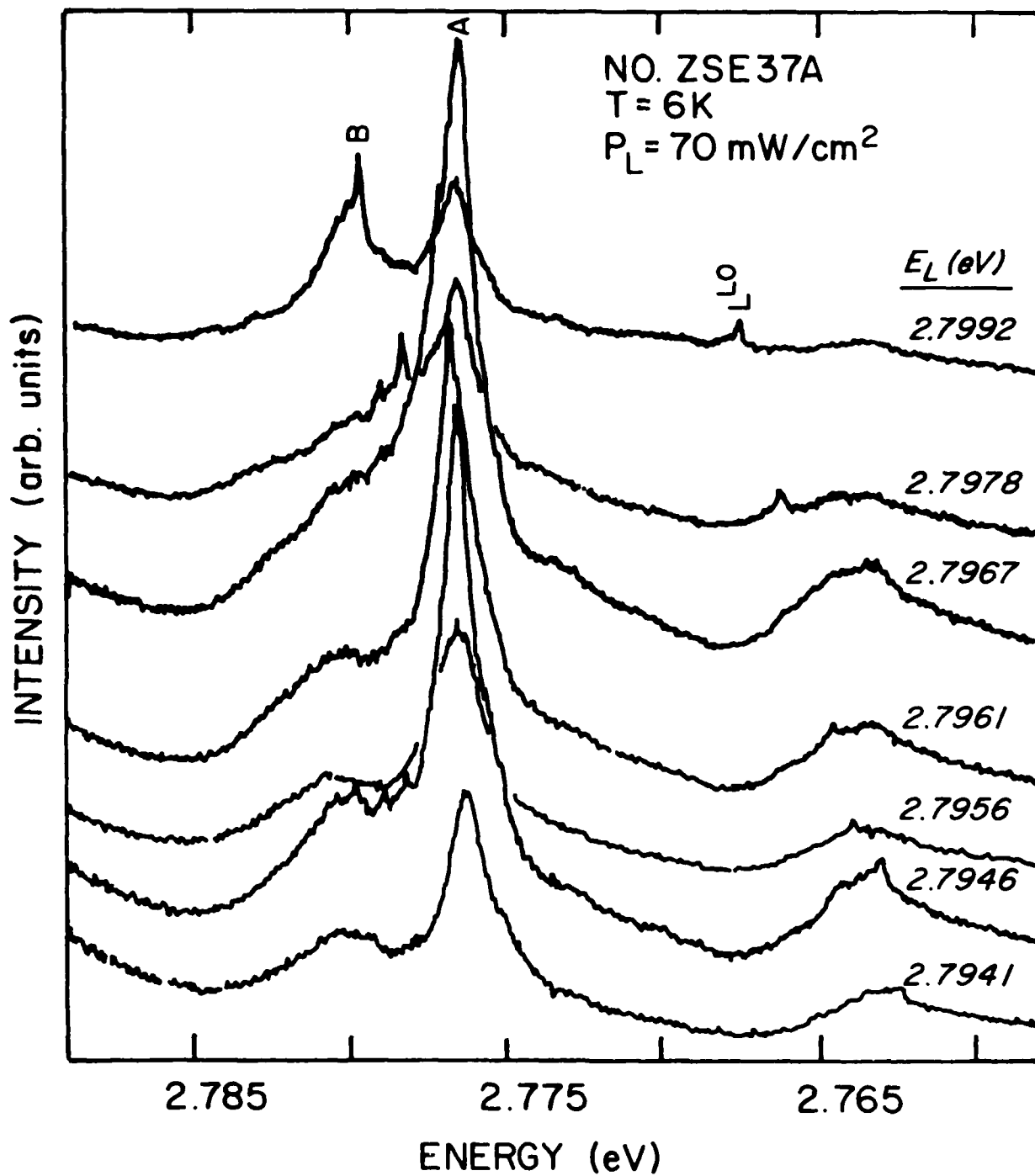


Figure 3-4. Two-electron and resonant Raman scattering signals obtained by resonantly exciting an undoped sample (ZSE37A) in the vicinity of the free exciton and donor-bound exciton peaks. The strong broad feature A is a two-electron transition due to Ga, while the weaker and narrower feature B is due to RRS from Cl.

We have shown, in agreement with the results of other researchers [15], that by using a new 6N+ purity Se which has only recently become available, we can reduce those features in the near-band-edge (NBE) PL spectrum associated with donors by a factor of 40 and, simultaneously, reduce the carrier concentration by more than a factor of 100. This result clearly indicates that the source of the residual donors is an extrinsic impurity. As discussed above, we feel that the culprit is Cl. This is the first of several times in this summary statement in which we will be stating our findings on the importance of controlling the starting material purity in this project. It is imperative that extremely pure Zn and Se and doping sources be used.

Theoretical studies of electron and hole transport in ZnSe were performed during the course of this research contract. One of these studies resulted in the first reported treatment of electron scattering in ZnSe, which also includes all major electron scattering mechanisms and solves the Boltzman transport equation under generalized Fermi-Dirac statistics [16]. This approach is dictated by the fact that the longitudinal polar optical phonons contribute significantly to the overall electron scattering. Hence a universal relaxation time cannot be defined. Therefore, it is necessary to use an iterative or variational procedure to combine all relevant scattering mechanisms. In this work, a variational procedure was chosen.

The basic approach used for electron transport was followed for hole transport, but the additional non-polar optical phonon scattering including interband and intraband scattering was calculated. The Boltzman transport equation was solved for light and heavy holes by the variational method [17] and without resort to a relaxation time approximation. The results predict an inherent mobility limit for holes in ZnSe at room temperature to be about  $100 \text{ cm}^2/\text{volt-second}$ .

Our theoretical study of the two-dimensional electron gas at a ZnSe-Zn (S, Te) heterointerface found that the electron mobility could be as high as  $3 \times 10^5 \text{ cm}^2/\text{v. sec.}$  at 4.2K in this case, and that measurements of the mobility could be used as a probe of strain at this interface [18].

In addition, the theoretical program included a study of the application of free-carrier absorption (FCA) to n-ZnSe materials characterization. This work [19] is the first report of a treatment of FCA in n-ZnSe to include all the scattering mechanisms and to solve for the FCA coefficients exactly under generalized Fermi-Dirac statistics. The necessity to resort to an exact quantum theoretical model is dictated by the inapplicability of classical FCA theory. This originates from the fact that typical photon energies are comparable to electron energies at 300K; therefore, the fundamental assumption of classical theory that electrons can quasi-continuously gain energy from the electromagnetic field is violated.

### 3.2 Growth of MBE-ZnSe Epilayers on Alternate Substrates

Early attempts to grow epitaxial ZnSe reported on in the literature were principally by MO-CVD and MBE, although the LPE technique was used by several investigators. The substrate of choice has been GaAs, although some results were also reported on homo-epitaxial ZnSe and ZnSe on Ge. Due to the unavailability of high-quality ZnSe bulk-grown crystals, it is necessary to grow ZnSe hetero-epitaxially. Moreover, since defect-sensitive devices such as LED's, particularly lasers, are being contemplated, the choice of substrate material on which to deposit the ZnSe layers is of critical importance.

Our study of alternate substrate materials was motivated by the finite, albeit small, lattice mismatch between ZnSe and GaAs, and by reports in the literature which pointed to Ga outdiffusion from the substrate into the growing film as a major potential source of donors in unintentionally-doped ZnSe. The substrates chosen for this study were Ge (lattice mismatch 0.17% ) and Si (4% ). The use of Ge should obviate the autodoping problem while, at the same time, provide a better lattice match to ZnSe than does GaAs. On the other hand, we anticipated that there might be some unique problems arising from attempting to grow a heteropolar material on a homopolar substrate. Si, while it presents a greater lattice mismatch, is of sufficient technological importance to warrant some effort. In addition, it was expected to provide us with additional information about the hetero-homopolar growth problem mentioned above. We also looked at ZnSe growth on Ge buffer layers and on Ge/ZnSe superlattice buffers. The results of a short study on homo-epitaxial growth have appeared elsewhere [20] and will not be repeated in this report.

### 3.2.1 Ge Substrates

Ge is an interesting candidate substrate material for ZnSe epitaxy since the lattice mismatch is only  $\sim 0.17\%$ , and the thermal expansion coefficients of the two materials are also closely matched at room temperature ( $7 \times 10^{-6} \text{ }^\circ\text{C}^{-1}$  for ZnSe and  $5.8 \times 10^{-6} \text{ }^\circ\text{C}^{-1}$  for Ge). In addition, high-quality single crystal Ge wafers are available at relatively low cost.

The first epitaxial ZnSe layers were grown on thermally-cleaned Ge substrates, but these were found to be of poor quality. Subsequently, a technique for substrate preparation was developed which consisted of room temperature  $\text{Ar}^+$  sputtering followed by annealing at temperatures around  $400^\circ\text{C}$ . With this procedure [21] both oxygen and carbon are removed as indicated by the spectrum of Figure 3-5. Furthermore, the (100) Ge substrate cleaned in this fashion exhibited (2 x 2) surface reconstruction as illustrated by the RHEED pattern of Figure 3-6(a), and is indicative of a surface that is both clean and smooth on an atomic scale.

ZnSe layers were grown on sputtered and annealed (100) Ge using a variety of substrate temperatures and Zn/Se beam pressure ratios. The highest quality ZnSe layers, as judged by the PL response of the material, were grown with a beam pressure ratio of about unity and at a substrate temperature of  $300^\circ\text{C}$ . Figure 3-6(b) shows the RHEED pattern of a  $2 \text{ } \mu\text{m}$  thick layer grown under these conditions.

X-ray double-crystal rocking curve (DCRC) measurements and transmission electron microscopy were also used to characterize the epitaxial layers. It is interesting to note [22] that the DCRC linewidths were significantly and consistently larger for ZnSe grown on the (100) Ge than for ZnSe on (100) GaAs for layers of equal thicknesses as shown in Figure 3-7. Indeed, even for the thickest layers of  $\sim 6.5 \text{ } \mu\text{m}$ , the difference remained significant. This suggests that large residual, non-uniform strain associated perhaps with non-uniform bonding, micro-twins, stacking faults or dislocations, or a combination thereof, is present in the ZnSe/(100) Ge layers.

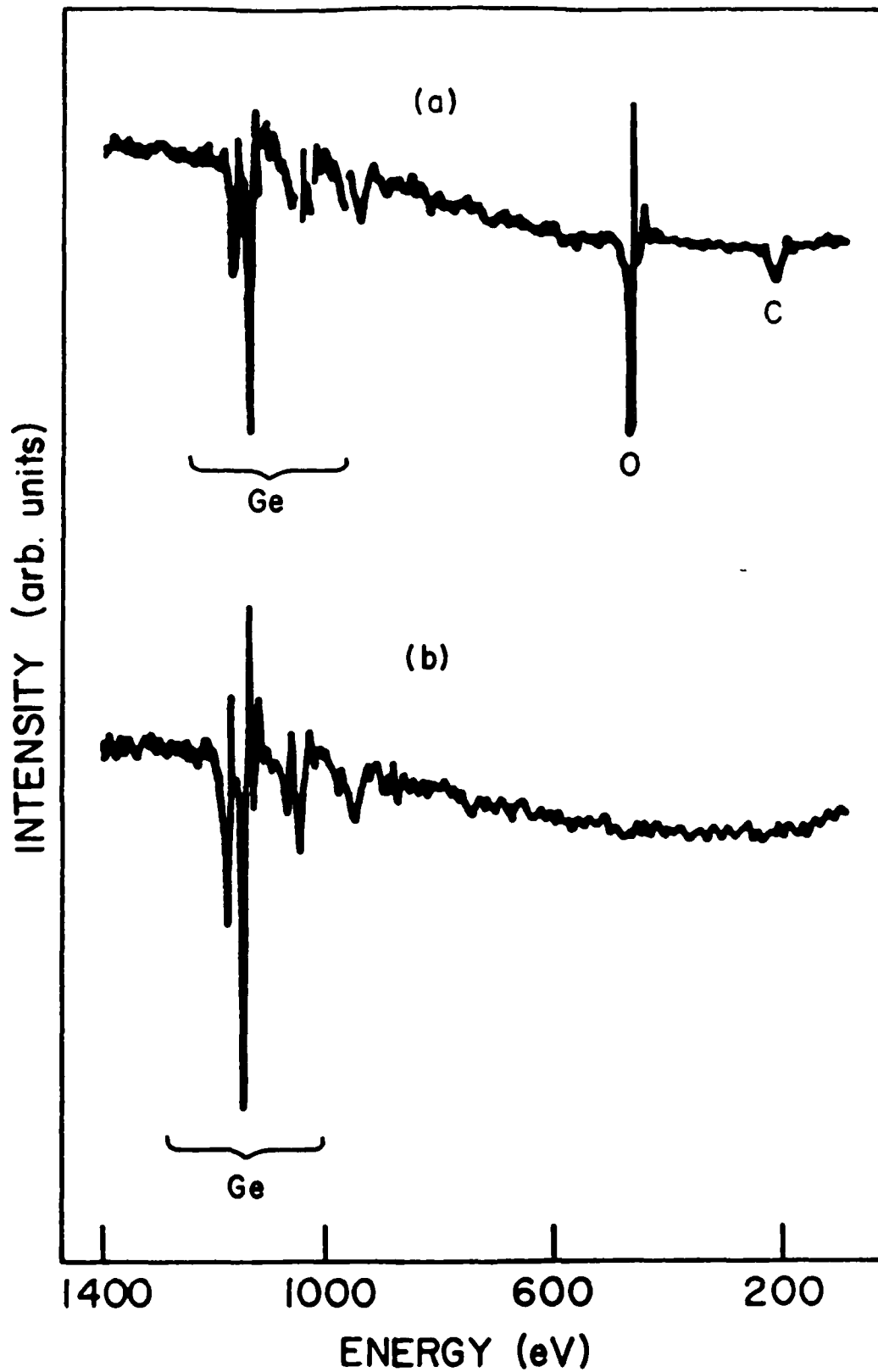
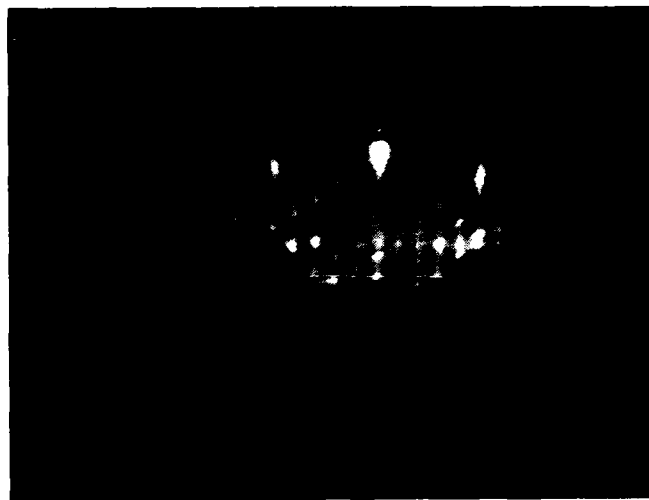
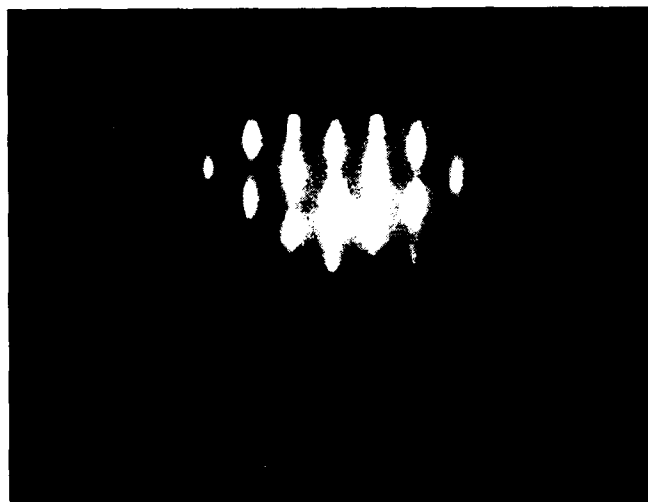


Figure 3-5. AES spectrum of a) untreated and b) sputter/annealed (100) Ge substrate showing the absence of both C and O.



(a)



(b)

**Figure 3-6.** RHEED patterns of Ge substrates.  
(a) A sputtered and annealed (100) Ge substrate.  
(b) RHEED of 2  $\mu\text{m}$  thick ZnSe layer on (100) Ge.

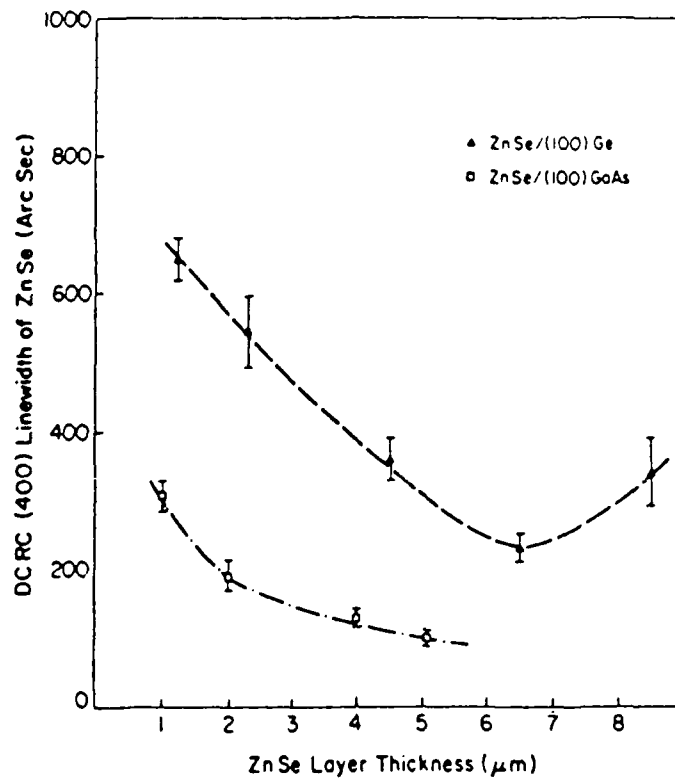


Figure 3-7. DCRC linewidths of ZnSe on (100) Ge and (100) GaAs versus layer thickness.

By way of contrast, the DCRC results suggest that the defect concentration in the ZnSe/(100) GaAs is much smaller; for a layer thickness of about 5  $\mu\text{m}$ , the DCRC linewidth is only 100 arc sec. The rapid reduction in the DCRC linewidth of ZnSe/(100) GaAs is not surprising in view of the single-crystal x-ray diffraction results [23] which suggest that epitaxial layer relaxation is essentially complete for layer thicknesses in excess of  $\sim 1.5 \mu\text{m}$ .

Another important observation, which may be related to the broad DCRC linewidths, is the large tilt of the (400) planes in ZnSe with respect to equivalent planes in the (100) Ge substrate. Tilts of as large as 1000 arc sec were observed [22] for ZnSe/(100) Ge layers. Again, by contrast, the measured tilt in the ZnSe/(100) GaAs system is typically less than 40 arc sec! The technique of tilt measurements and the attendant results are described in detail in Reference [22].

The results of the 4.2K PL measurements were found to be consistent with those of the DCRC measurements. Using the donor-bound exciton (DBE) linewidth as a measure of the material quality shows that the epitaxial

layer quality depends only weakly on the layer thickness (see Figure 3-8). Typical linewidths are about 1 meV. In fact, for a significant number of the best layers grown at or near optimum conditions, DBE linewidths of as low as 0.6 meV were obtained. For ZnSe grown on (100) Ge, linewidths of 1 meV were only observed for layers thicker than  $\sim 6 \mu\text{m}$ . Given that the DBE linewidths are also broadened by lattice inhomogeneities, the PL and DCRC analyses suggest that high concentrations of defects propagate into the ZnSe/(100) Ge layers even for thicknesses as large as  $6 \mu\text{m}$  in spite of the 0.17% mismatch. While for ZnSe/(100) GaAs layers, the dislocation propagation is not as extensive even for layers  $\sim 1 \mu\text{m}$  thick. Indeed, the results suggest that dislocations in ZnSe/(100) GaAs layers would appear to be confined to the substrate/layer interface.

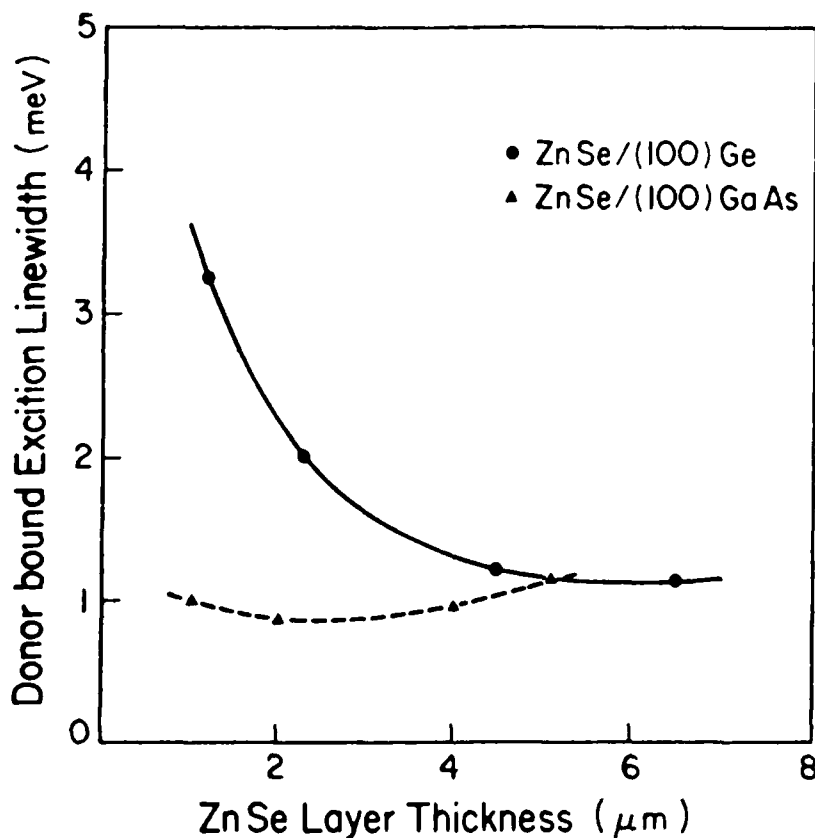


**Figure 3-8.** DBE linewidth of ZnSe layers on (100) Ge and (100) GaAs substrates.

The results of cross-sectional TEM analysis of  $2 \mu\text{m}$  thick ZnSe/(100) Ge and ZnSe/(100) GaAs layers support the above postulate. It was found that in the case of the ZnSe/(100) Ge layer, dislocations are present throughout the layer, whereas in the ZnSe/(100) GaAs layer, the dislocation network is confined to the first  $0.5 \mu\text{m}$  of material at the substrate/layer interface.

The reasons for the creation of the large dislocation densities in ZnSe grown on (100) Ge are unclear at present. However, it should be noted that ZnSe grown on (100) Ge with Ge buffers that vary in thickness from 1000 Å to 2 μm show significant improvement in material quality. Indeed, the DBE linewidth for ZnSe layers 2 μm thick grown on 0.6 μm thick Ge buffers at near optimum growth conditions was found to be about 0.7 meV. This is comparable with the best ZnSe grown on (100) GaAs to date.

Finally, the tilt between the (400) planes of ZnSe and the (100) Ge substrate was also found to exhibit a strong dependence on both film thickness and misorientation of the substrate surface from the (100) plane. The models proposed so far to explain the observations are at best crude, and certainly more work is required to elucidate the phenomenon.

SIMS analysis of films grown on Ge and on GaAs substrates revealed no less Ga in the ZnSe/Ge films than was found in the ZnSe/GaAs, so it no longer appears to be necessary to consider Ge substrates in order to avoid Ga autodoping.

### 3.2.2 Si Substrates

The concept of integrating compound semiconductors with Si is technologically attractive because of the promise of integrating high-speed electronic devices and optoelectronic devices with Si technology. In particular, considerable attention has recently been focused on the hetero-epitaxial growth of the technologically important semiconductor GaAs on Si. In addition, we have reported [24, 25] on the growth of ZnSe on Si. Although the application areas are different in these two cases, the experimental difficulties should be similar, as the lattice mismatch is approximately 4% in both cases. Our attempts to reduce the stress caused by this large mismatch by growing Ge and/or Ge/ZnSe superlattice buffer layers will be discussed in subsequent sections.

We reported [26] that the growth of single crystal ZnSe epilayers on (100) Si could be accomplished only if the growth was initiated very slowly. The surface was first exposed to just a Zn beam, and then the Se beam pressure was ramped up to its final value over a period of about 15 minutes. The low-temperature PL spectra for the resulting films were dominated by a strong, narrow peak ( $I_1^z$ ) at 2.788 eV which we proposed to be due to an acceptor-bound exciton.

### 3.2.3 Ge Buffer Layers

In order to avoid replication of substrate defects in the ZnSe epitaxial layer, and to provide an atomically smooth surface on which to initiate growth, Ge buffer layers were deposited on the sputter/annealed Ge surfaces prior to growth of the ZnSe layer. Ge layers were also grown on (100) Si substrates that were cleaned using the hot-sputter technique discussed earlier [24]. The growth temperature was 330°C and the growth rate was typically 0.33  $\mu\text{m/hr}$ . On initiation of the growth, the Si (2 x 1) surface reconstruction was replaced by the (2 x 2) reconstruction of the Ge surface. The Ge RHEED pattern is indicative of an atomically smooth (100) Ge surface. ZnSe layers grown on the Ge buffer to a thickness of 2 to 3  $\mu\text{m}$  appear to be rather rough as indicated by the RHEED patterns. PL measurements suggest that, indeed, the ZnSe layer quality is similar to that of the single-crystal ZnSe layers grown directly on the Si substrate.

It is worth noting, however, that the incorporation of the Ge buffer permitted the initiation of the ZnSe growth at regular growth rates. This is in contrast to our earlier reported results obtained growing ZnSe directly on Si [24].

### 3.2.4 ZnSe/Ge Superlattice Buffer Layers

The growth of superlattice (SL) buffer layers as a means to relieve strain and to confine impurities and mechanical defects to the substrate layers is becoming widely used in a variety of epitaxial growth systems. We have grown ZnSe/Ge SL buffer layers on (100) Si substrates prior to initiating growth of ZnSe epilayers.

Growth conditions were similar to those described above for the Ge buffer and ZnSe layer. The ZnSe and Ge layer thicknesses in the superlattice were both approximately 300Å. Whereas the ZnSe RHEED pattern appeared to deteriorate with each subsequent ZnSe layer, that of the Ge remained the same and showed a (2 x 2) reconstruction pattern. When deposition of extremely thin (i.e., about 60Å) alternate layers was attempted, a RHEED pattern characteristic of polycrystalline material developed. We conclude that a minimum alternate layer thickness greater than 60Å is required in order to maintain epitaxy in the ZnSe/Ge system under these growth conditions.

Two-period and ten-period superlattices were used as buffers between the ZnSe layer and the underlying (100) Si substrates. The results indicate that for the two-period superlattice buffer, the 2  $\mu\text{m}$  thick ZnSe epitaxial layer showed very good surface morphology as shown in Figure 3-9. In addition, cross-sectional TEM studies indicate a considerable reduction in the dislocation density in the ZnSe layer. Finally, 4.2K PL spectra show dominant excitonic emission for ZnSe on the two-period superlattice buffer. For ZnSe layers grown directly on the Si substrate, the emission spectrum is dominated by defect-related emission peaks such as  $\gamma_0$  and deep-level emission (see Figure 3-10). Quite narrow bound-exciton peaks ( $\sim 2$  meV linewidths) were measured from layers grown on the two-period superlattice indicating relatively high quality material. Indeed, by comparison, the bound-exciton linewidths for 2  $\mu\text{m}$  thick ZnSe grown in (100) Ge was typically 1.8 meV. The PL spectra recorded from layers grown on a ten-period superlattice showed little or no improvement over those obtained by growing ZnSe directly on Si. The mechanism responsible for the deterioration in the quality of the ZnSe layers in the thicker superlattices requires further investigation.

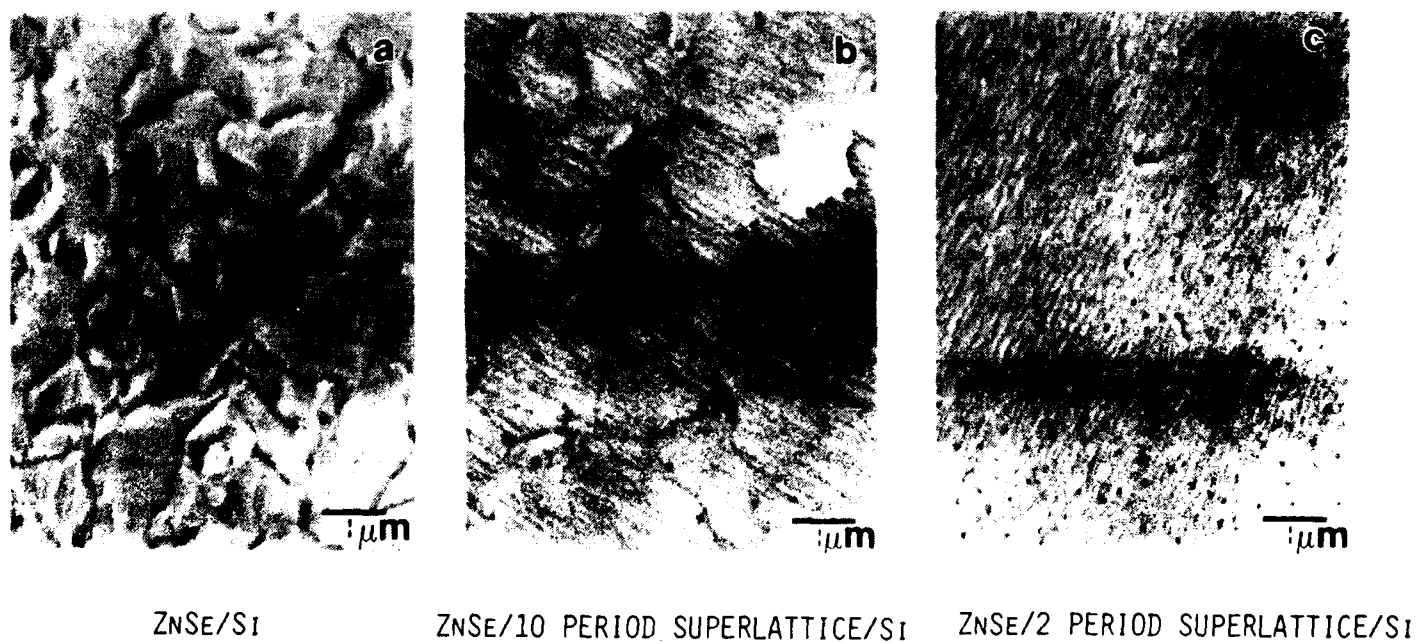


Figure 3-9. SEM micrographs of surface morphologies of ZnSe layers grown directly on Si and with superlattice buffers incorporated.

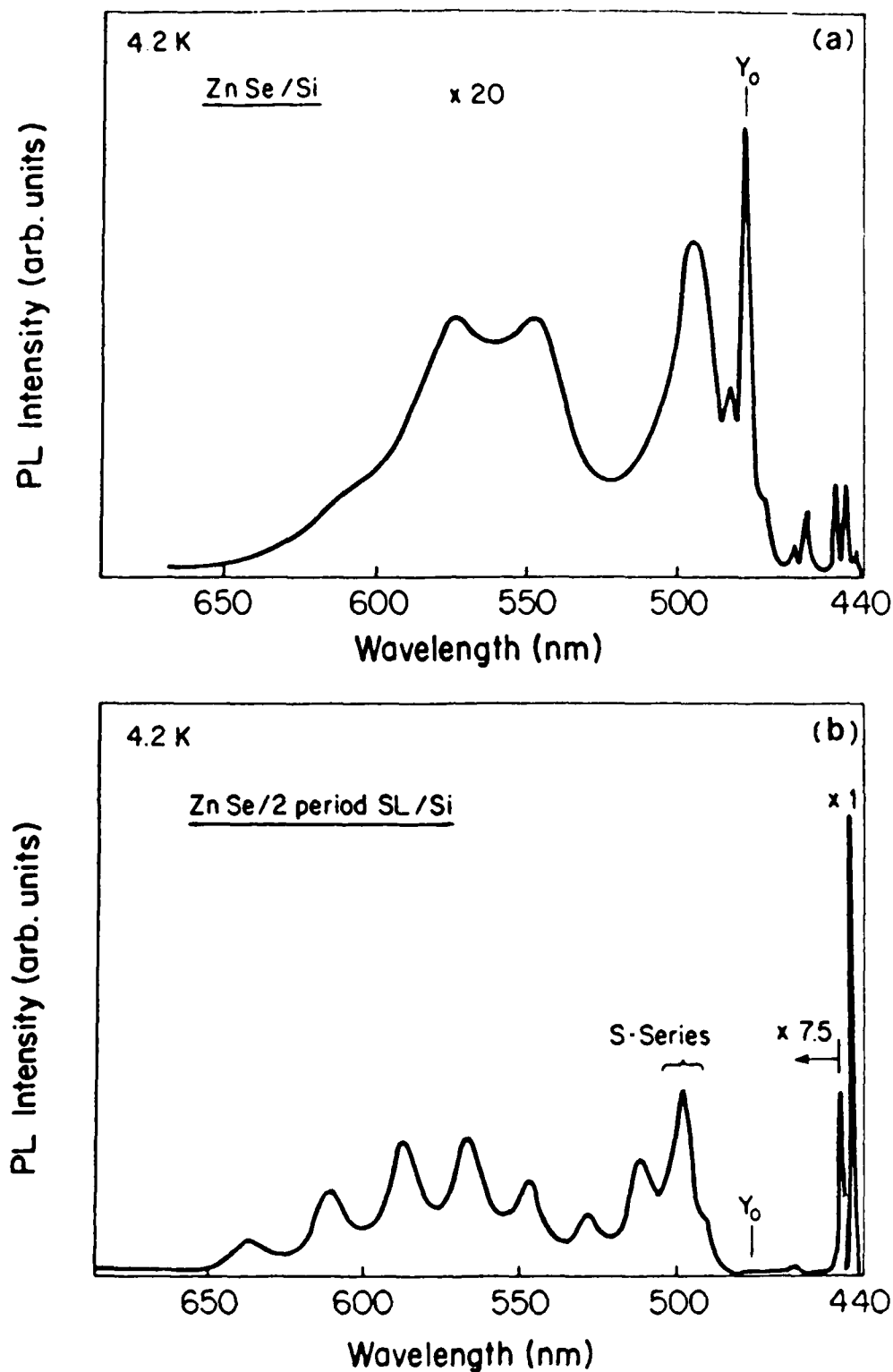


Figure 3-10. 4.2K PL spectrum of ZnSe on (100) Si with a two-period superlattice is dominated by excitonic emission. The PL emission spectrum of ZnSe grown directly on (100) Si is dominated by defect-related emission peaks.

### 3.3 p-Doping of ZnSe Films

The principal objective of this program of research was to investigate the possibility of obtaining p-type conductivity ZnSe. Previous attempts at growing this material by any growth technique were unsuccessful. The material appeared invariably to be either highly resistive and fully compensated or n-type. It was argued that on the basis of thermodynamics, the wide bandgap II-VI material would be highly compensated by native defects; in particular, ZnSe and especially ZnS could not be made p-type. The experimental results provided strong support for this thesis. However, there was also experimental evidence in the literature which suggested that compensation in ZnSe was principally due to unintentionally incorporated impurities. In fact, there were tantalizing reports that  $N^+$  ion-implanted ZnSe could be used to make p-n junctions, and that p-type conductivity could be obtained using Li. However, the results were not, or could not be, reproduced in other laboratories. Nonetheless, these results suggested that the question of making ZnSe p-type was still not satisfactorily answered, and that there was still a realistic possibility for blue/blue-green light-emitting devices. This notwithstanding, ZnSe has other attractive physical characteristics, such as its non-linear optical properties that make further investigation of the growth of this material worthwhile.

The p-doping candidates which have been studied in our laboratories to date are the following: N, P, Sb, Li, and Na. The results of these studies will be described for each of these elements in turn.

#### 3.3.1 N

Nitrogen doping of ZnSe films on (100) GaAs substrates was performed simply by bleeding  $N_2$  gas into the growth chamber through a high-precision leak valve and by allowing the establishment of the prescribed  $N_2$  pressures in the MBE chamber during growth. The growth conditions selected were a substrate temperature of 330°C and a beam pressure ratio of 10. Under these conditions, the layers were found to have low-temperature PL spectra dominated by free-excitonic related emission [27]. The layers were grown on sputter-cleaned/annealed GaAs substrates to a thickness of about 0.7  $\mu\text{m}$ .

Figure 3-11(a) shows the 4.2K PL excitonic spectrum recorded from the unintentionally-doped layer. Free excitonic-related emission is seen to dominate the spectrum. For the case of the N-doped layer, the spectrum is seen to be dominated by the acceptor-bound exciton peak ( $I_1$ ) at an energy of 2.793 eV. See Figure 3-11(b). In addition, the figure shows that the ratio of the acceptor-bound to the donor-bound exciton peaks is large. This is consistent with the further observation that the D-A pair emission is weaker than the dominant acceptor-bound excitonic emission.

Electrical measurements performed on the nitrogen-doped ZnSe samples have proven to be very difficult due to the high-resistivity of these samples. However, although the samples were found to be too resistive for Hall measurements, the carrier type could be determined from contact studies. The results indicate that the material is high-resistivity n-type, in spite of the low-temperature PL results.

SIMS measurements of the N-doped samples were seriously hindered by the large background concentration of nitrogen in the SIMS chamber. An attempt was made to determine the nitrogen concentration in the ZnSe, but the results are inconclusive. However, the relatively narrow linewidth of the acceptor-bound exciton peak ( $\sim 1.1$  meV) suggests a low nitrogen concentration.

### 3.3.2 P

We have incorporated P into the growing ZnSe layers at concentrations in excess of  $1 \times 10^{17} \text{ cm}^{-3}$  using a P-compound ( $\text{Zn}_3\text{P}_2$ ) source [28]. A series of films grown using different  $\text{Zn}_3\text{P}_2$ -cell temperatures showed that the incorporation of donors, apparently from the  $\text{Zn}_3\text{P}_2$  source, begins at a lower temperature than that at which P begins to be incorporated into the film. As the  $\text{Zn}_3\text{P}_2$ -cell temperature increases, the acceptor concentration increases more slowly than the donor concentration. The increased donor concentration must be due to extrinsic donors from contaminated  $\text{Zn}_3\text{P}_2$  source material, rather than to intrinsic defects accompanying the incorporation of acceptor atoms. With decreasing growth temperature, the concentration of acceptors increases while the mobility and the net (electron) carrier concentration decrease. In the PL spectra we find a dramatic increase in the deep level emission as we incorporate more P-atoms. See Figure 3-12. Thus, it appears that phosphorous is not a good candidate for p-type doping in ZnSe.

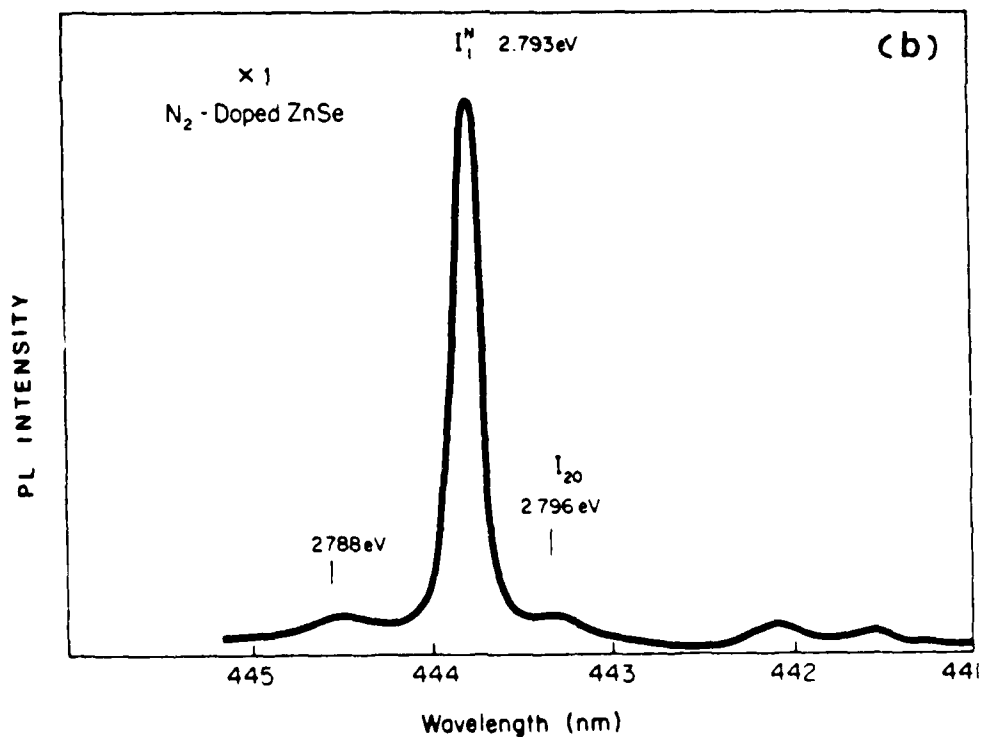
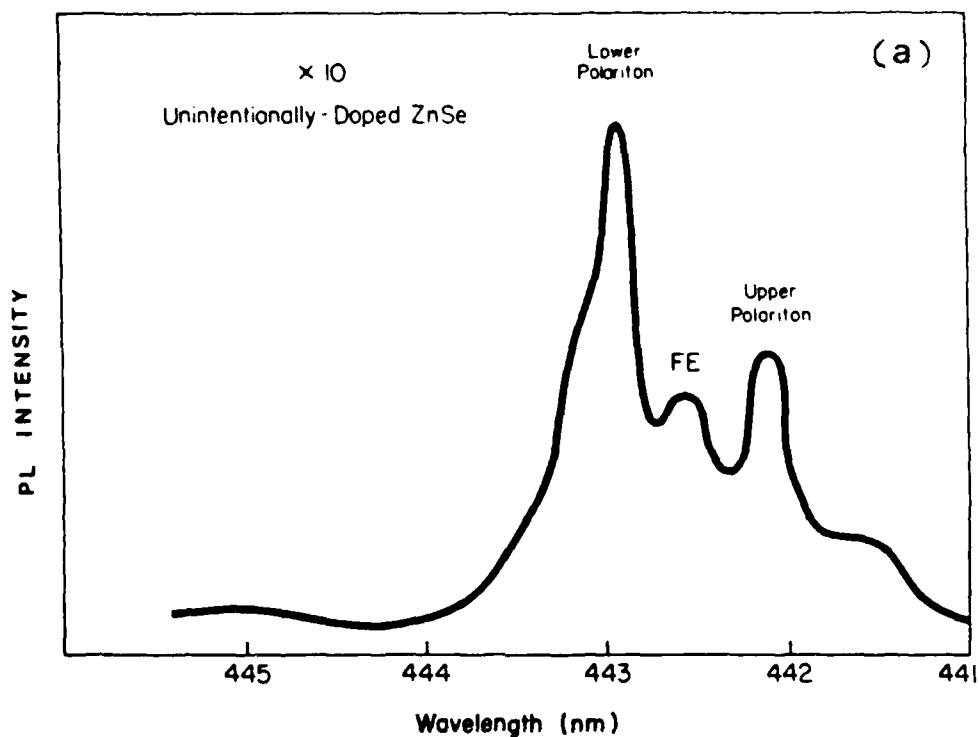


Figure 3-11. (a) 4.2K PL excitonic spectrum of unintentionally-doped ZnSe is dominated by free excitonic-related emission. (b) Spectrum of n-doped ZnSe layer is dominated by the acceptor-bound excitonic peak,  $I_1$ .

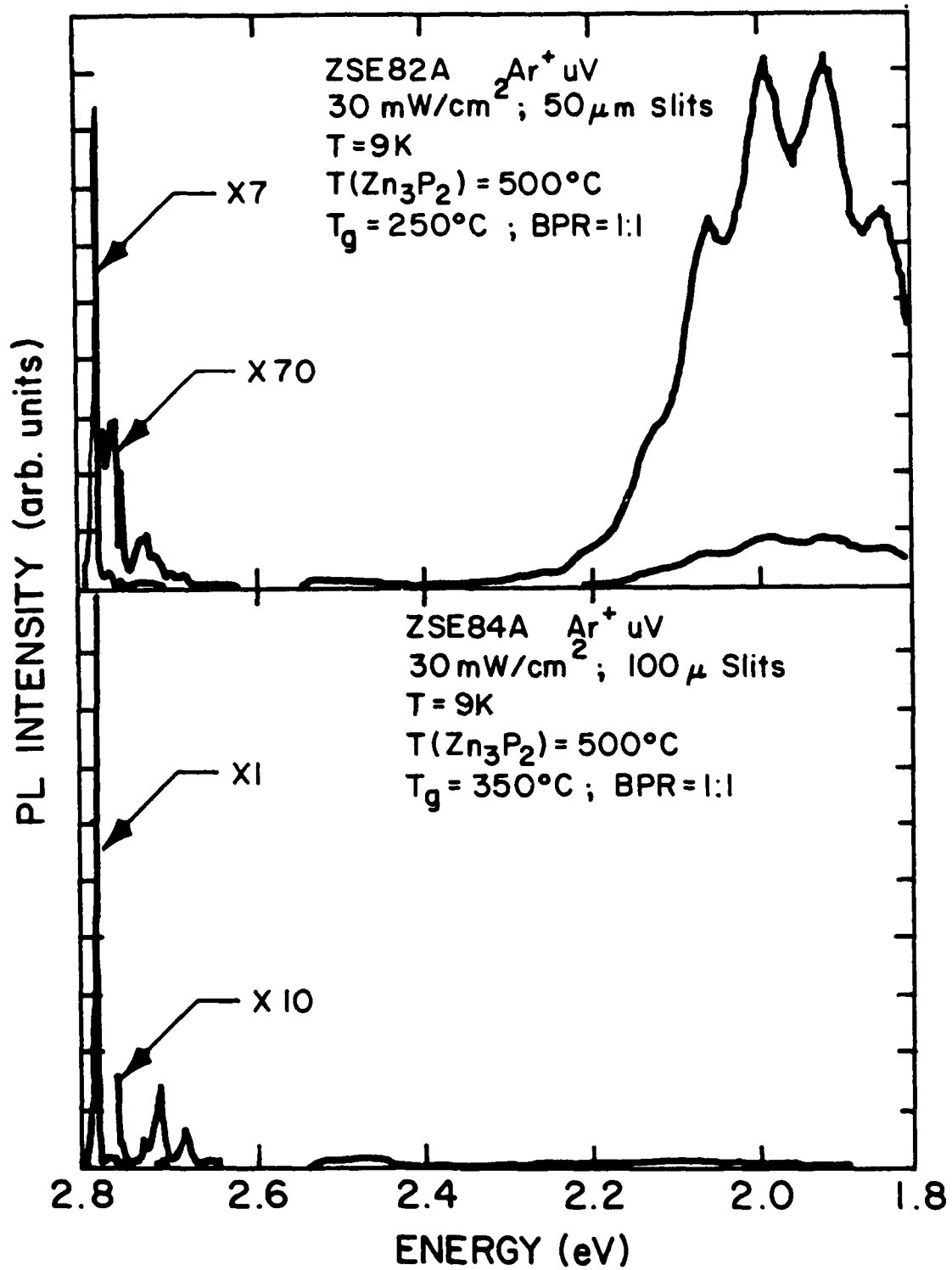


Figure 3-12. 9K PL spectra of lightly (lower) and a heavily (upper) phosphorous-doped ZnSe films, showing a dramatic increase in the deep level emission as the P-concentration increases.

While it is possible to incorporate P atoms into the ZnSe lattice, at even modest levels P begins to form deep levels rather than shallow acceptor states. Behavior of this sort had been proposed to explain some earlier attempts at P-doping in ZnSe [29] and our results support those suggestions. In this case, our knowledge of the ZnSe MBE growth matrix space and our attempts to use this information to alter the incorporation of P were of no avail. P simply appears to be an unsuitable p-doping candidate.

### 3.3.3 Sb

Of the Group V elements which are candidate p-type dopants substituting for Se in the ZnSe lattice, only Sb to our knowledge has not been investigated as a potential dopant. N, As, and P were used in dopant studies. Nitrogen was also used as reported above, but so far these efforts did not produce low-resistivity p-type material. However, recent work has shown [30] that Sb forms a shallow acceptor in CdTe.

Sb-doped ZnSe layers were grown and characterized using low-temperature PL, DCRC, and SIMS measurement techniques [31]. Sb concentrations were determined using an impinging ion beam of approximately 1 microampere  $O^+$  with positively-charged secondary ions at masses 121 and 123 amu being detected. Quantitation was achieved using standards prepared by ion implantation of known doses of  $^{121}\text{Sb}$  into epitaxial ZnSe layers with the peak implanted Sb concentration reaching about  $7 \times 10^{18} \text{cm}^{-3}$ . The detection limit by SIMS for Sb in ZnSe is estimated to be about  $5 \times 10^{15} \text{cm}^{-3}$ . The layers in this study were all grown on conducting GaAs substrates [oriented  $2^\circ$  off (100) towards (110)] in order to reduce charging effects in the SIMS measurements.

Analysis of SIMS measurements [31] suggest that at the optimum growth conditions, namely  $330^\circ\text{C}$  and a Zn/Se beam pressure ratio of unity, the Sb incorporation coefficient is  $\sim 10^{-2}$ . Furthermore, the analysis indicates it is possible to incorporate Sb to concentrations as high as  $10^{19} \text{cm}^{-3}$ . However, at these concentrations the layer is found to be optically dead. Indeed, RHEED measurements of these layers indicate a mixed polycrystalline/single crystalline material. On the other hand  $(2 \times 1)$  reconstructed ZnSe surfaces were observed with Sb concentrations less than  $10^{17} \text{cm}^{-3}$ .

When the substrate was exposed to moderate Sb flux levels, it is interesting to note that:

- (i) the 1/2-order diffraction lines in the (110) azimuth, normally associated with Se-stabilization, became intense, and
- (ii) the Kikuchi bands were better defined upon initial opening of the Sb shutter.

Such RHEED observations would normally be indicative of an improvement in the crystallographic quality of the surface.

Low temperature PL measurements of Sb-doped layers with Sb concentrations less than  $10^{17} \text{ cm}^{-3}$  indicate that neither acceptor-bound excitonic emission nor donor-acceptor pair transitions were detected in the spectra. However, the analysis also indicated that defect-related emission lines were enhanced with the increasing concentration of Sb impurities. For example, the so-called  $I_1^{\text{deep}}$  emission line at 445.5 nm and the  $Y_0$  and  $S_0$  bands, attributed in the literature to extended defects, were observed to increase significantly in intensity with increasing Sb concentration.

Thus, although it appears that Sb can be incorporated quite readily in MBE-grown ZnSe to concentrations in excess of  $10^{19} \text{ cm}^{-3}$  (single-crystal limit,  $\geq 10^{19} \text{ cm}^{-3}$ ), the impurity does not appear to produce a shallow acceptor. The results suggest that p-type ZnSe appears unlikely by MBE using Sb as the dopant species.

Recently, we have been able to improve the quality of the Sb-doped films by illuminating the surface with an  $\text{Ar}^+$ -ion laser during growth. We find that the films' surface morphology improves when the growth is laser assisted. In spite of this improvement, Sb still appears to be an unsuitable p-dopant in ZnSe. However, the experience we have gained in laser-assisted growth will be transferable to our studies of other systems.

#### 3.3.4 Li

Li has been used for doping of ZnSe in two previous reports of p-type conversion, one by a bulk-growth method [32] and the other by MOCVD [33]. There have been no previous reports in the literature of attempts to use Li in MBE growth.

We have undertaken an extensive study of Li-doping of MBE-grown ZnSe. The results of this study have been quite promising, culminating in the first demonstration of p-type ZnSe by MBE growth.

We have incorporated Li concentrations as high as  $5 \times 10^{19} \text{ cm}^{-3}$  as determined by SIMS. The low-temperature PL spectrum for heavily Li-doped material (Figure 3-13) is dominated by a strong, narrow acceptor-bound exciton peak, and there is little donor-acceptor pair (DAP) emission, in spite of the fact that the Li source material that was used was only of moderate purity. SIMS analysis has indicated the presence of a large number of impurities in the Li-doped films that were not present in the undoped films. These impurities bear a one-to-one correspondence to those present in the Li source material. While unintentionally-incorporated donor impurities may be compensating some of the Li acceptors, our I-V measurements using various combinations of Au and In contacts (Figure 3-14) did show evidence of p-type conduction, although the film resistivities were quite high [34]. More recent measurements have given indications that the actual hole concentrations may be considerably larger than what our I-V measurements have led us to believe. Our previous work on intrinsic ZnSe has proved quite valuable in the Li-doping study as it has suggested to us ways to alter the mode of incorporation of Li by altering the Zn/Se beam-pressure ratio (BPR). Our success in this study gives us reason to be optimistic about the prospects for achieving high-conductivity p-ZnSe by Li-doping. We intend to pursue this approach using higher-purity starting material obtained by locating a vendor who can supply such material or by doing our own distillation of available Li metal. With purer starting materials, we will be compensating fewer of our incorporated Li acceptors. Then as we continue to adjust the growth conditions we should be able to optimize the carrier (hole) concentrations. Our studies of Li diffusion have alerted us to potential problems arising from diffusion of Li ions through the lattice. These difficulties will have to be taken into account in the design of devices based on this material.

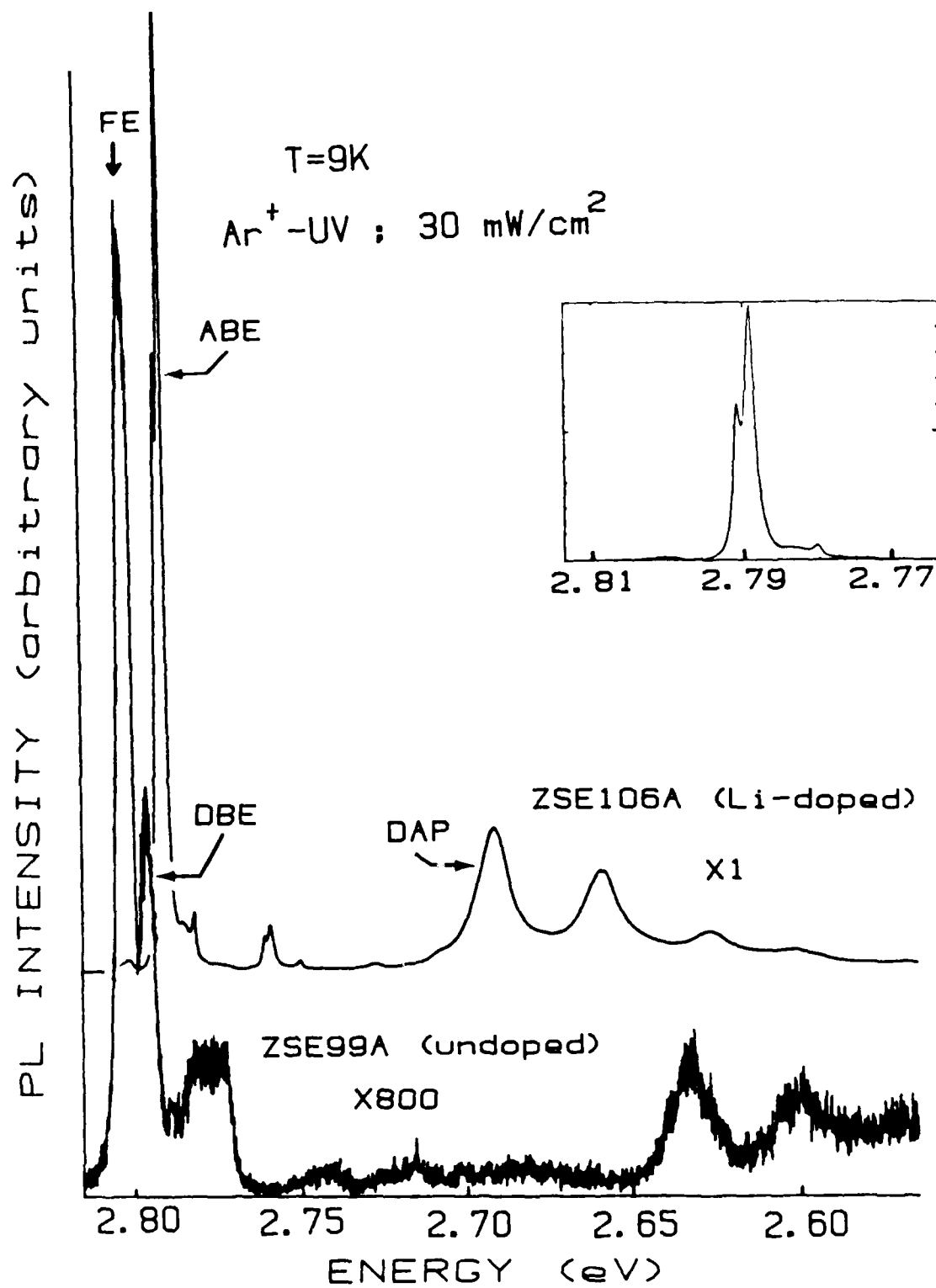


Figure 3-13. 9K PL spectra for an undoped (ZSE99A, lower curve) and a Li-doped (ZSE106A, upper curve) ZSE film. The inset shows the near-band-edge emission for the Li-doped film. The ABE emission is seen to be a doublet.

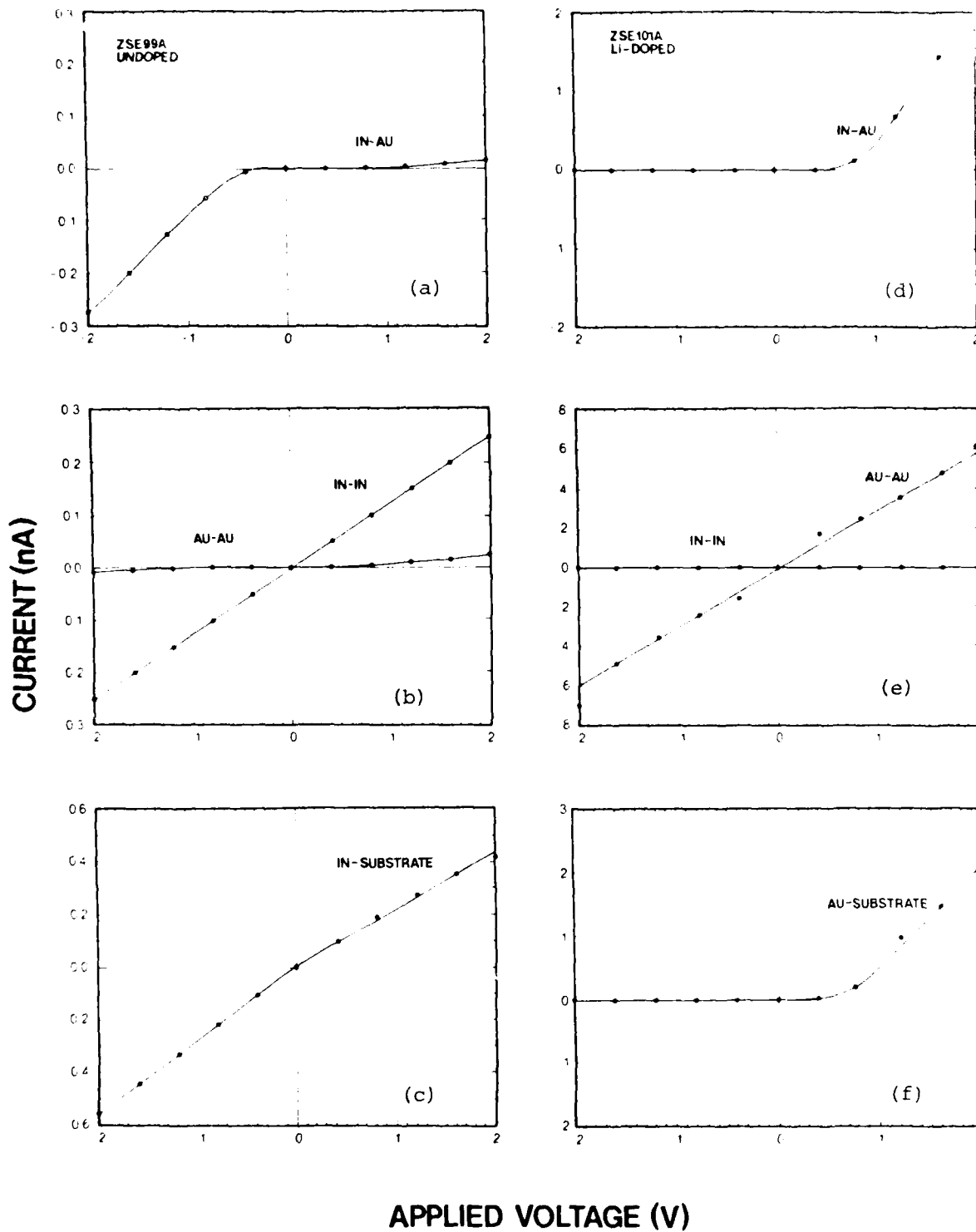


Figure 3-14. I-V characteristics for an undoped [ZSE99A, (a) - (c)] and a Li-doped [ZSE101A, (d) - (f)] ZnSe film using different metal contacts and electrode configurations. The In contact is positive for (a) - (c) and the Au contact is positive for (d) - (f).

### 3.3.5 Na

Based on considerations of ionic radius, Na is expected to be an excellent candidate for p-doping in ZnSe. There have been preliminary reports in the literature on Na-doping by MBE [35, 36]; they found some evidence for Na incorporation through the appearance of DAP emission in the PL spectrum.

As was the case with Li, the major problem seems to be to find a suitable source of Na. We have approached this problem in two ways, using first a compound source,  $\text{Na}_2\text{Se}$ , and secondly a unique proprietary source.

Using a source of  $\text{Na}_2\text{Se}$ , we have found very strong evidence that the source material was heavily contaminated and acted as a source of donors which caused our films to become more strongly n-type as we attempted to incorporate more acceptors [28]. PL measurements were dominated by a donor-bound exciton peak which grew in strength as the Na-cell temperature increased, confirming the incorporation of additional donors. This increase in the DBE peak began at relatively low Na-cell temperatures, even before any donor-acceptor pair spectra appeared or before the Na concentration exceeded the lower level of detectability in SIMS. Selectively-excited PL measurements indicated the presence of enhanced levels of Cl in the films, and this was confirmed quantitatively by SIMS. The Cl concentration exceeds the Na concentration and, in fact, is very nearly equal to the measured free electron concentration. The K concentration is also much higher in the film than in the Na starting material. Apparently these species are either preferentially emitted by the source or preferentially incorporated into the film. In either case, this result is critical since it suggests that, in all previous trials at Na-doping, contaminants were incorporated in concentrations exceeding those of the Na. Therefore, the actual behavior of Na in ZnSe had never been tested, but rather the effects produced by the unintentionally incorporated impurities.

In order to obtain a much cleaner Na beam, we have begun using a 3M proprietary source of Na, referred to in these reports as Na source #2. Our measurements using this source indicate that we are indeed getting a clean Na beam from this source. The quadrupole mass analyzer in the MBE chamber can detect nothing but Na coming from the source, and SIMS analysis reveals no incorporated impurities, other than Na, at levels in excess of those in an undoped film. Electrically, these films have high-resistivity but are

still n-type. PL spectra for lightly-Na-doped films show some DAP emission, indicating the incorporation of Na into the lattice. However as the Na concentration increases, the PL spectra are increasingly dominated by a large, broad band near 2.6 eV. See Figure 3-15. A  $\gamma_0$  peak at this energy has been ascribed to the presence of impurities near extended dislocation loops. We are looking into the possibility that either the Na is encouraging the propagation of dislocation loops from the interface into the growing film, or that the Na is itself causing the formation of extended defects in the lattice. Several questions remain to be answered about the suitability of Na as a p-type dopant in ZnSe, but we are gaining confidence that we are, for the first time, exploring the intrinsic behavior of Na itself as an impurity in ZnSe.

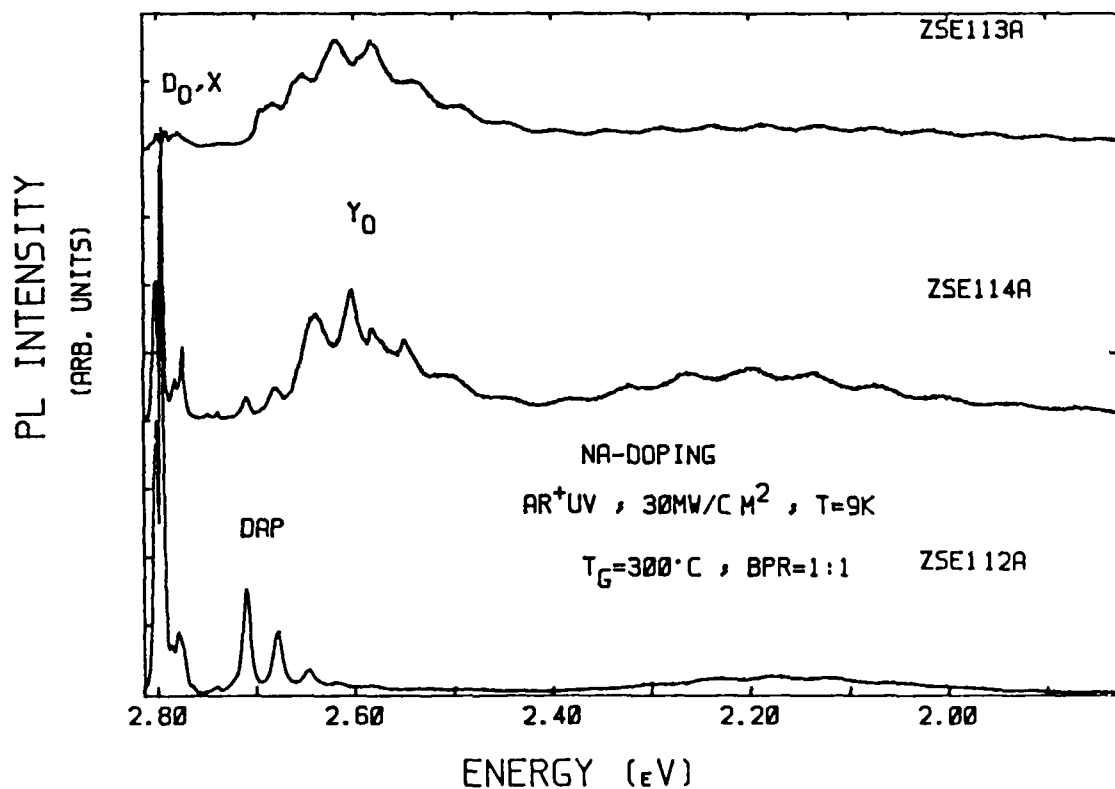


Figure 3-15. 9K PL spectra for three Na-doped samples. The Na concentration was increased in this series by increasing the Na source oven temperature.  $T_G = 300^\circ\text{C}$  and BPR = 1:1 for all three samples.  $[\text{Na}] = 3 \times 10^{16}$ ,  $2.5 \times 10^{17}$ , and  $1 \times 10^{18} \text{ cm}^{-3}$  for samples ZSE112A, ZSE114A, and ZSE113A, respectively.

### 3.4 Electron-Beam Pumping of ZnSe Laser Cavities

In order to study the lasing properties of ZnSe prior to constructing a suitable p-n junction for carrier injection, we have used a pulsed high voltage electron beam source to inject carriers into ZnSe cavities prepared by cleaving MBE-grown ZnSe films on their GaAs substrates. We have observed and reported lasing in 2  $\mu\text{m}$ -thick films [37] with thresholds as low as 4  $\text{A}/\text{cm}^2$  (at 40 kV, temperature 16 - 100K), comparable to the best results obtained in thicker films of material grown by alternate techniques. The threshold increased with increasing incident electron accelerating voltage,  $V_{acc}$ , reflecting the penetration of the beam beyond the ZnSe film at this small thickness. Later, working with thicker films ( $t = 4 - 4.5 \mu\text{m}$ ), we found the threshold reduced to less than 2  $\text{A}/\text{cm}^2$  (40 kV, 16K) [38]. See Figure 3-16. With this reduced threshold, we were able to observe lasing at temperatures as high as room temperature. Our study of the lasing wavelength and our measurements of the gain profiles have lead us to a tentative identification of an exciton-electron scattering process as the lasing mechanism in the low temperature ( $< 100\text{K}$ ) regime [38]. We have recently reported the results of our comparison of lasing thresholds in MBE- and OMVPE (or MOCVD)-grown materials [39]. We find that the MBE-grown films exhibit lower thresholds than their OMVPE counterparts by a factor of at least 2.5. However, we feel that this difference is due in large part to a poorer surface morphology on the OMVPE films, rather than to an intrinsic superiority of the MBE material for this purpose.

### 3.5 Metal Contacts to ZnSe

We have undertaken contact studies in order to (i) understand and characterize the formation of Ohmic and Schottky contacts to n- and p-type ZnSe, and (ii) to improve the adhesion of contacts to ZnSe for subsequent wire bonding during device fabrication.

We have developed procedures for making Ohmic contacts to n-ZnSe which have a reliability rate of better than 95%. These procedures involve placing and pressing small chips of In metal onto the sample surface, and then annealing in an Ar-H gas mixture at 300°C for 5 minutes.

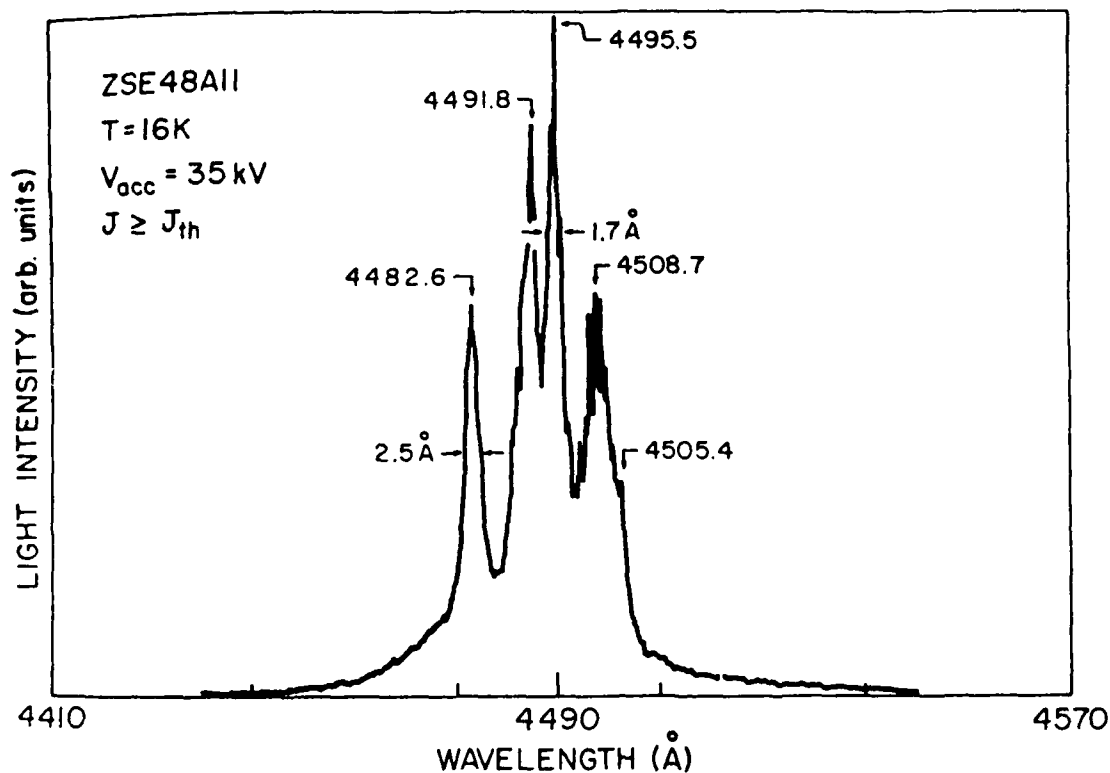


Figure 3-16. 16K lasing spectrum of a 4.3  $\mu\text{m}$  ZnSe cavity at 35 kV and an electron beam current just above threshold ( $J_{th} = 2 \text{ A/cm}^2$ ).

Although our procedures for making contacts to n-ZnSe for routine laboratory measurements have been extremely successful, this approach is not appropriate for actual optoelectronic device fabrication since these contacts are not optically transparent and not adaptable to thin film techniques. Several studies have been done in attempting to develop thin film Ohmic contacts to ZnSe. These include the evaporation of thin In contacts, evaporation of Al contacts, evaporation of In alloys, and construction of layered contacts.

Indium is the most commonly-used metal for making Ohmic contacts to n-ZnSe. We have found evidence for island formation of In, due to the high surface tension of In, and correlated this behavior with diminished contact performance. We have found that a thin Al overlayer prevents strong segregation of the In, which then forms a continuous layer.

Further attempts to reduce the problem of island formation seen with evaporated In were made by introducing a thin wetting layer prior to the deposition of the In contact. In this study a thin film of Ni

(approximately 5-10 Å) was used as the wetting layer. The insertion of the thin Ni wetting layer was successful in suppressing the formation of islands. The electrical properties of the contacts, however, were still not adequate for use in device applications.

The understanding of Ohmic contact formation to p-ZnSe is far from adequate at this time. The only reports of Ohmic contacts to p-ZnSe in the literature are for Au. From our measurements on Li-doped films we have found that the contact characteristics for Au on p-ZnSe are very poor. First of all, it was found that the majority of the applied voltage is dropped across the contact rather than across the bulk of the semiconductor. Secondly, the adhesion of Au to ZnSe is very poor. Our initial attempts at forming Ohmic contact to p-ZnSe relied on the evaporation of Au. The "as deposited" contacts did not show good Ohmic behavior and all subsequent heat treatments caused further degradation of the contacts. The substitution of evaporated Cu for Au resulted in better adhesion of the contact, but no improvement (or degradation) was found in the electrical properties.

It is generally found that forming Ohmic contact to p-type semiconductors is more difficult than making Ohmic contact to n-type materials. Increasing the bandgap of the semiconductor also generally increases the difficulty of Ohmic contact formation. In our lab we have found that reliable contacts to n-ZnSe can be made under certain situations, but that good contacts to p-ZnSe have not been possible.

A second fundamental application of metal/semiconductor contacts is in the formation of Schottky barriers. For Schottky barrier contacts, we find that the reproducibility and reliability of the contacts increases in the order Au, Au/Pd, Au/Cr, Au/Al; i.e., in order of increasing reactivity of the metal used. Planar Au Schottky barrier measurements, when compared to transverse measurements through a ZnSe/n<sup>+</sup>-GaAs interface, indicate that interface band discontinuity is largely responsible for the low forward bias current observed in Schottky barrier structures. Analyzing the I-V results using a thermionic emission model, we have found an interface barrier height of  $0.4 \pm 0.2$  eV.

#### 4.0 REFERENCES

1. Quarterly Technical Progress Report No. 3, Blue-Green Laser Diode Research Program. Prepared under DARPA Contract No. N00014-85-C-0552, January, 1987.
2. Quarterly Technical Progress Report No. 4, Blue-Green Laser Diode Research Program. Prepared under DARPA Contract No. N00014-85-C-0552, Rev. May, 1987.
3. H. Nagai, J. Appl. Phys., 45, 3789 (1974).
4. M. Kroemer, K.J. Polasko, and S.C. Wright, Appl. Phys. Lett., 36 763 (1980).
5. J.C. Phillips, "Bonds and Bands in Semiconductors," Academic Press, London and New York (1973).
6. L. Pauling, "The Nature of the Chemical Bond," Cornell University Press, New York (1960).
7. S. Myhajlenko, J.L. Batstone, H.J. Hutchinson and J.W. Steeds, J. Phys. C: Solid State Phys. 17, 6477 (1984).
8. R.N. Bhargava, R.J. Seymour, B.J. Fitzpatrick, and S.P. Herko, Phys. Rev. B 20, 2407 (1979).
9. G.F. Neumark, B.J. Fitzpatrick, P.M. Harnack, S.P. Kerko, R. Kosai, and R.N. Bhargava, J. Electrochem. Soc: S. State Sci. and Technol. 127, 983 (1980).
10. H. Cheng, J.M. DePuydt, J.E. Potts, S.K. Mohapatra, and T.L. Smith, in Proc. of SPIE Conf. on Growth of Compound Semiconductors (SPIE v.796; Bay Point, Fl; March, 1987), p.91. J.M. DePuydt, H. Cheng, J.E. Potts, T.L. Smith, and S.K. Mohapatra, J. Appl. Phys. 62, 4756 (1987).
11. J.E. Potts, H. Cheng, S. Mohapatra, and T.L. Smith, J. Appl. Phys, 61, 333 (1987).
12. J. Kleiman, R.M. Park, S.B. Qadri, J. Appl. Phys. 61, 2067 (1987).
13. T.L. Smith, H. Cheng, S.K. Mohapatra, and J.E. Potts, J. Vac. Sci. and Technol. B 5, 1326 (1987).
14. J.E. Potts, T.L. Smith, and H. Cheng, in Proc. of SPIE Conf. on Modern Optical Characterization Techniques for Semiconductors and Semiconducting Devices (SPIE v.794, Bay Point, FL, March, 1987), p.27.
15. T. Mitsuyu, K. Ohkawa and O. Yamazaki, Appl. Phys. Lett. 49, 1348 (1986).
16. H.E. Ruda, J. Appl. Phys. 59, 1220 (1986).
17. H.E. Ruda, J. Appl. Phys. 59, 3516 (1986).
18. H.E. Ruda, submitted to J. Appl. Phys.
19. H.E. Ruda, J. Appl. Phys. 61, 3035 (1987).

20. H.E. Ruda, R.M. Park, H.A. Mar and N.M. Salansky, J. Vac. Sci. and Technol. B 3, 1637 (1985).
21. R.M. Park and H.A. Mar, J. Mater. Res., 1 (4), 543 (1986).
22. R.M. Park, J. Kleiman, and H.A. Mar, Proceedings of SPIE: Growth of Compound Semiconductors, 26-27, March, 1987, Bay Point, Florida.
23. J. Kleiman, R.M. Park, and S.B. Qadri, J. Appl. Phys., 61 (5), 2067 (1987).
24. R.M. Park and H.A. Mar, Appl. Phys. Lett., 48 (8), 529 (1986).
25. R.M. Park, J. Kleiman, and H.A. Mar, J. Cryst. Growth (1987), accepted for publication.
26. R.M. Park and H.A. Mar, Appl. Phys. Lett. 48, 529 (1986).
27. Quarterly Technical Progress Report No. 3, pp. 49-55, R.M. Park, H.A. Mar, and N.M. Salansky, J. Appl. Phys, 58 (2), 1047 (1985).
28. J.M. DePuydt, T.L. Smith, J.E. Potts, H. Cheng, and S.K. Mohapatra, Proc. Third Int'l. Conf. on II-VI Semiconductors, Monterey, CA, July, 1987 (to be published in J. Cryst. Growth).
29. T. Yao and Y. Okada, Jpn. J. Appl. Phys., 25, 821 (1986).
30. R.N. Bicknell, N.C. Giles, and J.F. Schetzina, Appl. Phys. Lett., 49 (25), 1735 (1986).
31. R.M. Park, J. Kleiman, H.A. Mar, and T.L. Smith, submitted to Applied Physics Letters.
32. J. Nishizawa, K. Itoh, Y. Okuno, and F. Sakurai, J. Appl. Phys. 57, 2210 (1985).
33. H. Kukimoto, presented at Semicond. Conf.; Tokyo; March, 1987.
34. H. Cheng, J.M. DePuydt, J.E. Potts and T.L. Smith, Appl. Phys. Lett. 52, 147 (1988).
35. T. Yao and T. Taguchi, to appear in J. Electr. Mater.
36. T. Yao and T. Takeda, to appear in J. Vac. Sci. and Technol.
37. J.E. Potts, T.L. Smith and H. Cheng, Appl. Phys. Lett. 50, 7 (1987).
38. T.L. Smith, J.E. Potts, and H. Cheng, 1987 Conf. on Lasers and Electro-Optics; Baltimore, MD; April 27-May 1, 1987.
39. J.E. Potts, T.L. Smith, H. Cheng, B. Yang and B.W. Wessels, Proc. Third Int'l. Conf. on II-VI Semiconductors, Monterey, CA, July, 1987 (to be published in J. Cryst. Growth).

## 5.0 PUBLICATIONS RESULTING UNDER ONR CONTRACT NO. N00014-85-C-0552

The following is a list of publications resulting from full or partial support by DARPA under ONR Contract No. N00014-85-C-0552.

### 5.1 Refereed Papers

"Effects of Beam Pressure Ratios on Film Quality in MBE Growth of ZnSe", H. Cheng, S.K. Mohapatra, J.E. Potts and T.L. Smith, *J. Cryst. Growth* 81, 512 (1987); publ. proc. of Fourth Int'l. Conf. on MBE; York, UK; Sept., 1986.

"X-Ray Diffractometry Measurements of Lattice Parameter Dependence on Layer Thickness for the ZnSe/GaAs System Grown by MBE"; S.B. Qadri, R.M. Park, J. Kleinman and H.A. Mar, *J. Cryst. Growth* 81, (1987); publ. proc. of Fourth Int'l. Conf. on MBE; York, UK; Sept., 1986.

"Effect of Elastic Strain on the Energy Band Gap in Heteroepitaxially Grown ZnSe", J.E. Potts, H. Cheng, S.K. Mohapatra and T.L. Smith, *J. Appl. Phys.* 61, 333 (1987).

"Electron Beam Pumped Lasing in ZnSe Grown by Molecular Beam Epitaxy", J.E. Potts, T.L. Smith and H. Cheng, *Appl. Phys. Lett.* 50, 7 (1987).

"Growth and Photoluminescence Characterization of ZnSe Layers Grown on (100) Ge by Molecular Beam Epitaxy"; R.M. Park and H.A. Mar, *J. Mater. Res* 1, 543 (1986).

"Molecular Beam Epitaxial Growth of High Quality ZnSe on (100) Si"; R.M. Park and H.A. Mar, *Appl. Phys. Lett.*, 48, 529 (1986).

"A Theoretical Analysis of Electron Transport in ZnSe"; H.E. Ruda, *J. Appl. Phys.* 59, 1220 (1986).

"Determination of the Onset of Plastic Deformation in ZnSe Layers Grown on (100) GaAs by Molecular Beam Epitaxy"; J. Kleinman, R.M. Park and S.B. Qadri, *J. Appl. Phys.* 61, 2067 (1987).

"A Theoretical Study of Electron Mobility in a Two-Dimensional Electron Gas Confined at a Lattice-Matched ZnSe-Zn (S,Te) Heterointerface"; H.E. Ruda, submitted to *J. Appl. Phys.*

"Application of Free Carrier Absorption to n-ZnSe Materials Characterization"; H.E. Ruda, *J. Appl. Phys.* 61, 3035 (1987).

"Theoretical Study of Hole Transport in ZnSe"; H.E. Ruda, *J. Appl. Phys.* 59, 3516 (1986).

"Secondary Ion Mass Spectrometry Studies of Al, Ga, and In Unintentional Donors in ZnSe Epilayers on GaAs"; T.L. Smith, H. Cheng, S.K. Mohapatra and J.E. Potts; *J. Vac. Sci. Technol. B* 5, 1326 (1987).

"Growth of Undoped ZnSe on (100) GaAs by Molecular Beam Epitaxy: An Investigation of the Effects of Growth Temperature and Beam Pressure Ratio"; J.M. DePuydt, H. Cheng, J.E. Potts, T.L. Smith and S.K. Mohapatra; *J. Appl. Phys.*, 62, 4756 (1987).

"Detection and Control of Impurity Incorporation in MBE-Grown ZnSe"; J.M. DePuydt, T.L. Smith, J.E. Potts, H. Cheng and S.K. Mohapatra, to appear in J. Cryst. Growth; publ. proc. Third Int'l. Conf. on II-VI Semiconductors; Monterey, CA; July, 1987.

"ZnSe and ZnSe/Ge Epilayers Grown on (100) Si by Molecular Beam Epitaxy"; R.M. Park, H.A. Mar and J. Kleiman, to appear in J. Cryst. Growth; publ. proc. of Third Int'l. Conf. on II-VI Semiconductors; Monterey, CA; July, 1987.

"Electron-Beam-Pumped Lasing in Epitaxial ZnSe Thin Films"; J.E. Potts, T.L. Smith, H. Cheng, B. Yang and B. Wessels, to appear in J. Cryst. Growth; publ. proc. Third Int'l. Conf. on II-VI Semiconductors; Monterey, CA; July, 1987.

"Room Temperature Excitonic Optical Nonlinearities of MBE-Grown ZnSe Thin Films"; N. Peyghambarian, S.H. Park, S.W. Koch, A. Jeffery, J.E. Potts and H. Cheng; to appear in Appl. Phys. Lett. (Jan. 11, 1988).

"Growth of p-type ZnSe:Li by Molecular Beam Epitaxy"; H. Cheng, J.M. DePuydt, J.E. Potts and T.L. Smith, Appl. Phys. Lett. 52, 147 (1988).

"Elastic Properties of Epitaxial ZnSe (001) Films on GaAs Measured by Brillouin Spectroscopy"; S. Lee, B. Hillebrands, G.I. Stegeman, H. Cheng, J.E. Potts and F. Nizzoli; to appear in J. Appl. Phys.

"Evidence for the Existence of Guided Longitudinal Acoustic Phonons in ZnSe Films on GaAs"; B. Hillebrands, S. Lee, G.I. Stegeman, H. Cheng, J.E. Potts and F. Nizzoli; subm. to Phys. Rev. Lett.

"On Accurate Epilayer Tilt Determination by Double Crystal Rocking Curve X-Ray Analysis"; J. Kleiman, R.M. Park and H.A. Mar; to be published in Journal of X-Ray Science and Technology.

"Antimony-Doped ZnSe Grown by Molecular Beam Epitaxy"; R.M. Park, J. Kleiman, H. Mar and T.L. Smith; to be published in the Journal of Applied Physics, April, 1988.

"Band Gap Discontinuities for Ge/ZnSe (100) and Si/ZnSe (100): A Photoemission Study"; F. Xu, M. Vos, J.P. Sullivan, Lj. Atanasoska, S.G. Anderson, J.H. Weaver and H. Cheng, submitted to Phys. Rev. B.

"On Epilayer Tilt in ZnSe/Ge Heterostructures Prepared by Molecular Beam Epitaxy", J. Kleiman, R.M. Park and H. Mar; submitted to J. Appl. Phys.

## 5.2 Published Conference Proceedings (not refereed)

"Molecular Beam Epitaxial Growth of ZnSe on (100) GaAs Substrates"; H. Cheng, J.M. DePuydt, J.E. Potts, S.K. Mohapatra and T.L. Smith; to appear in SPIE Conf. Proc. #796, Growth of Compound Semiconductors; Bay Point, FL; March, 1987, p.91.

"Photoluminescence Studies of Donors in MBE-Grown ZnSe"; J.E. Potts, T.L. Smith and H. Cheng; to appear in SPIE Conf. Proc. #794, Modern Optical Characterization Techniques for Semiconductors and Semiconductor Devices; Bay Point, FL; March, 1987, p.27.

"Molecular Beam Epitaxial Growth of ZnSe on (100) GaAs and (100) Ge: A Comparative Study of Material Quality"; R.M. Park, J. Kleiman and H.A. Mar; to appear in SPIE Conf. Proc. #796, Growth of Compound Semiconductors"; Bay Point, FL; March, 1987, p.86.

"Defect Characterization of MBE Grown ZnSe/GaAs and ZnSe/Ge Heterostructures by Cross-Sectional and Planar Transmission Electron Microscopy"; S.B. Sant, J. Kleiman, M. Melech, R.M. Park, G.C. Wetherly, R.W. Smith and K. Rajan; Fifth Int'l. Conf. on Microscopy of Semiconducting Materials; Univ. of Oxford; Oxford, UK; April, 1987.

"Excitonic Optical Nonlinearities in ZnSe Thin Films"; J.E. Potts and N. Peyghambarian; invited presentation at SPIE Conf. on Optical Nonlinearities; Los Angeles, CA; Jan., 1988.

### 5.3 Oral Presentations (no published proceedings)

"Molecular Beam Epitaxial Growth of ZnSe: A Progress Report"; H. Cheng, S.K. Mohapatra, J.E. Potts and T.L. Smith, Midwest MBE Users Group Meeting; Eden Prairie, MN; October 7, 1986.

"Molecular Beam Epitaxy of ZnSe for Visible Light Optoelectronic Devices"; T.L. Smith, Univ. of Illinois Physical Electronics Annual Workshop; Champagne-Urbana, IL; April, 1987.

"Electron Beam Pumped Lasing in MBE-Grown ZnSe"; T.L. Smith, J.E. Potts and H. Cheng; 1987 Conf. on Lasers and Electro-Optics; Baltimore, MD; April, 1987.

"Room Temperature Excitonic Optical Nonlinearities of MBE-Grown ZnSe Thin Films"; S.H. Park, A. Jeffery, R. Morgan, S.W. Koch, N. Peyghambarian, J.E. Potts and H. Cheng; 1987 Conf. on Lasers and Electro-Optics; Baltimore, MD; April, 1987.

"Process-Related Defects in ZnSe Grown by MBE", J. Kleiman, R.M. Park, H.A. Mar, K. Rajan; TMS/AIME Symposium on Dislocations and Interfaces in Semiconductors; Phoenix, AZ; January 25-29, 1988.

"A Study of Anomalous-Colored Regions in MBE-Grown ZnSe", J. Kleiman, H.A. Mar, R.M. Park and G.C. Weatherly; 15th Annual Conf. on Physics and Chemistry of Semiconductor Interfaces; Asilomar, CA; Feb. 1-3, 1988.

"Femtosecond Dynamics of Excitonic Optical Nonlinearities of MBE-Grown ZnSe Thin Films", S.H. Park, B. Fleugel, R. Morgan, M. Joffre, S.W. Koch, N. Peyghambarian, J.E. Potts and H. Cheng; CLEO'88; Baltimore, MD; April 21, 1988.

### 5.4 In Preparation

"Interface Phonon Modes in Epitaxial ZnSe Films"; J.E. Potts, H. Cheng and R. Merlin.

"Photoluminescence and Electrical Properties of As-Grown and Post-Annealed ZnSe"; S.K. Mohapatra, G.A. Haugen, J.E. Potts and J.M. DePuydt, SPIE Conf. on Advances in Semiconductors and Superconductors; Physics and Device Applications; Newport Beach, CA; March 13-18, 1988.

END

DATE

FILMED

5-88

DTIC